Geotechnical and Structures Laboratory

**US Army Corps
of Engineers**®
Engineer Research and
Development Center

Field Testing and Load Rating Report, Bridge S-1090, Camp Casey, South Korea

Brett Commander, Jesse Grimson, Wilmel Varela-Ortiz   May 2008
Terry R. Stanton, Carmen Y. Lugo, and Gerald M. Hansler

Field Testing and Load Rating Report, Bridge S-1090, Camp Casey, South Korea

Brett Commander and Jesse Grimson

Bridge Diagnostics, Inc.
1965 57th Court North, Suite 106
Boulder, CO 80301-2826

Wilmel Varela-Ortiz, Terry R. Stanton, and Carmen Y. Lugo

Geotechnical and Structures Laboratory
U.S. Army Engineer Research and Development Center
3909 Halls Ferry Road
Vicksburg, MS 39180-6199

Gerald M. Hansler

Eighth U.S. Army
Seoul, South Korea

Final report

Prepared for   Headquarters, Installation Management Command (IMCOM)
                 Arlington, VA 22202

Abstract: In June 2007, Bridge Diagnostics, Inc. (BDI), was contracted by the U.S. Army Corps of Engineers to perform live-load testing and load rating on Bridge S-1090 at Camp Casey, South Korea, in conjunction with two other structures, S-4360 and S-1801. The general goal of the live-load testing was to obtain and then utilize field measurements to verify an analytical model from which accurate load ratings could be obtained. A more specific purpose of the load test was to determine if the use of the Heavy Equipment Transporter System (HETS) to transport an M1A1 tank across the bridge was more or less severe than the M1A1 tank crossing on its own.

Controlled load tests were performed with a three-axle dump truck, an empty HETS, an M1A1 tank, and a HETS carrying an M1A1 tank. The load test data were examined to obtain a direct comparison of load responses from the different load configurations. The conclusion obtained directly from the load test data was that the HETS/M1A1 load combination produced lower stresses than the M1A1 tank by itself. Subsequent modeling and analysis of the bridge further verified that the HETS was the best option for transporting the M1A1 across the bridge. Load ratings were performed for the standard American Association of State Highway and Transportation Officials (AASHTO) vehicles and several military load configurations in accordance with AASHTO Load and Resistance Factor Design–Bridge Design Specifications 2004 and Manual for Condition Evaluation and Load and Resistance Factor Rating of Highway Bridges 2003. It was found that the structure can safely carry all of the AASHTO vehicles and military load configurations considered in this report.

Contents

Report Documentation Page

Figures and Tables

Figures

Tables

Preface

This report describes the load testing process and analytical results conducted for Bridge S-1090 at Camp Casey, South Korea. The load test was one of three tests performed in June 2007 to obtain more accurate bridge load ratings with respect to the Heavy Equipment Transporter System and other heavy military load configurations. This project was arranged and supervised by Terry R. Stanton of the U.S. Army Engineer Research and Development Center (ERDC).

The work was performed by Bridge Diagnostics, Inc. (BDI), under Contract No. W912HZ-07-C-0045, and by personnel of the Structural Engineering Branch (StEB), ERDC Geotechnical and Structures Laboratory (GSL). This report was prepared by Jesse Grimson and Brett Commander of BDI; Wilmel Varela-Ortiz, Terry R. Stanton, and Carmen Y. Lugo, GSL; and LTC Gerald M. Hansler, Deputy Assistant Chief of Staff, Eighth U.S. Army. Technical review of the document was performed by Dr. Mihan H. McKenna and Sharon Garner, StEB.

The Army Bridge Inspection Program is sponsored by the Army Transportation Infrastructure Program (ATIP) of the Headquarters, Installation Management Command (IMCOM), Arlington, VA. The IMCOM provided funding for this investigation. Questions should be directed to Ali A. Achmar, IMCOM ATIP Program Manager (210-295-2038).

This publication was prepared under the overall project supervision of James S. Shore, Chief, StEB; Dr. Robert L. Hall, Chief, Geosciences and Structures Division; Dr. William P. Grogan, Deputy Director, GSL; and Dr. David W. Pittman, Director, GSL.

COL Richard B. Jenkins was Commander and Executive Director of ERDC. Dr. James R. Houston was Director.

Unit Conversion Factors

Multiply	By	To Obtain
degrees Fahrenheit	(F-32)/1.8	degrees Celsius
feet	0.3048	meters
foot-pounds force	1.355818	joules
inches	0.0254	meters
inch-pounds (force)	0.1129848	newton meters
miles per hour	0.44704	meters per second
pounds (force)	4.448222	newtons
pounds (force) per foot	14.59390	newtons per meter
pounds (force) per inch	175.1268	newtons per meter
square feet	0.09290304	square meters
square inches	6.4516 E-04	square meters
tons (force)	8,896.443	newtons

1 Introduction and Results Summary

The Bridge Diagnostics, Inc. (BDI), Structural Testing System (STS) was used to measure strain at 56 locations on the superstructure while it was subjected to various controlled load tests. Load configurations included a three-axle dump truck, an M1A1 tank, an empty Heavy Equipment Transporter System (HETS), and a HETS hauling an M1A1 tank. Direct comparisons of response data were made to evaluate the relative difference in load responses from the different load configurations. It was found that the M1A1 tank produced the greatest flexural stresses on the bridge.

The load test data were then used to "calibrate" an analytical finite element model of the superstructure, which was in turn used to develop load ratings using the Load and Resistance Factor Design (LRFD) design manual and Load and Resistance Factor Rating (LRFR) manual. Load ratings were performed for several American Association of State Highway and Transportation Officials (AASHTO) and military load configurations. The analysis and load rating results further verified that the use of the HETS to transport the M1A1 tank produced less stress than the M1A1 tank by itself.

Table 1 presents the controlling load rating factors (RF) for each vehicle and the corresponding locations at which they occur. Flexural moment at the end-sections of the beam beyond the cover plates controlled all load ratings.

Table 1. Critical load rating factors and weights.

Rating Vehicle	Location	LRFR - Inventory		LRFR - Operating	
		RF	Tonnes	RF	Tonnes
HS-20	Interior end span	2.67	87.2	3.46	113.0
HS-26	Interior end span	2.05	67.1	2.66	87.0
HS-30	Interior end span	1.78	58.1	2.31	75.4
Type 3	Interior end span	3.39	129.2	4.39	167.4
Type 3S2	Interior end span	4.08	266.5	5.29	345.5
Type 3-3	Interior end span	3.76	272.9	4.87	353.7
M1A1*	Exterior end span	1.74	106.7	2.26	138.3
Empty HETS*	Interior end span	5.45	212.6	7.06	275.5
HETS with M1*	Interior end span	2.15	225.8	2.79	292.6
Korean HETS*	Interior end span	2.45	181.1	3.18	234.7
PLS	Interior end span	2.23	138.5	2.89	179.6
MLC60 (wheeled)*	Interior end span	2.48	135.0	3.21	175.0
MLC60(tracked)*	Interior end span	2.03	110.5	2.63	143.2
MLC70 (wheeled)*	Exterior end span	2.15	136.5	2.79	177.0
MLC70 (tracked)*	Exterior end span	1.81	114.9	2.35	149.0
* Single lane loading only.					

2   Structural Testing Information

Bridge S-1090 is located at Camp Casey in South Korea. It is a four-span, noncontinuous, steel beam bridge. The bridge consists of six beam lines and a reinforced concrete deck. The spans are roughly 12 m each, and the abutment and pier supports are in perpendicular alignment to the roadway. The steel beams are rolled sections with cover plates welded to the bottom flange. Shear stud connectors were specified on the design plans, indicating the deck was to be composite with beams for all live-load applications. It was noted during the instrumentation process that the actual span lengths and beam cross-section dimensions varied slightly from those specified in the plans.

The bridge was instrumented with 56 standard strain transducers, as shown in Figure 1 through Figure 3. Controlled load tests were performed with a three-axle dump truck driven slowly (<7 kph) across the bridge along three prescribed lateral paths. In addition to the dump truck, live-load tests were performed with an M1A1 tank, an empty HETS, and a HETS loaded with an M1A1 tank. Strains were measured simultaneously on all sensors at a rate of 40 Hz during the entire load cycle. The longitudinal truck position was measured and recorded remotely and stored with the strain data.

Information specific to this load test can be found in Table 2, and the field notes are presented in Appendix B. Vehicle gross-weights and wheel rollout distances, for each load configuration, are provided in Table 3 through Table 6. Footprints of each vehicle, including wheel weights, are shown in Figure 4 through Figure 7. All vehicle weights were obtained onsite with the use of portable scales so each wheel pair was measured separately.

Appendix C provides an outline of the general field testing procedures, Appendix D contains the specifications on the BDI strain transducers, and Appendix E summarizes specifications of the BDI Structural Testing System.
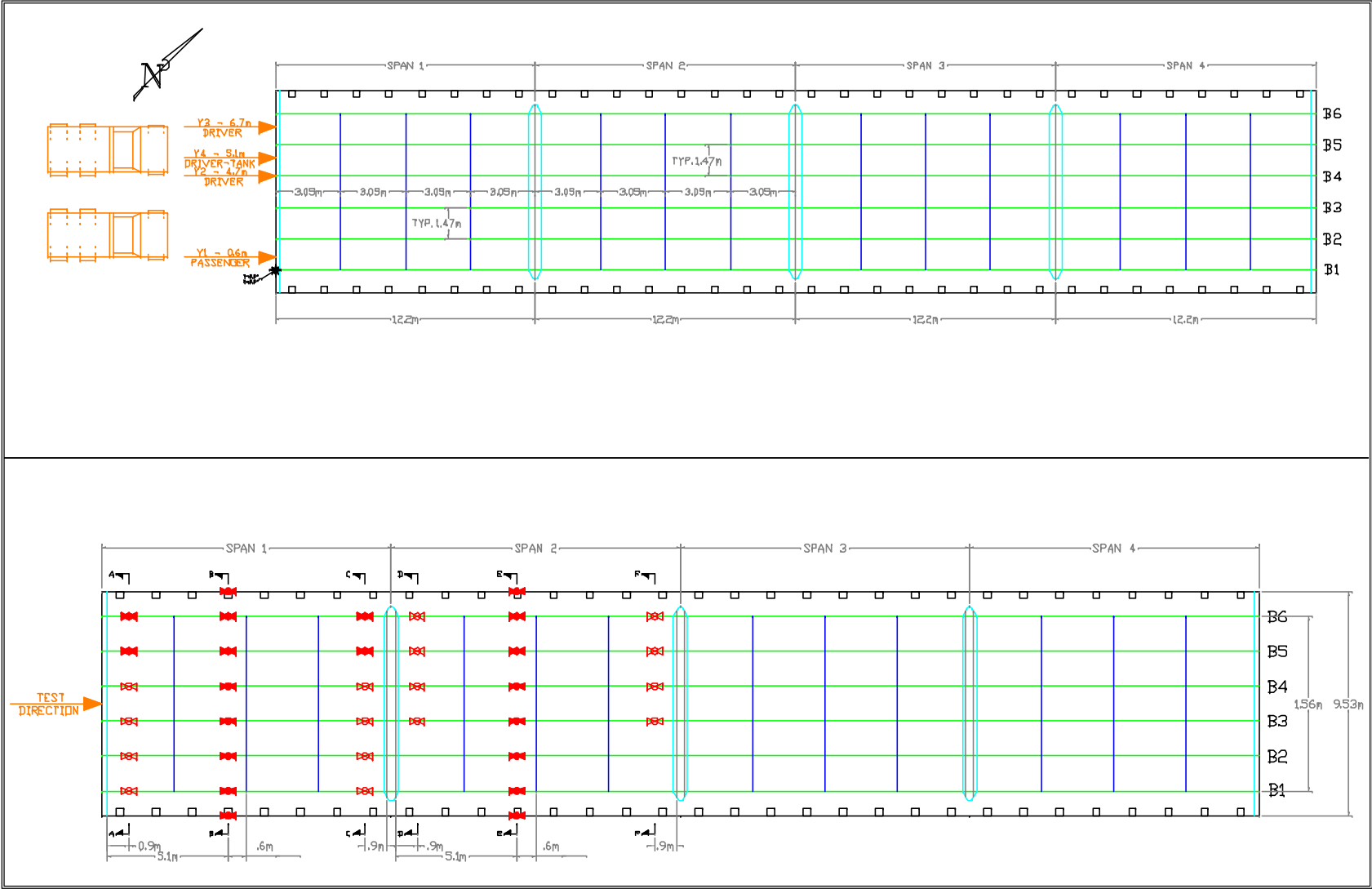
Figure 1. Gage layout.
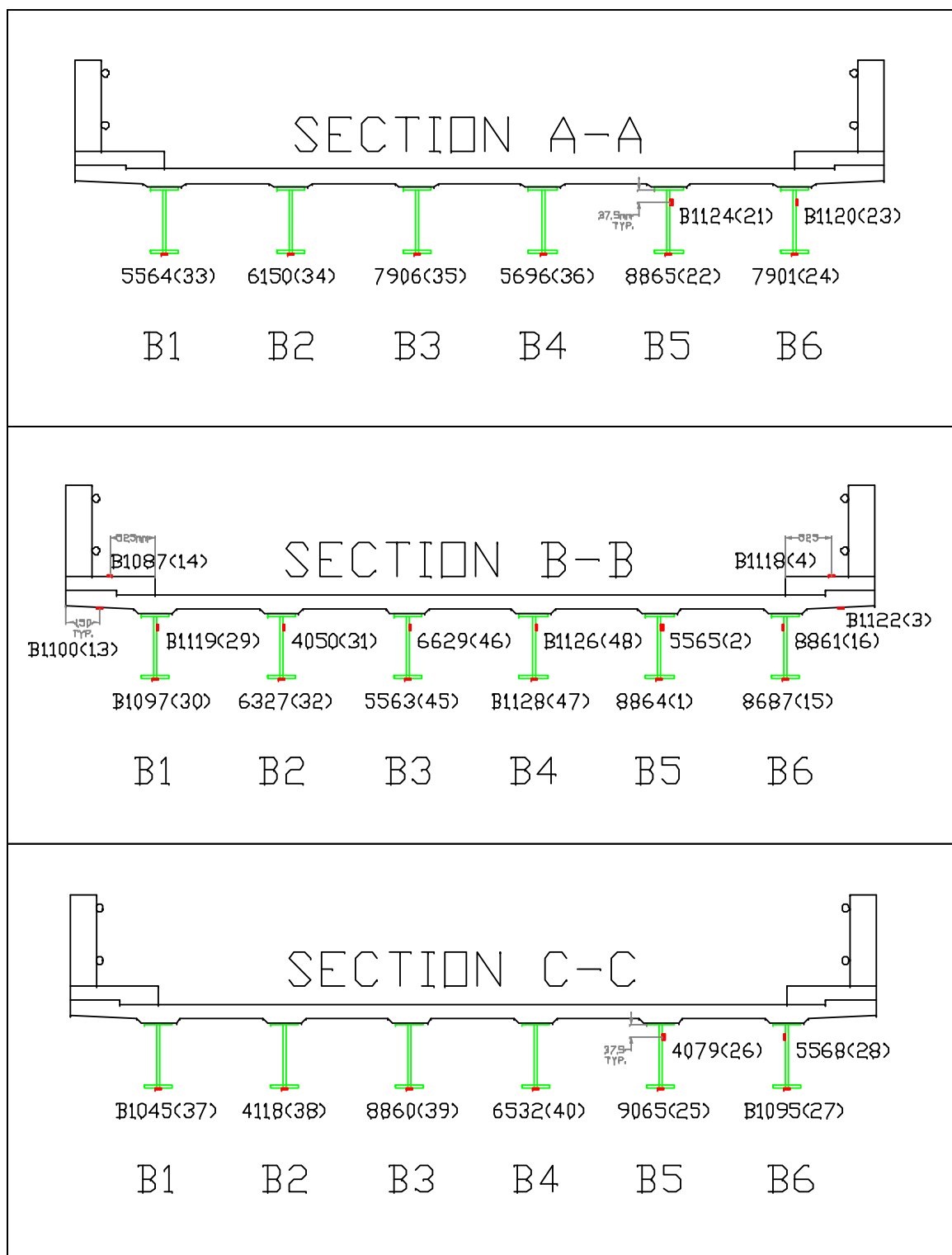
Figure 2. Instrumentation details, cross sections AA-CC.
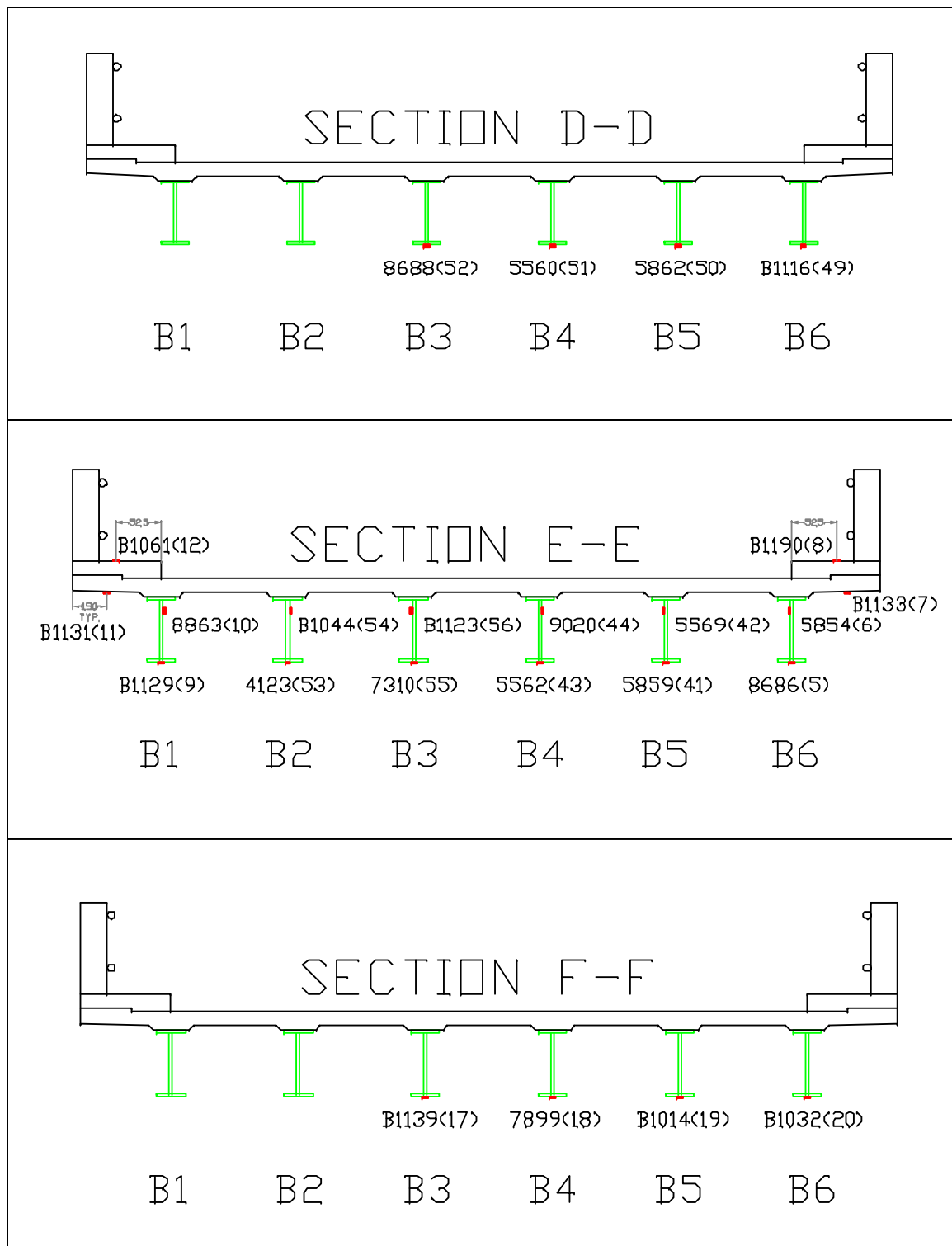
Figure 3. Instrumentation details, cross sections DD-FF.

Table 2. Structure description and testing notes.

Item	Description
Structure Name	S-1090
Year Constructed/Renovated	Unknown/1984 Assume steel yield strength, Fy = 248 MPa (36 ksi), based on USACE load rating 2007.
BDI Project Number	060701-303
Testing Date	June 16, 2007
Client's Structure ID #	S-1090
Location/Route	Camp Casey, South Korea
Structure Type	Steel girder with reinforced concrete deck
Total Number of Spans	4 (noncontinuous)
Span Length(s)	Span 1: 12.2 m, Span 2: 12.2 m, Span 3: 12.2 m, Span 4: 12.2 m
Skew	0 deg
Structure/Roadway Width	7.31 m/9.53 m
Beams	(6) Beam lines @ 1.47 m (4'-10") rolled steel beams with cover-plates
Deck Type	Reinforced concrete 163 mm (6.5 in.)
Other Structure Info	N/A
Spans Tested	2
Test Reference Location (X=0,Y=0)	Edge of sidewalk, northeast corner
Test Vehicle Direction	Northeast
Test Beginning Point	-3 m + ½ wheel revolution from expansion joint
Lateral Load Position(s)	3
Number/Type of Sensors	56 strain transducers
STS Sample Rate	40 Hz (66 Hz and 100 Hz for high-speed tests)
Number of Test Vehicles	3
Structure Access Type	Ladder and scaffolding.
Structure Access Provided by	USACE (U.S. Army Corps of Engineers)
Traffic Control Provided by	USACE
Total Field Testing Time	8 hr
Field Notes	See Appendix B
Visual Condition	Good condition

Data Files
    1090DT-1.dat
    1090DT-2.dat
    1090DT-3.dat
    1090DT-4.dat
    1090DT-5.dat
    1090DT-6.dat
    1090DT-7.dat
    1090DT-8.dat
	Lateral Truck Position and Notes
	    Dump truck @ Y1
	    Dump truck @ Y1
	    Dump truck @ Y2
	    Dump truck @ Y2
	    Dump truck @ Y3
	    Dump truck @ Y3
	    Dump truck @ Y3
	    Dump truck @ Y2 @ 32 kph - Brake test, Span 4

Item	Description
1090DT-9.dat	Dump truck @ Y2 @ 32 kph
1090DT-10.dat	Dump truck @ Y2 @ 32 kph - Brake test, Span 4
1090M1-1.dat	M1 tank @ Y4
1090M1-2.dat	M1 tank @ Y4
1090M1-3.dat	M1 tank @ Y4 - 10 kph
1090M1-4.dat	M1 tank @ Y4 - 10 kph – Brake test, Span 4
1090HET-1.dat	HETS empty trailer @ Y2 – 0.6 m off to right at start
1090HET-2.dat	HETS empty trailer @ Y2 - good
1090HET-3.dat	HETS empty trailer @ Y2 - good
1090HET-4.dat	HETS empty trailer @ Y2 - 32 kph
1090HET-5.dat	HETS empty trailer @ Y2 - 32 kph – Brake test, Span 4
1090HETM1-1.dat	HETS w/M1A1 tank @ Y2
1090HETM1-2.dat	HETS w/M1A1 tank @ Y2
1090HETM1-3.dat	HETS w/M1A1 tank @ Y2 - 32 kph
1090HETM1-3.dat	HETS w/M1A1 tank @ Y2 - 32 kph – Brake test, Span 4

Table 3. Testing vehicle information (dump truck).

Vehicle Type - Tandem rear axle dump truck (see Figure 4)	
Gross Vehicle Weight (GVW)	26380 kg
Wheel Rollout 5 Revs	16.4 m
# Crawl Speed Passes	7
# High Speed Passes and Brake Tests	4 (32 kph)
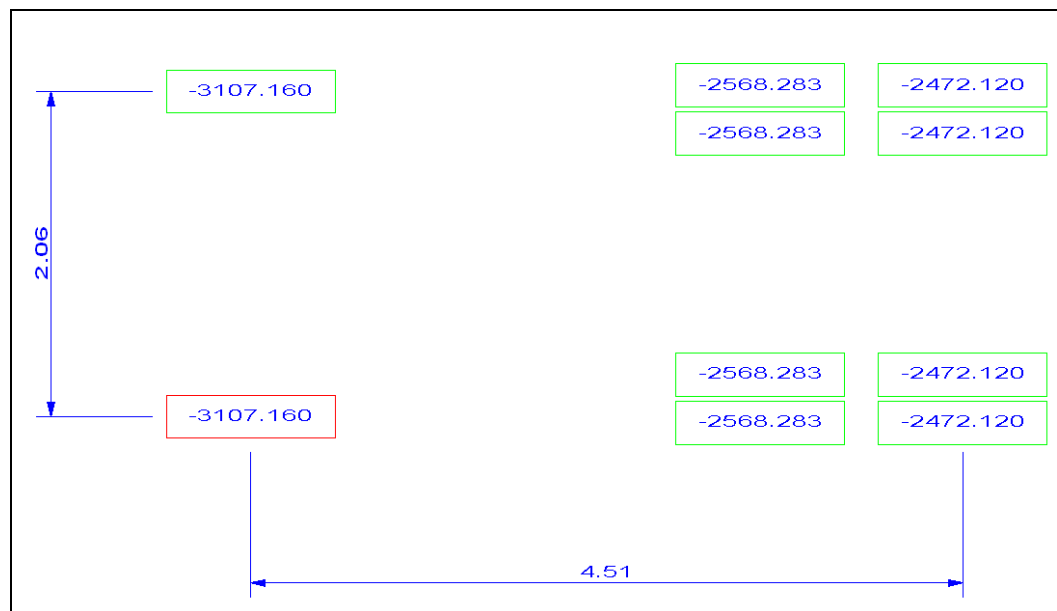
Figure 4. Tandem rear axle dump truck footprint.

Table 4. HETS with M1A1 vehicle information.

Vehicle Type – HETS with M1A1 Tank (see Figure 5)	
Gross Vehicle Weight (GVW)	109400 kg
Wheel Rollout 5 Revs	20.29 m
# Crawl Speed Passes	2
# High Speed Passes and Brake Tests	2 (32 kph)
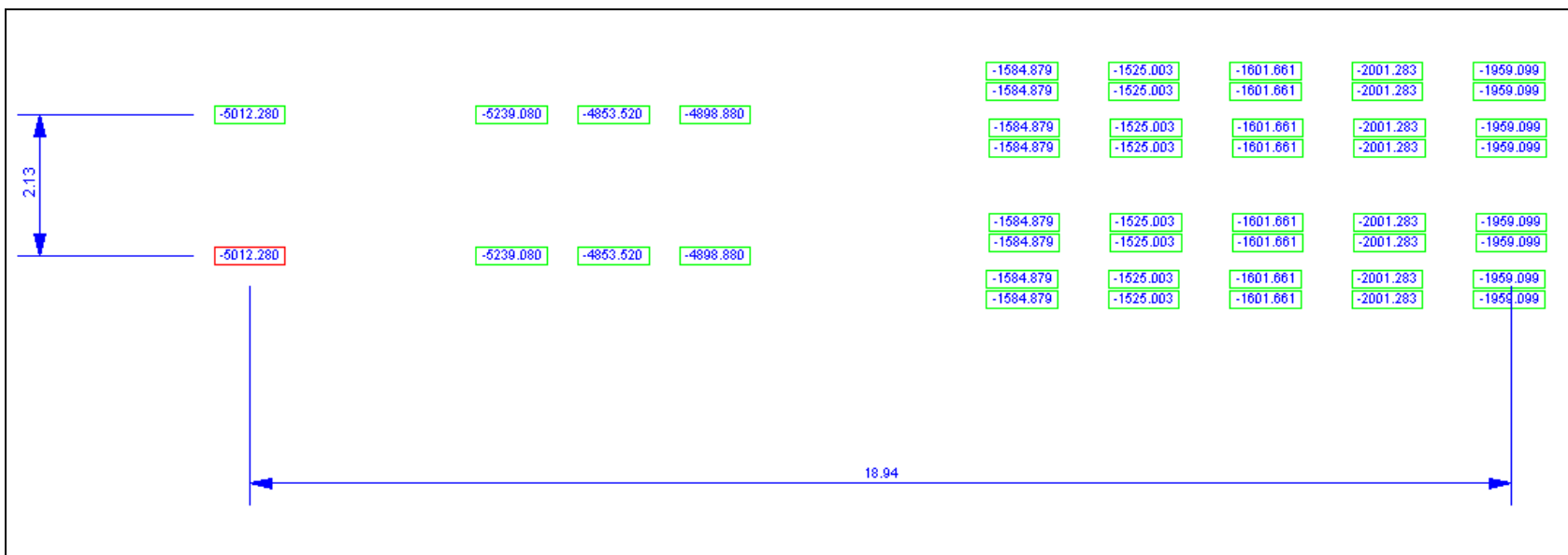
Figure 5. HETS with M1A1 tank footprint.

Table 5. Empty HETS vehicle information.

Vehicle Type – Empty HETS (see Figure 6)	
Gross Vehicle Weight (GVW)	46500 kg
Wheel Rollout 5 Revs	16.4 m
# Crawl Speed Passes	3
# High Speed Passes and Brake Tests	2 (32 kph)
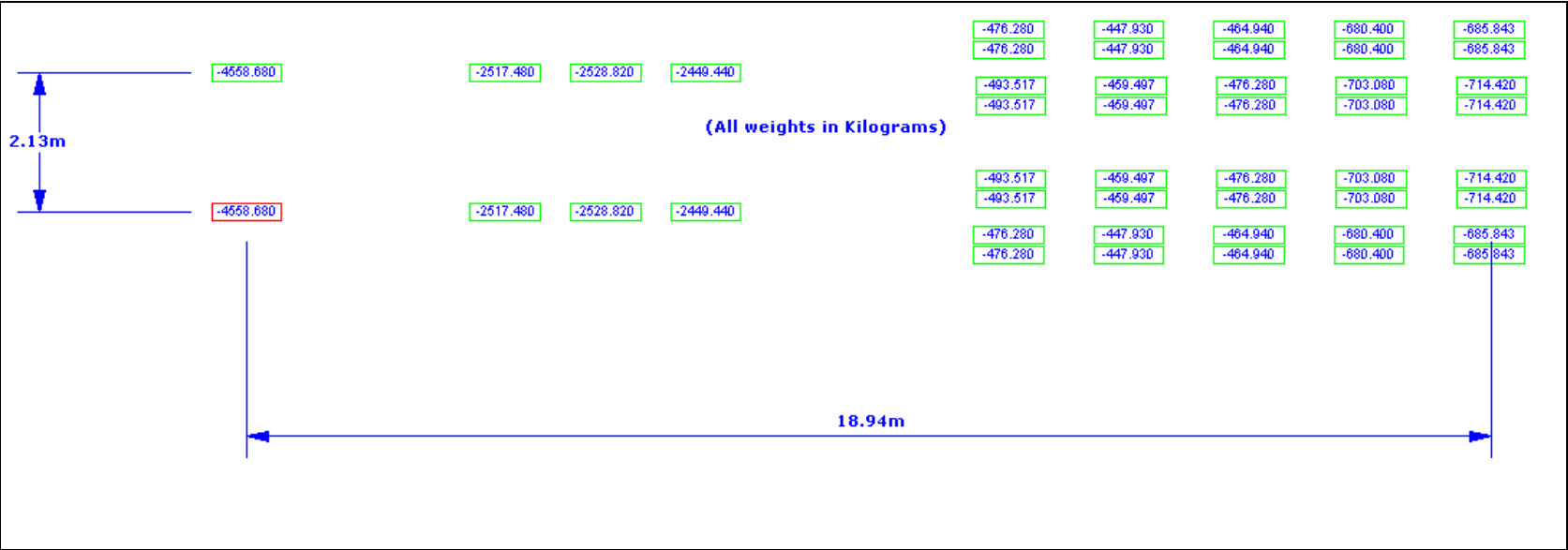
Figure 6. Empty HETS footprint.

Table 6. M1A1 tank vehicle information.

Vehicle Type – M1A1 Tank (see Figure 7)	
Gross Vehicle Weight (GVW)	71300 kg
Wheel Rollout 10 Revs	21.77 m
# Crawl Speed Passes	2
# High Speed Passes and Brake Tests	2 (10 kph)
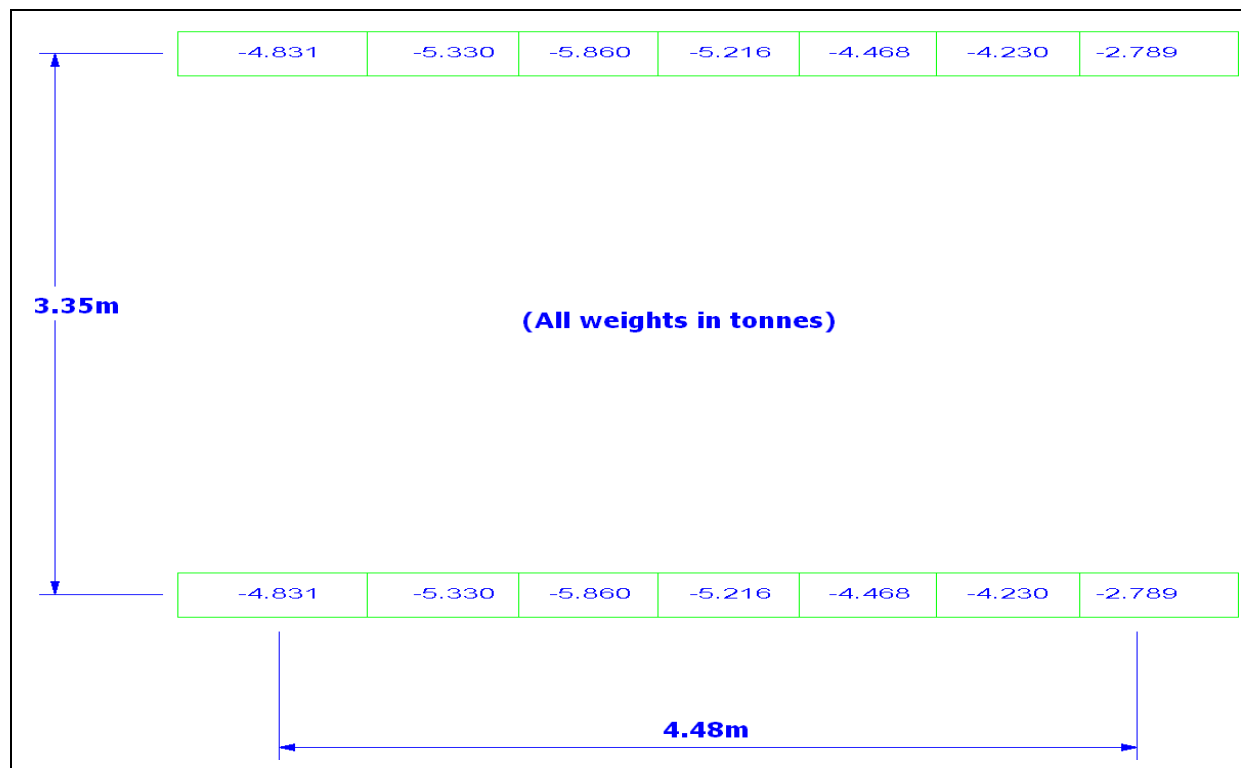
Figure 7. M1A1 tank footprint.

3   Preliminary Investigation of Test Results

All of the field data were first examined graphically to determine their
quality and to provide a qualitative assessment of the structure's live-load
response. Some of the indicators of data quality included reproducibility
between identical truck crossings, elastic behavior (strains returning to
zero after truck crossing), and any unusual-shaped responses that might
indicate nonlinear behavior or possible gage malfunctions.

In addition to providing a data "quality check," the information obtained
during the preliminary investigation was used to determine appropriate
modeling procedures and helped establish the direction that the analysis
should take. Several representative response histories are provided in
Appendix A.

The following sections summarize comments based on examination of the
load test data. In several cases, supporting data plots are referenced. All of
the measured data are shown in terms of stress in units of megapascals.
These values were obtained by multiplying the strain values by the modu-
lus of steel (E_s = 200,000 MPa). The data plots typically contain a series
legend providing an identification for each data series. In general, the
legend contains the gage ID and the data file name. Within the data file
name, it is possible to determine the bridge ID, the load vehicle, and the
pass number. A description of the truck paths can be found in Table 2 and
in the field notes in Appendix B. Most of the measured data are presented
in the form of stress histories in which the X-axis is shown as truck posi-
tion. The truck position value indicates the position of the vehicle's front
axle with respect to the structure's origin (X = 0.0, as shown in Figure 1).

Data observations for 26.38-tonne dump truck

Reproducibility and linearity

Responses from identical truck paths were very reproducible, as shown in
Figure 8. In addition, all stresses appeared to be linear with respect to load
magnitude (truck position) and all stresses returned to zero, indicating
that the structure was acting in a linear-elastic manner. The stress history
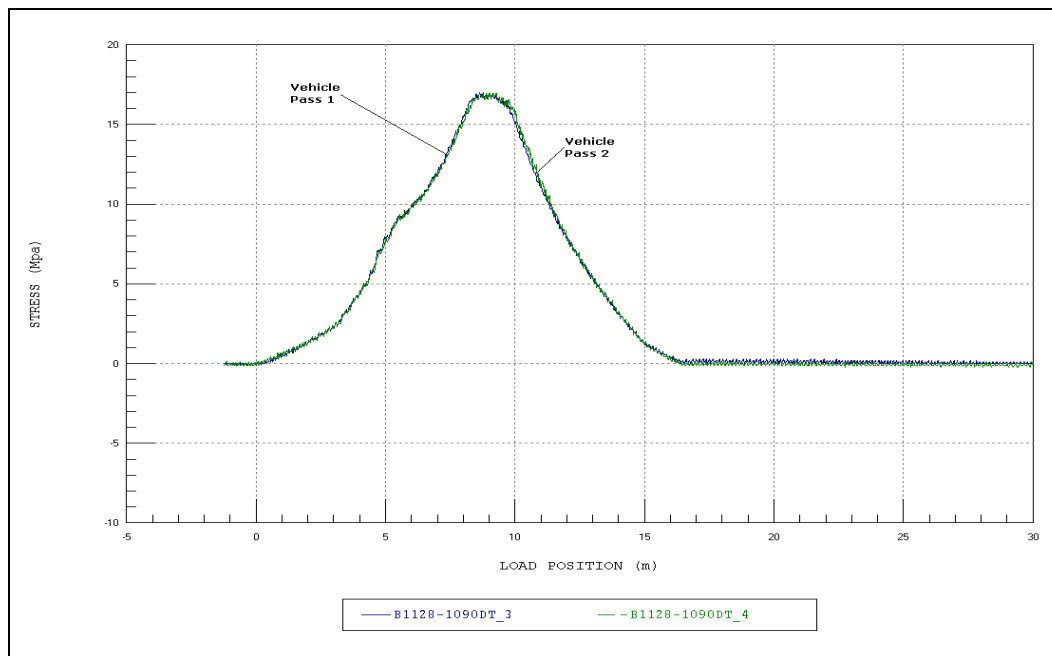
Figure 8. Reproducibility and linearity.

plots show the response from the midspan gage of Beam 4 at Span 1 with the vehicle traveling on Path Y2. All of the stress histories had a similar degree of reproducibility and linearity, indicating good quality data.

Distribution and symmetry

Midspan stress values from all beam lines were examined for the truck positions generating the maximum stress. The relative stress magnitude from each beam illustrates the structure's lateral load transfer character-istics. Figure 9 displays the bottom flange stress distribution across mid-span of Span 2 for the truck paths (Y1, Y2, and Y3). This plot shows that the structure is distributing the load in a symmetric manner. Note that the distribution of Path Y2 is slightly skewed to the right side. This is simply an indication that the prescribed lateral path was not precisely down the center of the structure.

Neutral axis values

At beam cross sections where two strain transducers were installed, neutral axis (NA) locations were estimated using the method described in Appendix G. The average interior beam NA value was 529 mm (21.2 in.), which was very close to the theoretical NA based on an effective flange width of 1450 mm (58 in.), 175-mm (7-in.) deck thickness, a 12.5-mm (0.5-in.) haunch, and a steel-to-concrete elastic modulus ratio of 8.
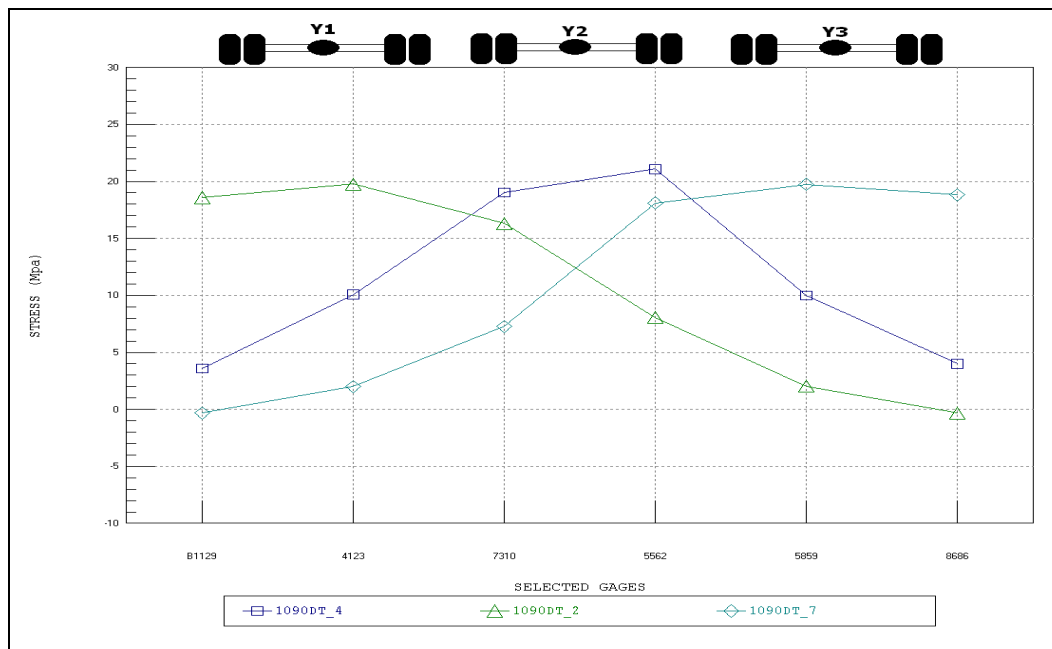
Figure 9. Lateral strain for Span 1, Paths Y1–Y3.

The average NA location for the exterior beam was approximately 600 mm (24.0 in.). This indicates that the thickened slab due to the sidewalk had a significant effect on the exterior beam stiffness. This observation, along with the relatively narrow bridge width, was highly relevant because the stiff exterior beams greatly altered the structure's lateral load transfer characteristics. Figure 10 and Figure 11 show bottom flange and upper web stress histories for an exterior and an interior beam. In both cases, the upper web gage was very close to the NA. It is apparent, however, that the NA is above the gage location at the exterior beam and below the gage location at the interior beam.

End-restraint

Most of the beam lines showed little axial or rotational end-restraint. This was expected since the structure was designed as four separate simple spans with an expansion joint between them. However, this was not found to be true for Beam Line 1 on the West Abutment. Figure 12 shows the bottom flange stress history near the abutment. The negative (compressive) stress as the truck approached midspan was an indication that end-restraint was present. The beam bearing condition cannot physically resist significant moment, but it can resist horizontal displacement of the bottom flange. Since the degree of end-restraint varied from beam to beam,
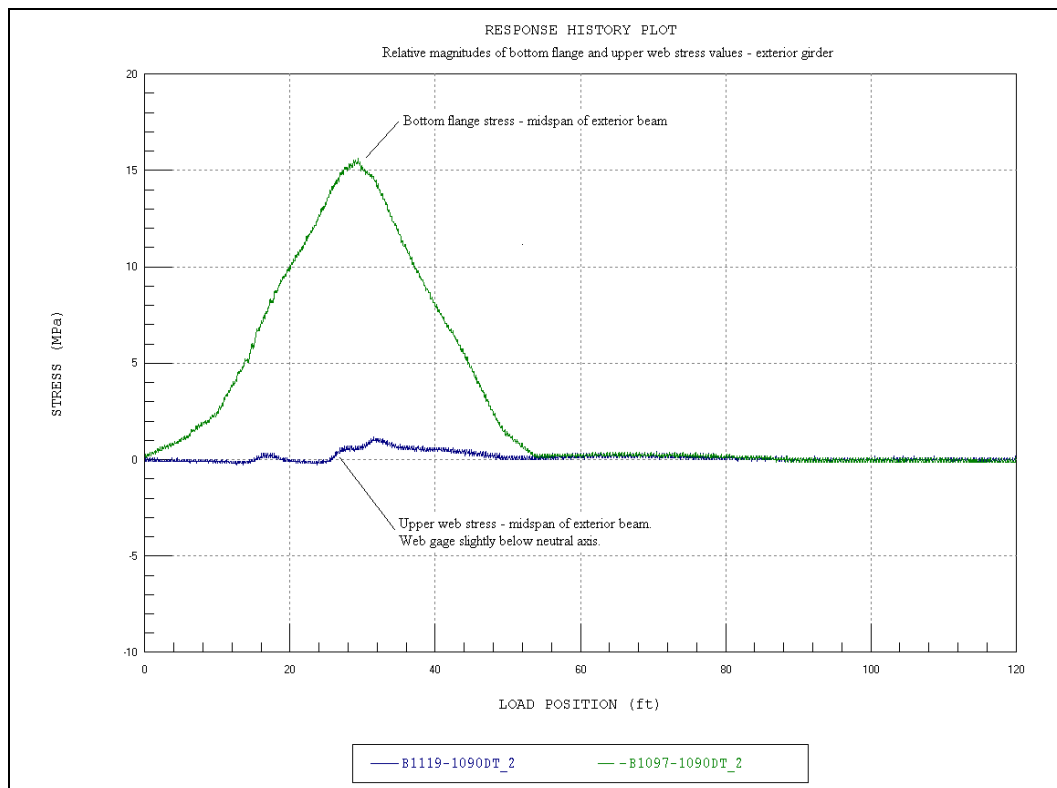
Figure 10. Bottom flange and upper web stress histories - exterior beam.
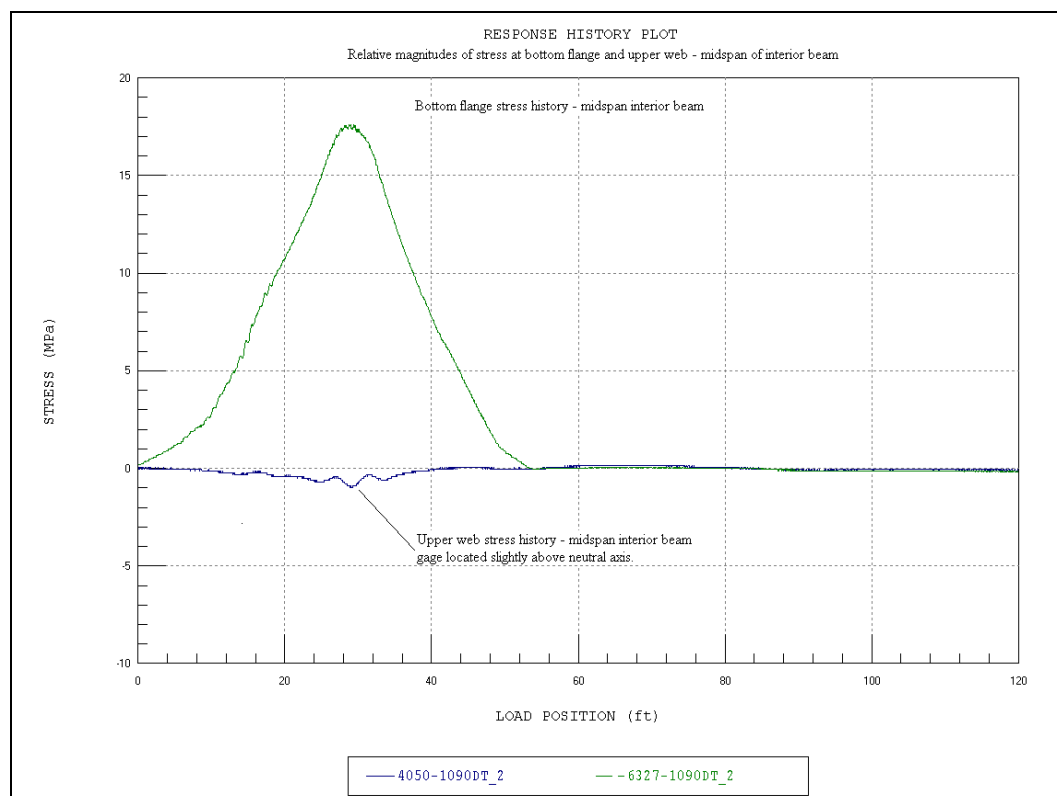
Figure 11. Bottom flange and upper web stress histories - interior beam.
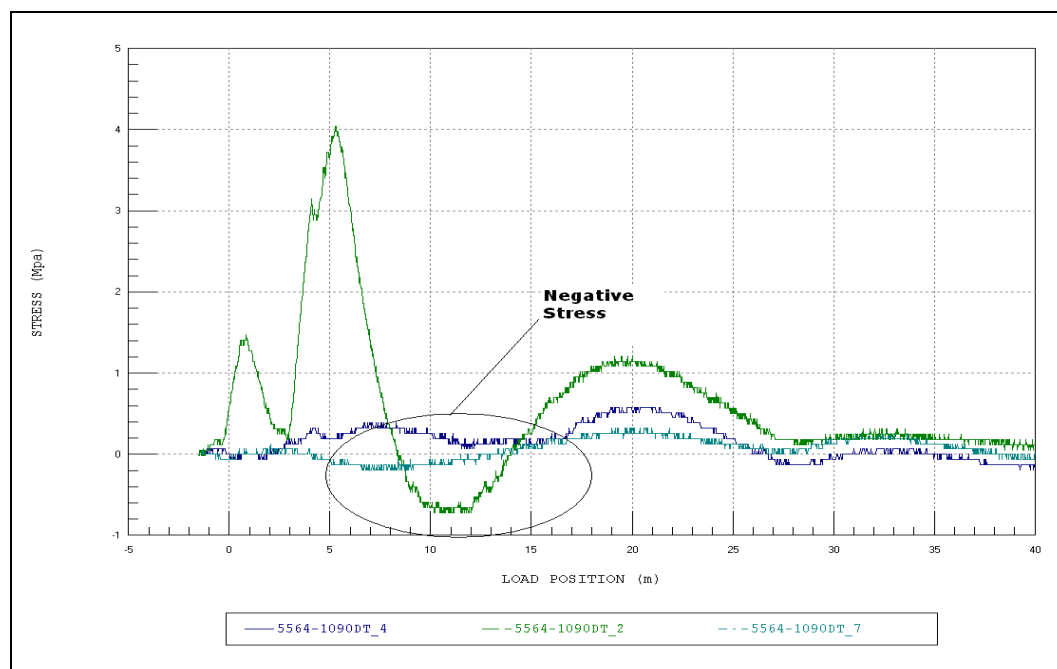
Figure 12. End-restraint near abutment and piers.

each beam support will likely require a unique spring type. The large variation also indicates the end-restraint is not highly reliable, so any resistance identified during the model calibration process should be ignored for rating.

Continuity

This structure exhibited slight continuity between spans. Figure 13 is a plot of the stress found in the west end of Beam 3, Span 2. The negative stress caused by the load as it moves from one span to the next is an indication of continuity. This was a typical response of all gage locations near the pier. The beams were not continuous, and there was an expansion joint in the deck over the piers. Therefore, the only means of load transfer between spans is the common translational movement of the beam's bottom flanges at the pier. This type of response is typical of multi-span noncontinuous structures. While the continuity was minimal and should be ignored for load rating purposes, accurate identification of the continuity is required to accurately identify the beam and deck stiffness parameters.
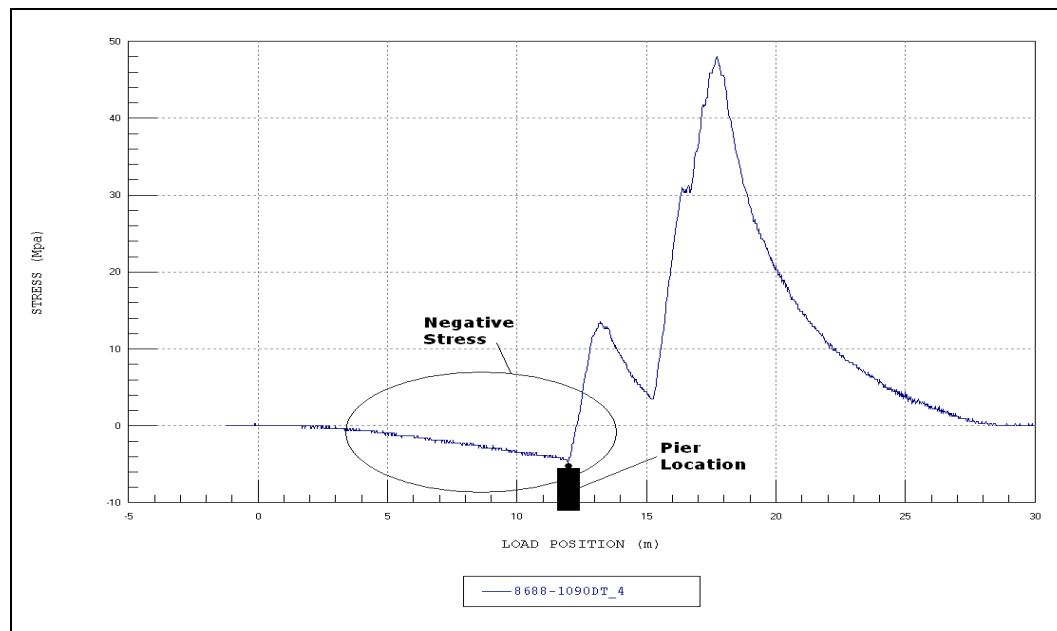
Figure 13. Continuity load response.

Gage malfunction

As shown in Figure 14, Gage 6150 was found to be malfunctioning and was not used in the modeling and correlation process. The constant noise generated by this gage is indicative of a damaged sensor.

Upper web gages

It was noticed that the upper web gages throughout the structure were placed very close to the NA of the individual sections, resulting in low strain responses. As a result, these readings will be used to evaluate the location of the NA only. The near-zero readings will not be useful in the model calibration process and will not be included in the model for data comparison.

Data review—load tests with military vehicles

In addition to testing with the loaded dump truck, several tests were run with specific military vehicles. The applied load configurations included a HETS transporting an M1A1 tank, an empty HETS, and the M1A1 tank by itself. General observations from these load tests are provided in the following sections.
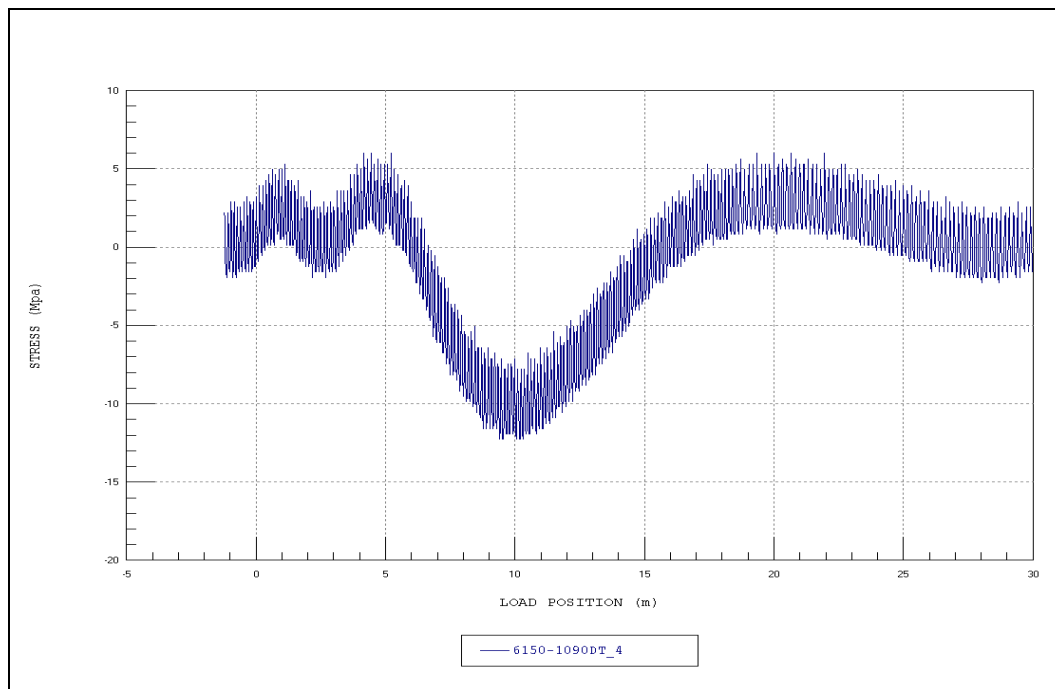
Figure 14. Malfunctioning gage.

Maximum stress magnitudes

The largest stress was generated by the M1A1 tank by itself. In fact, the maximum stress produced by an M1A1 tank at the center of Span 2 (Section E, Beam 4) was 20 percent greater than that obtained from the HETS transporting the tank. A comparison of maximum stress magnitudes from each gage location and each load configuration is provided in Table 7. A stress history comparison at midspan of Span 2 is shown in Figure 15.

Impact factors

Several high speed tests were conducted for the dump truck, empty HET, HET loaded with the M1A1 tank, and M1A1 tank alone. The measured increases in stress due to the impact and dynamic effects were typically less than 10 percent for all load configurations. The largest dynamic effects were generated by the slow-speed M1A1 tank. (Apparently, the engine vibrations of the tank were close to the natural frequencies of one of the bridges.) Figure 16 displays the slow- and high-speed stress history plot of the M1A1 tank on Beam 4, Section E.

Table 7. Maximum stress values generated by military vehicles (all values in megapascals).

Location	Transducer ID	HET with M1		HET (empty)		M1A1	
		Minimum MPa	Maximum MPa	Minimum MPa	Maximum MPa	Minimum MPa	Maximum MPa
Section A - B1 - Bottom	5564	-0.09	1.49	-0.12	0.60	-0.27	1.79
Section A - B2 - Bottom	6150	-4.27	1.59	-1.98	0.99	-15.65	24.51
Section A - B3 - Bottom	7906	-3.25	4.81	-0.85	4.43	-3.47	8.08
Section A - B4 - Bottom	5696	-0.06	11.18	-0.09	4.82	-0.69	12.81
Section A - B5 - Bottom	8865	-0.97	3.72	-0.33	1.28	-1.34	7.45
Section A - B5 - Top	B1124	-0.68	0.70	-0.30	0.20	-0.66	0.56
Section A - B6 - Bottom	7901	-0.11	1.95	-0.03	0.44	-0.06	2.18
Section A - B6 - Top	B1120	-0.12	0.80	-0.19	0.24	-0.17	0.73
Section B - B1 - Bottom	B1119	-0.71	0.42	-0.45	0.27	-0.95	0.37
Section B - B1 - Top	B1097	-0.18	5.76	-0.11	2.17	-0.15	10.02
Section B - B2 - Bottom	6327	-0.06	15.66	-0.07	5.99	-0.14	25.02
Section B - B2 - Top	4050	-0.82	0.36	-0.39	0.21	-1.43	0.29
Section B - B3 - Bottom	5563	-0.03	28.32	-0.04	11.11	-0.20	33.35
Section B - B3 - Top	6629	-0.54	1.25	-0.39	0.89	-1.06	0.43
Section B - B4 - Bottom	B1128	-0.10	27.03	-0.15	10.32	-0.18	31.29
Section B - B4 - Top	B1126	-0.19	2.09	-0.16	0.81	-0.18	0.46
Section B - B5 - Bottom	8864	-0.05	18.99	-0.11	5.93	-0.14	23.09
Section B - B5 - Top	5565	-0.28	0.95	-0.17	0.30	-0.48	0.45
Section B - B6 - Bottom	8687	0.00	8.81	-0.15	2.35	-0.18	9.86
Section B - B6 - Top	8861	-0.46	0.43	-0.45	0.15	-0.88	0.29
Section B - North Curb - Bottom	B1122	-0.15	0.49	-0.12	0.25	-0.15	0.53
Section B - North Curb - Top	B1118	-5.35	0.54	-1.64	0.39	-6.51	0.56
Section B - South Curb - Bottom	B1100	-0.10	0.28	-0.16	0.12	-0.19	0.19
Section B - South Curb - Top	B1087	-5.97	0.68	-2.52	0.40	-11.13	0.51
Section C - B1 - Bottom	B1045	-1.87	1.11	-0.57	0.73	-2.04	3.78
Section C - B2 - Bottom	4118	-1.69	4.78	-0.39	2.66	-1.27	13.04
Section C - B3 - Bottom	8860	-2.50	11.29	-0.67	6.25	-2.10	16.49
Section C - B4 - Bottom	6532	-1.72	12.35	-0.42	6.30	-1.47	17.54
Section C - B5 - Bottom	9065	-1.20	8.26	-0.26	3.06	-1.09	12.95

Location	Transducer ID	HET with M1		HET (empty)		M1A1	
		Minimum MPa	Maximum MPa	Minimum MPa	Maximum MPa	Minimum MPa	Maximum MPa
Section C - B5 - Top	4079	-1.49	0.44	-0.34	0.20	-2.27	0.30
Section C - B6 - Bottom	B1095	-0.74	2.36	-0.21	0.77	-0.76	3.12
Section C - B6 - Top	5568	-0.04	0.63	-0.05	0.11	-0.17	0.66
Section D - B 4 - Bottom	5560	-1.85	14.17	-1.10	4.59	-2.60	14.68
Section D - B3 - Bottom	8688	-2.00	12.65	-1.19	4.44	-2.54	13.31
Section D - B5 - Bottom	5862	-1.16	9.25	-0.72	2.40	-1.65	10.77
Section D - B6 - Bottom	B1116	-0.65	2.76	-0.29	0.78	-0.72	3.34
Section E - B1 - Bottom	B1129	-0.49	7.06	-0.23	2.77	-0.71	12.07
Section E - B1 - Top	8863	-0.88	0.29	-0.33	0.15	-1.16	0.23
Section E - B2 - Bottom	4123	-0.45	18.30	-0.20	6.81	-0.64	29.47
Section E - B2 - Top	B1044	-3.08	0.34	-1.69	0.32	-4.97	0.59
Section E - B3 - Bottom	7310	-0.68	28.41	-0.38	10.84	-0.79	36.66
Section E - B3 - Top	B1123	-3.96	0.63	-3.17	0.38	-7.25	0.72
Section E - B4 - Bottom	5562	-0.43	33.09	-0.28	11.79	-0.81	39.90
Section E - B4 - Top	9020	-0.93	2.12	-1.25	1.06	-3.01	2.02
Section E - B5 - Bottom	5859	-0.47	21.10	-0.21	6.29	-0.79	26.46
Section E - B5 - Top	5569	-0.23	0.48	-0.14	0.16	-0.75	0.45
Section E - B6 - Bottom	8686	-0.35	10.05	-0.16	2.64	-0.65	12.04
Section E - B6 - Top	5854	-0.29	0.17	-0.17	0.19	-0.59	0.30
Section E - North Curb - Bottom	B1133	-7.83	1.56	-2.45	0.52	-9.06	1.44
Section E - North Curb - Top	B1190	-5.18	0.45	-1.32	0.36	-6.35	0.61
Section E - South Curb - Bottom	B1131	-1.09	0.33	-0.41	0.18	-1.30	0.31
Section E - South Curb - Top	B1061	-5.62	0.26	-1.82	0.45	-8.44	0.55
Section F - B3 - Bottom	B1139	-2.62	9.36	-0.91	4.75	-2.90	14.20
Section F - B4 - Bottom	7899	-3.01	8.75	-0.99	5.15	-3.36	14.53
Section F - B5 - Bottom	B1014	-1.21	7.40	-0.34	2.34	-1.40	12.38
Section F - B6 - Bottom	B1032	-1.14	1.53	-0.31	0.55	-1.21	2.58
		Max Stress	33.09	Max Stress	11.79	Max Stress	39.90
		Min Stress	-7.83	Min Stress	-3.17	Min Stress	-15.65
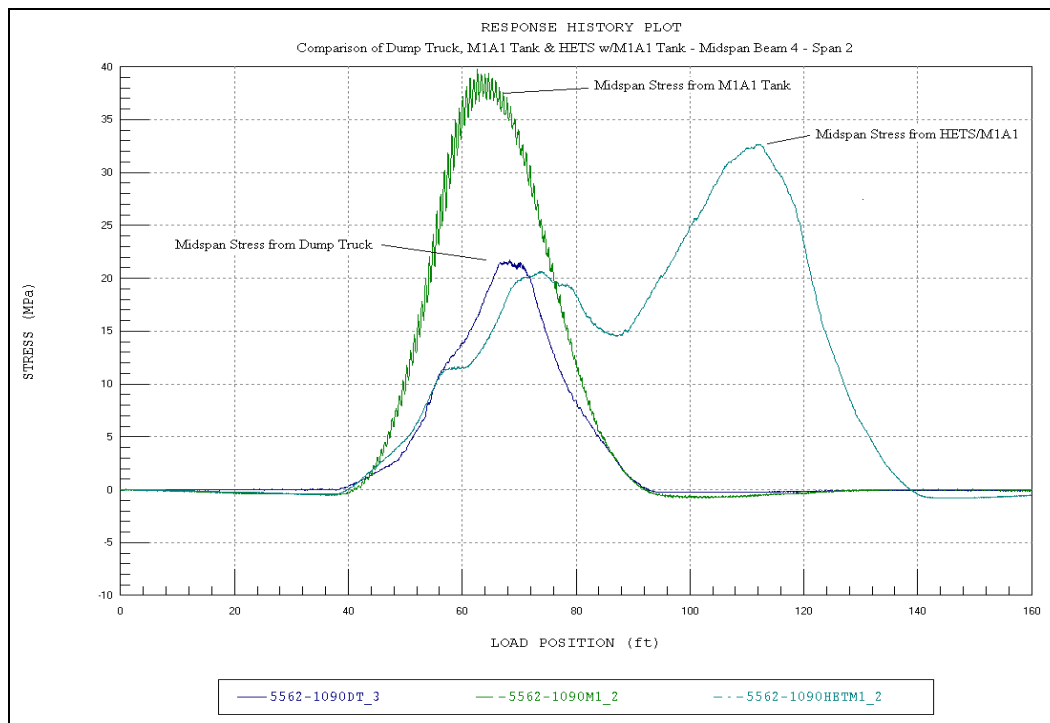
Figure 15. Comparison of midspan stress – dump truck, M1A1, and HETS with M1A1.
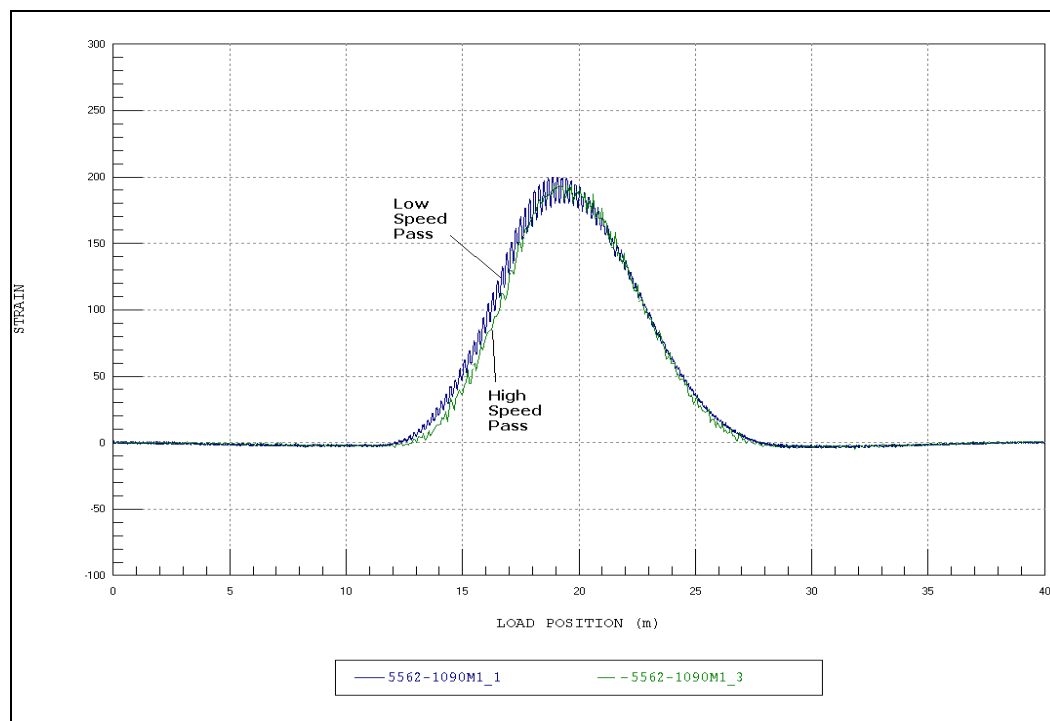
Figure 16. Dynamic effects of M1 tank at Beam 4, Section E.

Braking test

Several hard braking tests were conducted with the various testing vehicles. The vehicles were driven at the maximum safe speed when approaching the bridge. Once on the bridge, the vehicles decelerated as fast as possible until the vehicles achieved a complete stop. Except for the M1A1 tank, no significant increase in stress was detected between the braking tests and the regular high-speed crossings. The M1A1 tank braking test did create 10 to 15 percent greater strain response than the low-speed test. A typical brake test stress history for the HET vehicles can be seen in Figure 17. M1A1 tank brake test results are shown in Figure 18. Stress histories in these figures were obtained from Beam 4 near midspan of Span 1. Note that these plots are displayed as a function of time.
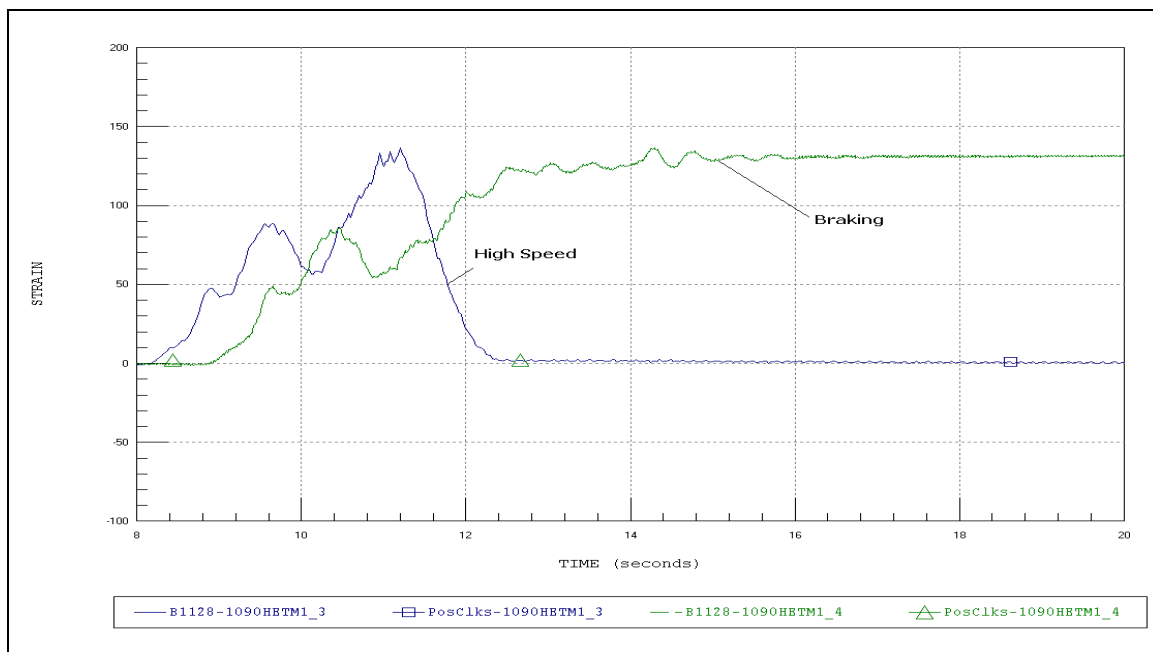
Figure 17 High-speed and braking comparison - HETS.
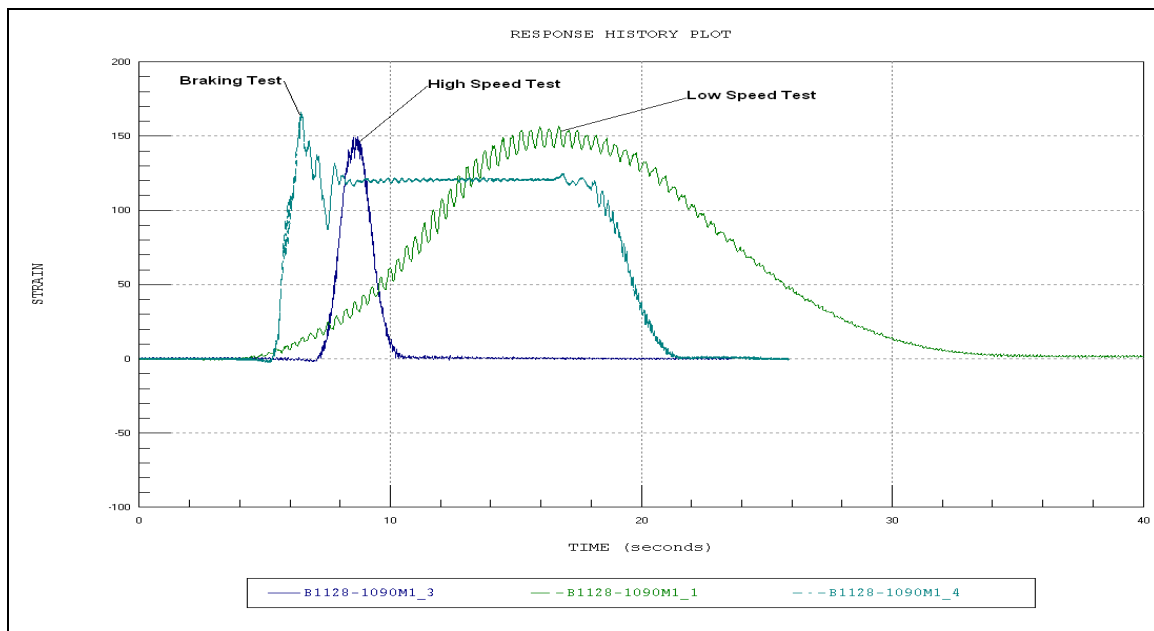
Figure 18. M1A1 tank braking test.

4   Modeling, Analysis, and Data Correlation

Discussion

Note that all of the above information was determined strictly by viewing the field data. The next step was to generate a representative finite element model, as illustrated in Figure 19. Because of the symmetry of the structure, it was necessary to test only two spans. All spans have the same beam sections, spacing, and length. Details regarding the structure model and analysis procedures are provided in Table 8.
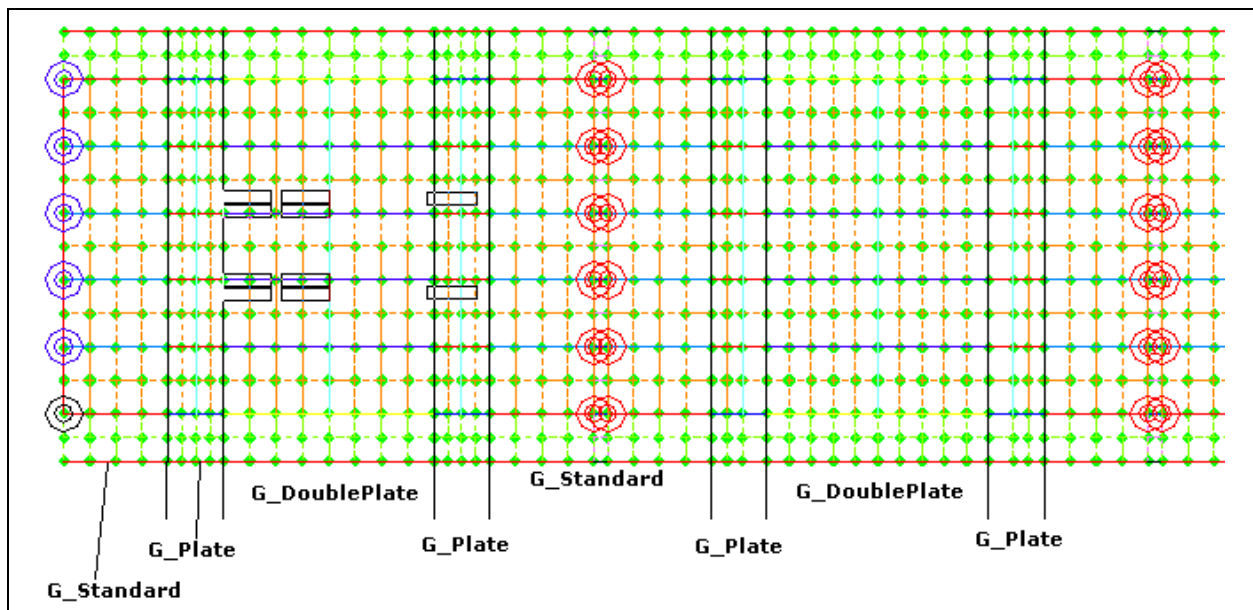
Figure 19. Finite element model of superstructure.

Once the model was developed, the load test procedures were essentially "reproduced" in the analyses. A two-dimensional (2-D) "footprint" of the load vehicle was applied to the model along the same paths that the actual test vehicle crossed the bridge. A direct comparison of strain values was made between the analytical predictions and the experimentally measured results. The initial model was then "calibrated" to the dump truck by modifying various properties and boundary conditions until the results matched those measured in the field. After the calibration was complete, the additional testing vehicles were applied to the calibrated model to confirm the accuracy of the model for other load conditions. A complete outline of this process is provided in Appendix G.

Table 8. Analysis and model details.

Analysis Type	Linear-elastic finite element - stiffness method.
Model Geometry	Planar-grid composed of shell elements, beam elements, and springs.
Nodal Locations	Nodes placed at all bearing locations and at corners of all shell elements.
Model Components	Shell elements for all deck components. Two-noded beam elements for beams, diaphragms and guardrails. Translational (horizontal) springs elements at each support.
Live-Load	2-D footprint of test truck consisting of 10 vertical point loads. The truck path was simulated by series of load cases with truck moving at 2-ft increments (70 truck positions per path).
Dead-Load	Self-weight of structure plus weight of guardrail uprights and pipe attached to the exterior of the structure.
Number of Load Case Positions Compared	70 x 3 lateral load paths = 210 load case positions compared.
Total Number of Strain Comparisons	31 strain points x 213 load positions = 6510 strain comparisons.
Model Statistics	1500 Nodes 2650 Elements 19 Cross-section/material types 210 Load cases 31 Gage locations at beam lower flanges (used for comparison)
Adjustable Parameters for Model Calibration	1. Axial springs at abutments and piers (F_x). 2. Slab Young's modulus (E). 3. Abutment and pier diaphragm torsional stiffness (J). 4. Midspan diaphragm moment of inertia (I_x) 5. Stringers moment of Inertia (I_x) 6. Link stiffness (E)

Note that the field measurements of the structure and beam cross sections did not match the provided set of plans. As a result, the beam dimensions provided in Figure 20 where used to define the cross-section properties.
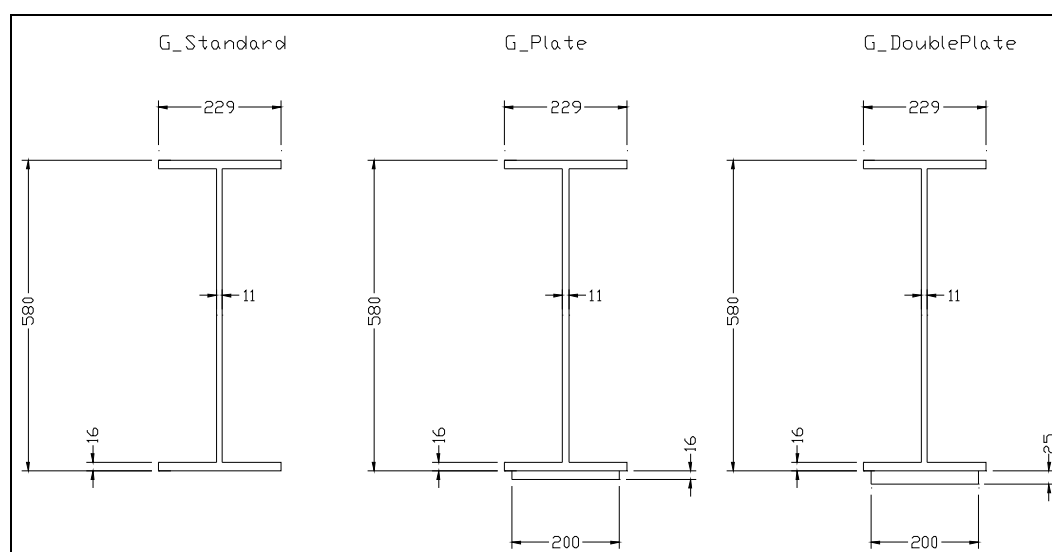
Figure 20. Beam cross-section measurements (all dimensions in millimeters).

Results

Deck stiffness

The resulting effective modulus of the reinforced concrete deck elements is generally a result of the actual concrete modulus, the density of flexural cracks in the deck, and the amount of reinforcing steel in the deck. The optimization resulted in a deck modulus slightly less than the initial estimate, indicating that the some flexural cracks are present. This result was relatively typical and is not an indication of a reduction in the concrete strength. The sidewalk slab modulus increased slightly from the initial estimate. It is not likely that the deck slab and sidewalk slab contain different grades of concrete. The resulting sidewalk modulus was likely artificially high in order to compensate for the stiffness provided by the railing, additional conduits, or dimensional errors.

Abutment and pier springs

The most realistic simulation of the existing beam bearing conditions was the use of an eccentrically placed horizontal spring. With exception to Beam 1 at the west abutment, the resulting beam bearing condition indicated that there was very little end-restraint. The west abutment beam support at Beam 1 had roughly three times the amount of resistance. This was likely just a matter of how tight the beams were bolted to the steel bearing plates. Realistic assessment of the bearing conditions was necessary to accurately evaluate the other stiffness parameters. Because of the type of bearing detail, any end-restraint should be ignored for load rating purposes.

Beam stiffness

The moment of inertia values calculated using Figure 20 dimensions were allowed to adjust ±10 percent for the interior stringers and ±15 percent for the exterior stringers. Both the interior and exterior stringer stiffness values increased. It is likely that the increased stiffness of the interior stringers occurs because the actual rolled section could not be identified from the field measurements and the stringers were in fact slightly stiffer than calculated. Variations in the deck properties can also influence the effective beam stiffness. The exterior stringer increase resulted from the contribution of the sidewalk and the guardrails. These results seemed reasonable since the sidewalk was significantly thicker than the slab, and the steel guardrails were relatively deep as well.

Following the optimization procedures, the model produced a 0.9911 correlation coefficient between the test and analysis strains. The parameter and model accuracy values used in the initial model and obtained for the final model are provided in Table 9. (See Appendix G for a description of each error value.)

Table 9. Model accuracy and parameter values.

Modeling Parameter		Initial Model Value	Final Model Value
Beam Bearing Springs (F_x) Note: All springs have eccentricity of -711.2 mm from center of deck.			
Abutment Springs (Translational –X)	(kN/mm)	0	0.0124
Pier Springs (Translational –X)	(kN/mm)	0	0.0045
B1_Abut_Spring (Translational –X)	(kN/mm)	0	0.0397
Slab Stiffness (E)			
Deck	(MPa)	21,080	20,866
Sidewalk	(MPa)	21,080	26,565
Beam Moment-of-Inertia (Ix)			
Girder Standard	(mm^4)	2584 x 106	2842 x 106
Girder Plate	(mm^4)	3648 x 106	3849 x 106
Girder Double Plate	(mm^4)	4251 x 106	4487 x 106
Exterior Girder Standard	(mm^4)	3026 x 106	3060 x 106
Exterior Girder Plate	(mm^4)	4249 x 106	4321 x 106
Exterior Girder Double Plate	(mm^4)	4951 x 106	4999 x 106
Diaphragm	(mm^4)	53.6 x 106	67.1 x 106
Error Parameters		**Initial Model Value**	**Final Model Value**
Absolute Error		19711.9	7637.5
Percent Error		13.5	1.8
Scale Error		4.7	1.0
Correlation Coefficient		0.9704	0.9911

In addition to the loaded dump truck, data comparisons were made with data from the empty HET, the HET/M1A1 combination, and the M1A1 tank. Comparison results from each vehicle are listed in Table 10. Overall, the correlation coefficients were 0.96 or greater, and it can be concluded that the final calibrated model was sufficient for predicting the stresses caused by heavier loads.

Table 10. Military vehicle accuracy and parameter values.

Error Parameters	Empty HET	HET with M1A1 Tank	M1A1 Tank
Absolute Error	11595.6	7831.6	5487
Percent Error	10.9	8.8	9.7
Scale Error	13.3	12.3	4.9
Correlation Coefficient	0.9727	0.9793	0.9588

5   Load Rating Procedures and Results

Procedures

The goal of producing an accurate model is to predict the structure's actual live-load behavior when subjected to design or rating loads. This approach is essentially identical to standard load rating procedures (AASHTO 2003), except that a "field-verified" model is used to determine shears and moments due to a given loading instead of a typical beam analysis combined with load distribution factors. (See Appendix H for a detailed outline of the load rating procedures.)

Once the finite element model has been calibrated to field conditions, a reality check must be performed to eliminate any secondary stiffening effects that may change over time or that may be unreliable with heavy loads. In the case of this bridge, the abutment springs, pier springs, and links between spans were set to zero for rating purposes. While these forces appear in the structure, it cannot be said with any certainty that they will remain in their current state for the lifespan of the structure. Removing these parameters from the rating model will provide slightly conservative results compared to the actual structure, but this will ensure that the load capacities are not overpredicted.

Shear and moment capacities were calculated using AASHTO (2004) and AASHTO (2003). For this structure, a condition factor of "fair" was selected based on the National Bridge Inventory rating of 6 reported in the 2005 Bridge Inspection Report provided by USACE. For a list of the load and resistance factors, refer to Tables H1 and H2.

The beam moment capacities were based on composite action between the steel beams and the concrete deck. This assessment was based on shear connector details shown in the renovation plans (29 May 1984) and also from the load test data. It was assumed that the composite action was available for live-load only. Therefore, the structure's dead-load was applied to a noncomposite model, and stresses were computed at all extreme fibers. The composite moment capacities were calculated by subtracting the noncomposite dead-load stresses from the yield stress and multiplying the difference by the composite section modulus of each section [(yield stress – dead-load stress) * S_{XC}]. The composite moment

capacities were used in the load rating calculations to resist all live-load and superimposed dead-loads. In this case, there was no wearing surface on the bridge, and all dead-loads were applied to the noncomposite model. Technically, the sidewalk, guard rail, and conduit loads should have been applied as superimposed loads on the composite model; therefore, the load rating calculations are slightly conservative. Since the shear capacities were dependent only on the steel web properties and not the composite action of the deck and beams, the shear capacities were not separated into noncomposite and composite values. The calculated positive moment capacity and shear capacity based on each unique stringer section are given in Table 11 and Table 12. A construction date for the original structure was unknown; the structure was renovated in 1984. A yield stress of 248 MPa (36 ksi) was used for all member capacities based on the current (2007) USACE load rating calculations.

Load ratings were computed for several AASHTO and military vehicles. The configuration and layout of all the vehicles used in the load rating is provided in Appendix H. The applied load paths for each of the loading vehicles are given in Table 13. For the standard-width vehicles, two-lane loading could be applied, resulting in a multi-lane presence factor of 1.00. As per AASHTO LRFD specifications, the single-lane load conditions were multiplied by a factor of 1.2. For all military vehicles except the PLS (palletized load system), only single-lane loading could be achieved. An impact factor of 33 percent was applied to all live-load responses.

All live-load configurations and superimposed dead-loads were applied to the composite rating model. One and two-lane loadings were considered for all standard width vehicles. Only single-lane loading could be considered for the wide military vehicles (axle widths greater than 3 m (10 ft)). For all single lane load configurations, the multi-presence load factor of 1.2 was applied as per AASHTO LRFD specifications. The applied load paths for each of the loading vehicles can be seen in Table 13.

Table 11. LRFD positive moment loading, section properties, and capacity for noncomposite and composite sections.

	Noncomposite Section					Composite Section				

Beam Section	$M_{DL\ Factored}$ kN-m	Ync mm	Ix_{nc} mm^4	Sx_{btm}-nc mm^3	σ_{DLbtm} mPa	Yc mm	Ix_c mm^4	$Sx_{btm}\ c$ mm^3	$\sigma_{Capacity}$ mPa	M_{LL} Capacity kN-m
G_Standard	106.50	303.8	8.626E+08	2.839E+06	37.5	585.978	2.842E+09	4.850E+06	210.7	1021.9
G_Plate	143.07	262.4	1.118E+09	4.262E+06	33.6	563.626	3.849E+09	6.830E+06	214.6	1465.9
G_DoublePlate	172.58	245.1	1.243E+09	5.070E+06	34.0	552.196	4.487E+09	8.126E+06	214.2	1740.3
EX_G_Standard	125.65	303.8	8.626E+08	2.839E+06	44.3	625.348	3.060E+09	4.893E+06	204.0	997.9
EX_G_Plate	168.35	262.4	1.118E+09	4.262E+06	39.5	607.06	4.320E+09	7.117E+06	208.7	1485.4
EX_G_DoublePlate	200.83	245.1	1.243E+09	5.070E+06	39.6	597.154	4.999E+09	8.371E+06	208.6	1746.2

Where:
- M_{DL} = maximum dead-load moment from a finite element analysis multiplied by a dead-load factor of 1.25 (AASHTO 3.4.1)
- Ync, Yc = locations of the neutral axes for the noncomposite and composite sections
- Sx-nc, Sx-c = section modulus values for the noncomposite and composite sections
- σ_{DL} = maximum tensile stress at the bottom flange due to dead-load
- σ_{cap} = live-load tensile stress capacity of the bottom flange of the composite section
- $M_{LL}\ cap$ = yield-based live-load capacity of the composite section

Table 12. LRFD beam shear capacity.
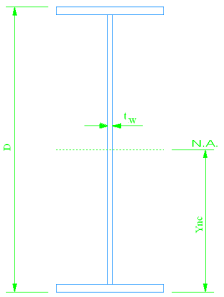
Beam Section	D mm	t_w mm	V_p kN	D/tw	C	V_n kN
G_Standard	573.024	11.176	921.9	51.3	1	921.9
G_Plate	573.024	11.176	921.9	51.3	1	921.9
G_DoublePlate	573.024	11.176	921.9	51.3	1	921.9
EX_G_Standard	573.024	11.176	921.9	51.3	1	921.9
EX_G_Plate	573.024	11.176	921.9	51.3	1	921.9
EX_G_DoublePlate	573.024	11.176	921.9	51.3	1	921.9

Where:

Vp = plastic shear force = $0.58 * F_y D t_w$ AASHTO 6.10.9.2

C = ratio of shear bucking resistance to shear yield strength and is a function of D/t_w (AASHTO 6.19.9.3)

Vn = nominal shear capacity

Table 13. Load path locations.

Rating Vehicle	Paths	Location
HS-20, HS-26, HS-30, Type 3, Type 3-3, Type 3S2, PLS	1	0.6 m (2 ft) from edge of north curb
	2	0.6 m (2 ft) from edge of south curb
	3	Driver side wheel on center line
	4	Passenger side wheel on center line
	5	Combines Paths 1 and 3
	6	Combines Paths 2 and 4
HETS, M1, MCL60, MLC70	1	0.6 m (2 ft) from edge of north curb
	2	0.6 m (2 ft) from edge of south curb
	3	Center line of roadway

Results

Table 14 contains the load and resistance factors used in the load rating calculations. An example computation of an inventory and operating load rating factor is provided for Section G_Standard:

Table 14. Rating factor calculation for HS-20 (G_Standard).

Moment capacity available for superimposed dead-load and live-load at Section G_Standard	M_{Cap}	1021.9	kN-m
Superimposed dead-load applied to composite model—wearing surface and railing	DW	0.0	kN-m
Live-load effect (HS-20)	LL	164.42	kN-m
Resistance factor for steel in flexure	Φ_b	1.00	
Condition factor (good)	φ_c	1.00	
System factor (multiple girders)	φ_s	1.00	
LRFD load factor for structural components and attachments	γ_{DC}	1.25	
Live-load factor	γ_{LL}	1.75 1.35	Inventory Operating
Dynamic influence (impact) factor	IM	1.33	
Using Equation H1: RF_{Inv} = [(1.0)(1.0)(1021.9) – (1.25*0.00)] / (1.75*164.42*1.33) = **2.67** RF_{Opr} = [(1.0)(1.0)(1021.9) – (1.25*0.00)] / (1.35*164.42*1.33) = **3.47**			

Table 15 presents the maximum superimposed dead-load and maximum live-load for each section along with the calculated load rating factors. The lowest load rating factor is the controlling factor for the bridge and is used to determine the maximum weight for a particular load configuration. All load ratings were controlled by moment at the standard beam sections (no cover plate).

Table 15. Maximum live-load moments and vehicle load rating factors.

| Location | Responses [kN-m] | | Inventory | Operating |
	Dead-load	Live- load	RF	RF
HS-20				
G_Standard	0.00	164.42	2.67	3.47
G_Plate	0.00	211.49	2.98	3.87
G_DoublePlate	0.00	240.63	3.11	4.04
Ext_G_Standard	0.00	126.20	3.40	4.42
Ext_G_Plate	0.00	172.59	3.70	4.81
Ext_G_DoublePlate	0.00	201.12	3.73	4.85
HS-26				
G_Standard	0.00	213.75	2.05	2.67
G_Plate	0.00	274.94	2.29	2.98
G_DoublePlate	0.00	312.82	2.39	3.11
Ext_G_Standard	0.00	164.06	2.62	3.40
Ext_G_Plate	0.00	224.37	2.85	3.70
Ext_G_DoublePlate	0.00	261.46	2.87	3.73
HS-30				
G_Standard	0.00	246.63	1.78	2.31
G_Plate	0.00	317.24	1.99	2.58
G_DoublePlate	0.00	360.95	2.07	2.69
Ext_G_Standard	0.00	189.30	2.27	2.95
Ext_G_Plate	0.00	258.89	2.47	3.21
Ext_G_DoublePlate	0.00	301.68	2.49	3.23
Type 3				
G_Standard	0.00	129.36	3.39	4.41
G_Plate	0.00	167.55	3.76	4.89
G_DoublePlate	0.00	189.64	3.94	5.12
Ext_G_Standard	0.00	97.72	4.39	5.71
Ext_G_Plate	0.00	134.06	4.76	6.19
Ext_G_DoublePlate	0.00	157.17	4.77	6.20
Type 3-3				
G_Standard	0.00	107.48	4.08	5.30
G_Plate	0.00	138.19	4.56	5.93
G_DoublePlate	0.00	155.48	4.81	6.25
Ext_G_Standard	0.00	81.01	5.29	6.88
Ext_G_Plate	0.00	111.56	5.72	7.44
Ext_G_DoublePlate	0.00	128.33	5.85	7.61
Type 3S2				
G_Standard	0.00	116.68	3.76	4.89
G_Plate	0.00	152.12	4.14	5.38
G_DoublePlate	0.00	177.02	4.22	5.49
Ext_G_Standard	0.00	87.00	4.93	6.41
Ext_G_Plate	0.00	121.11	5.27	6.85
Ext_G_DoublePlate	0.00	146.81	5.11	6.64

Location	Responses [kN-m]		Inventory	Operating
	Dead-load	Live- load	RF	RF
PLS				
G_Standard	0.00	196.63	2.23	2.90
G_Plate	0.00	263.60	2.39	3.11
G_DoublePlate	0.00	309.06	2.42	3.15
Ext_G_Standard	0.00	160.72	2.67	3.47
Ext_G_Plate	0.00	225.21	2.83	3.68
Ext_G_DoublePlate	0.00	274.58	2.73	3.55
Empty HET				
G_Standard	0.00	80.57	5.45	7.09
G_Plate	0.00	107.09	5.88	7.64
G_DoublePlate	0.00	121.21	6.17	8.02
Ext_G_Standard	0.00	51.17	8.38	10.89
Ext_G_Plate	0.00	73.03	8.74	11.36
Ext_G_DoublePlate	0.00	90.04	8.33	10.83
M1A1 Tank				
G_Standard	0.00	223.91	1.96	2.55
G_Plate	0.00	308.11	2.04	2.65
G_DoublePlate	0.00	377.19	1.98	2.57
Ext_G_Standard	0.00	246.44	1.74	2.26
Ext_G_Plate	0.00	346.25	1.84	2.39
Ext_G_DoublePlate	0.00	424.93	1.77	2.30
HET with M1A1 Tank				
G_Standard	0.00	204.01	2.15	2.80
G_Plate	0.00	278.08	2.27	2.95
G_DoublePlate	0.00	331.75	2.25	2.93
Ext_G_Standard	0.00	145.52	2.95	3.84
Ext_G_Plate	0.00	210.20	3.04	3.95
Ext_G_DoublePlate	0.00	265.17	2.83	3.68
Korean HET				
G_Standard	0.00	179.12	2.45	3.19
G_Plate	0.00	239.18	2.63	3.42
G_DoublePlate	0.00	291.87	2.56	3.33
Ext_G_Standard	0.00	149.70	2.86	3.72
Ext_G_Plate	0.00	214.01	2.98	3.87
Ext_G_DoublePlate	0.00	266.73	2.81	3.65
MLC 60 (Tracked)				
G_Standard	0.00	216.72	2.03	2.64
G_Plate	0.00	291.85	2.16	2.81
G_DoublePlate	0.00	352.35	2.12	2.76
Ext_G_Standard	0.00	199.59	2.15	2.80
Ext_G_Plate	0.00	284.48	2.24	2.91
Ext_G_DoublePlate	0.00	353.94	2.12	2.76

Location	Responses [kN-m]		Inventory	Operating
	Dead-load	Live- load	RF	RF
MLC 60 (Wheeled)				
G_Standard	0.00	177.20	2.48	3.22
G_Plate	0.00	231.47	2.72	3.54
G_DoublePlate	0.00	259.75	2.88	3.74
Ext_G_Standard	0.00	168.32	2.55	3.32
Ext_G_Plate	0.00	229.23	2.78	3.61
Ext_G_DoublePlate	0.00	263.83	2.84	3.69
MLC 70 (Tracked)				
G_Standard	0.00	242.17	1.81	2.35
G_Plate	0.00	328.69	1.92	2.50
G_DoublePlate	0.00	400.18	1.87	2.43
Ext_G_Standard	0.00	236.48	1.81	2.35
Ext_G_Plate	0.00	335.15	1.90	2.47
Ext_G_DoublePlate	0.00	415.51	1.81	2.35
MLC 70 (Wheeled)				
G_Standard	0.00	199.95	2.20	2.86
G_Plate	0.00	262.71	2.40	3.12
G_DoublePlate	0.00	301.03	2.48	3.22
Ext_G_Standard	0.00	199.70	2.15	2.80
Ext_G_Plate	0.00	271.58	2.35	3.06
Ext_G_DoublePlate	0.00	315.58	2.38	3.09

6   Conclusions and Recommendations

Several useful results were obtained directly from the load test data. It was observed that the bridge responded in a linear-elastic manner for all load configurations. The structure's response behavior was symmetric, and there was no sign of distress in any of the measurements.

Direct comparisons of the responses were made for the different applied load configurations. In particular, the measurements from the M1A1 tank crossing and the HETS hauling an M1A1 tank were examined. It was observed that, for all gage locations, the tank by itself generated the greatest flexural stresses. The greatest midspan stress obtained from the tank was approximately 20 percent greater than the HETS/M1A1 combination.

Various high-speed and braking type load tests were performed to evaluate the range of increased stress that could be expected with the military load configurations. The largest dynamic effect was measured from the M1A1 tank crossing at slow speed. Apparently, the tank vibrations were close to the natural frequency of the bridge superstructure. Some variations in stress magnitudes (in the range of 10 percent) were detected and were likely the result of impact. Brake tests with the M1A1 tank indicated a potential increase in flexural stress of approximately 10 percent. No significant stress increase was noted with the other load configurations. This indicates the 33 percent impact factor specified by AASHTO would be conservative for all load conditions.

Model calibration and subsequent load rating results verified that the bridge responses were linear-elastic. Rating results also indicated that the use of the HETS to transport an M1 tank is preferable to direct loading with the tank. However, all applied load configurations could cross Bridge S-1090 within inventory load limits (inventory rating factors all greater than 1.0).

At the time of this test, all structural components were visually rated as fair to good. Load rating results presented here are only valid with the bridge in its current condition. Any excessive deterioration or damage to the bridge components would alter the bridge's load rating. No attempt was made during this project to evaluate any substructure components.

References

American Association of State Highway and Transportation Officials. 2004. *AASHTO LRFD bridge design specifications*. 3d ed. (includes 2005 and 2006 Interims). Washington, DC.

_____. 2003. *Manual for the condition evaluation and load and resistance factor rating (LRFR) of highway bridges*. Washington, DC.

Commander, B. 1989. An improved method of bridge evaluation: Comparison of field test results with computer analysis. MS thesis, Univ. of Colorado, Boulder.

Gerstle, K. H., and M. H. Ackroyd. 1990. Behavior and design of flexibly-connected building frames. *Engineering Journal, AISC* 27(1):22-29.

Goble, G., J. Schulz, and B. Commander. 1992. *Load prediction and structural response*. Final Report, FHWA DTFH61-88-C-00053. Boulder, CO: University of Colorado.

Lichtenstein, A. G. 1995. *Bridge rating through nondestructive load testing*. Technical Report NCHRP Project 12-28(13)A. National Cooperative Highway Research Program.

Schulz, J. L. 1989. Development of a digital strain measurement system for highway bridge testing. MS thesis, Univ. of Colorado, Boulder.

_____. 1993. In search of better load ratings. *Civil Engineering*, ASCE 63(9):62-65.

Appendix A: Measured and Computed Stress Comparisons

While statistical terms provide a means of evaluating the relative accuracy of various modeling procedures or help determine the improvement of a model during a calibration process, the best conceptual measure of a model's accuracy is by visual examination of the response histories. The graphs presented as Figures A1–A31 show the measured and computed stress histories from each truck path. In each graph, the continuous lines represent the measured stress at the specified gage location as a function of dump truck position as it traveled across the bridge. In all cases, the measured stress is the product of the measured strain and the modulus of steel (200,000 MPa). Computed stresses are shown as markers at discrete truck intervals in the same color as the test stress curve.

The following data comparisons indicate that an accurate model was established—certainly within the applicable load factors used for load rating. In general, the analytical results overpredicted the measurements but, on occasion, did underpredict the measurements. A certain amount of error can be expected, even under the best of conditions. Factors that typically result in differences between measured and calculated responses include the following:

* Variations between the actual truck paths and the modeled path will always exist.
* The real structure will always exhibit secondary response behavior that cannot be simulated by a two-dimensional grid model. For example, localized behavior due to the vertical pressure of the wheel loads can have a substantial effect on the measurements. An extremely refined three-dimensional model of the beams would be required to simulate this type of response.

End-restraints provided by beam bearings that are intended to be simple supports are often highly variable and nonlinear. These end-restraints are simulated as accurately as possible with linear springs but are generally removed from the model prior to load rating.
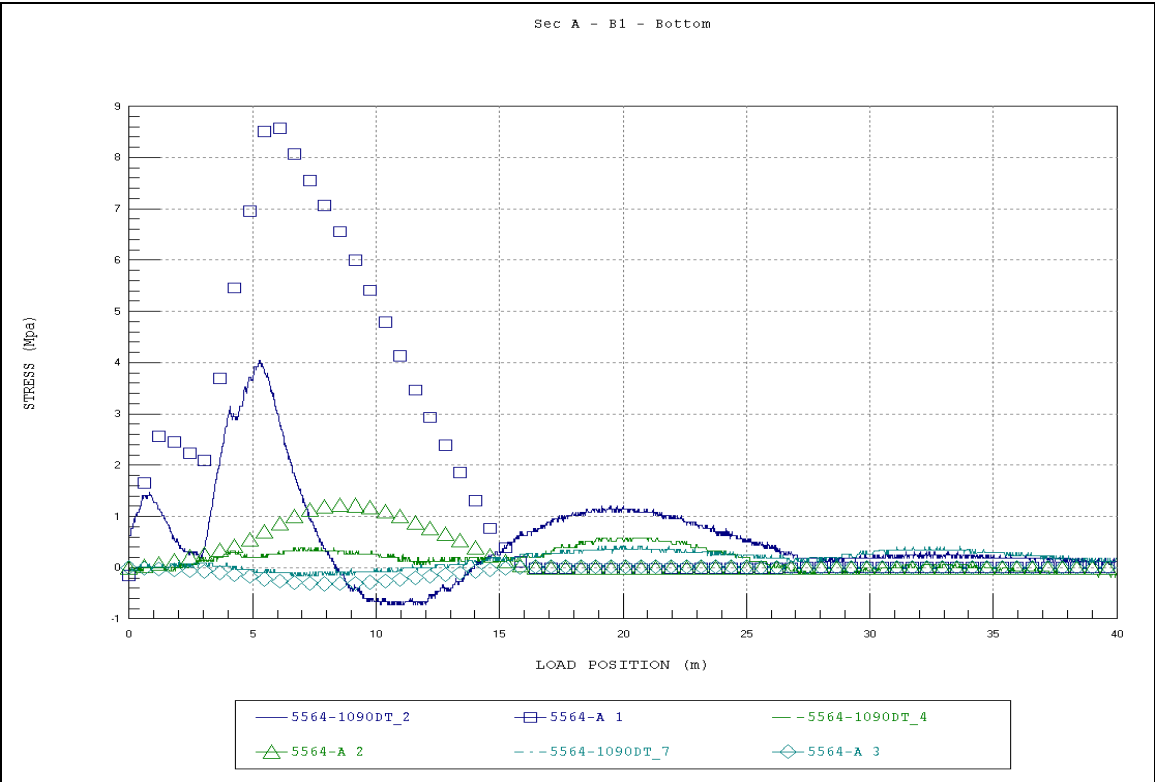
Figure A1. Section A – B1 – bottom.

Figure A2. Section A – B3 – bottom.

Figure A3. Section A – B4 – bottom.

Figure A4. Section A – B5 – bottom.

Figure A5. Section A – B6 – bottom.

Figure A6. Section B – B1 – bottom.

Figure A7. Section B – B2 – bottom.

Figure A8. Section B – B3 – bottom.

Figure A9. Section B – B4 – bottom.

Figure A10. Section B – B5 – bottom.

Figure A11. Section B – B6 – bottom.
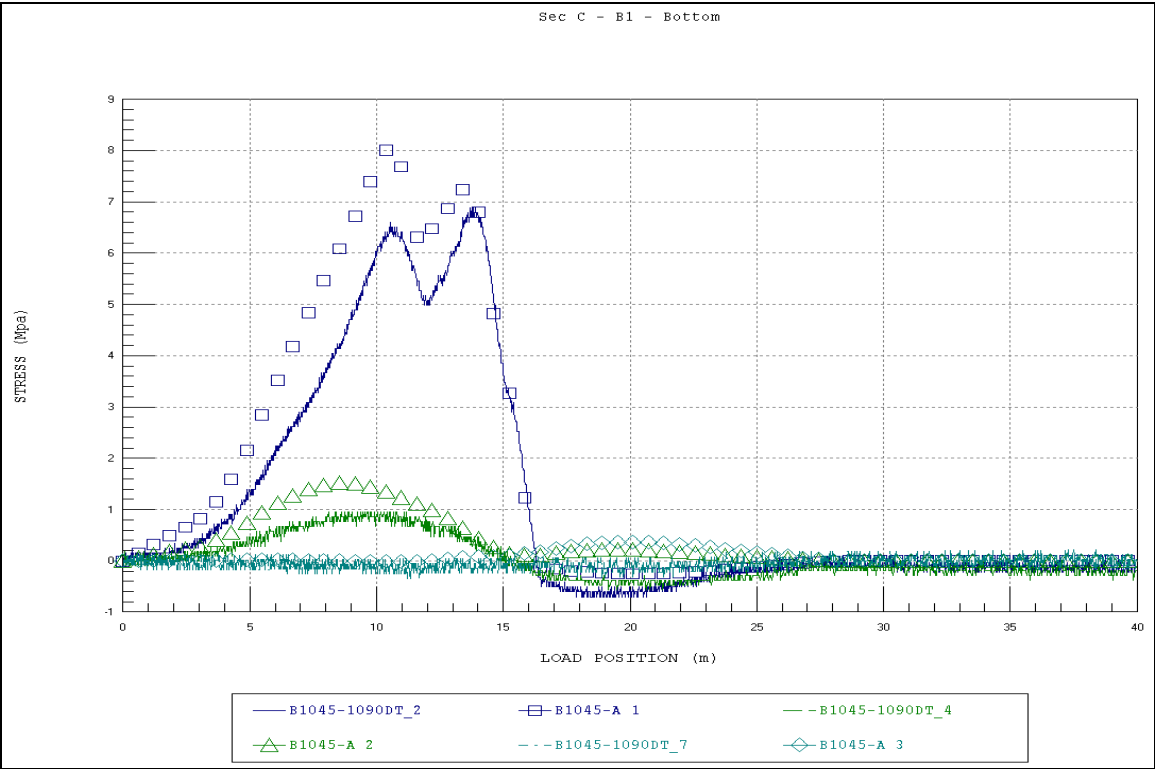
Figure A12. Section C – B1 – bottom.
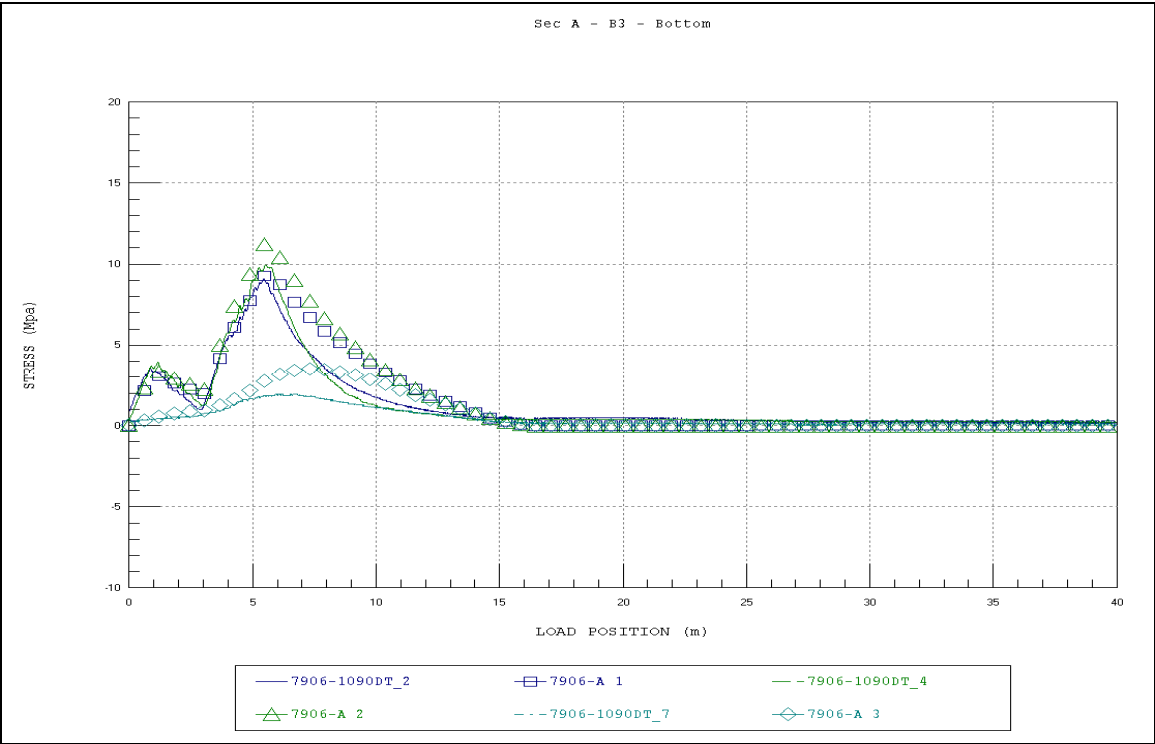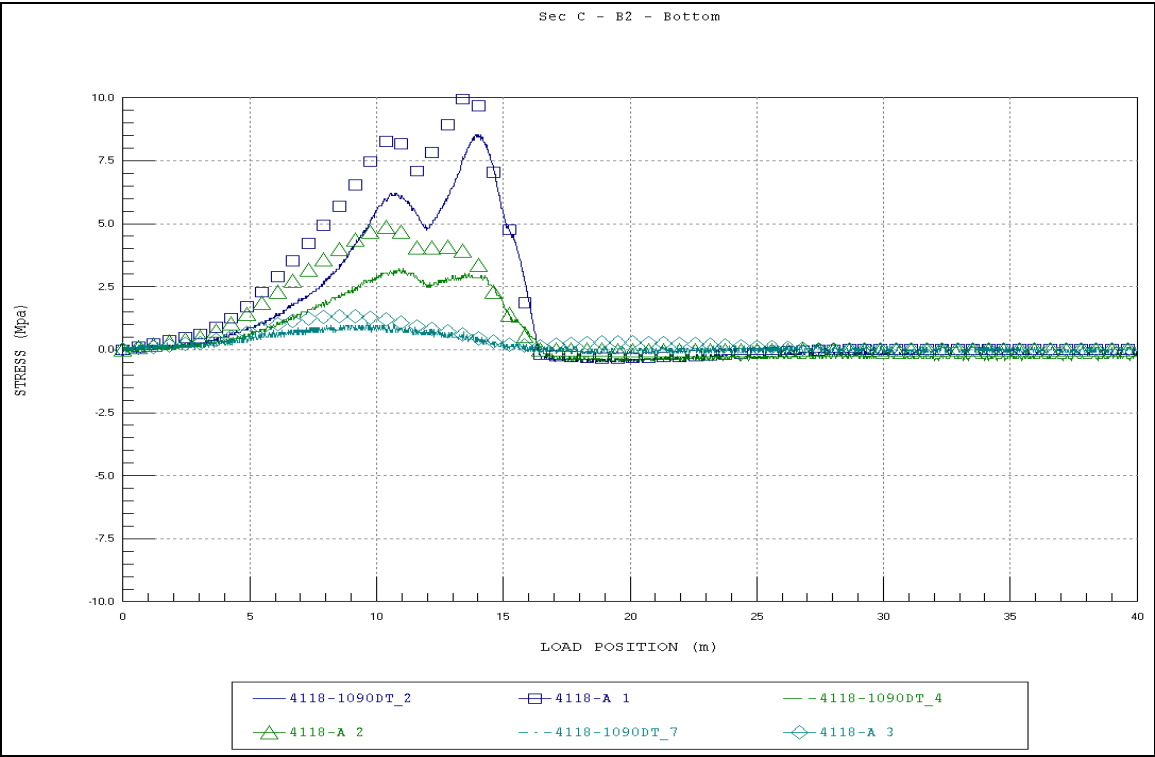
Figure A13. Section C – B2 – bottom.
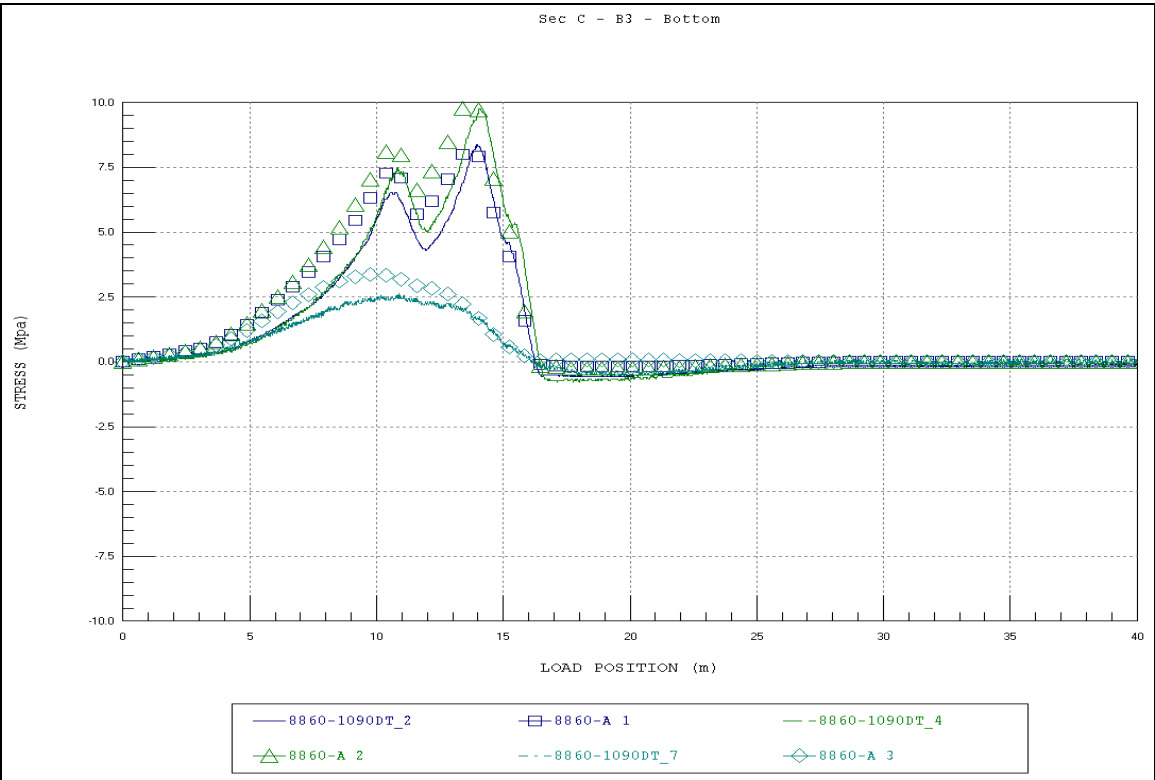
Figure A14. Section C – B3 – bottom.
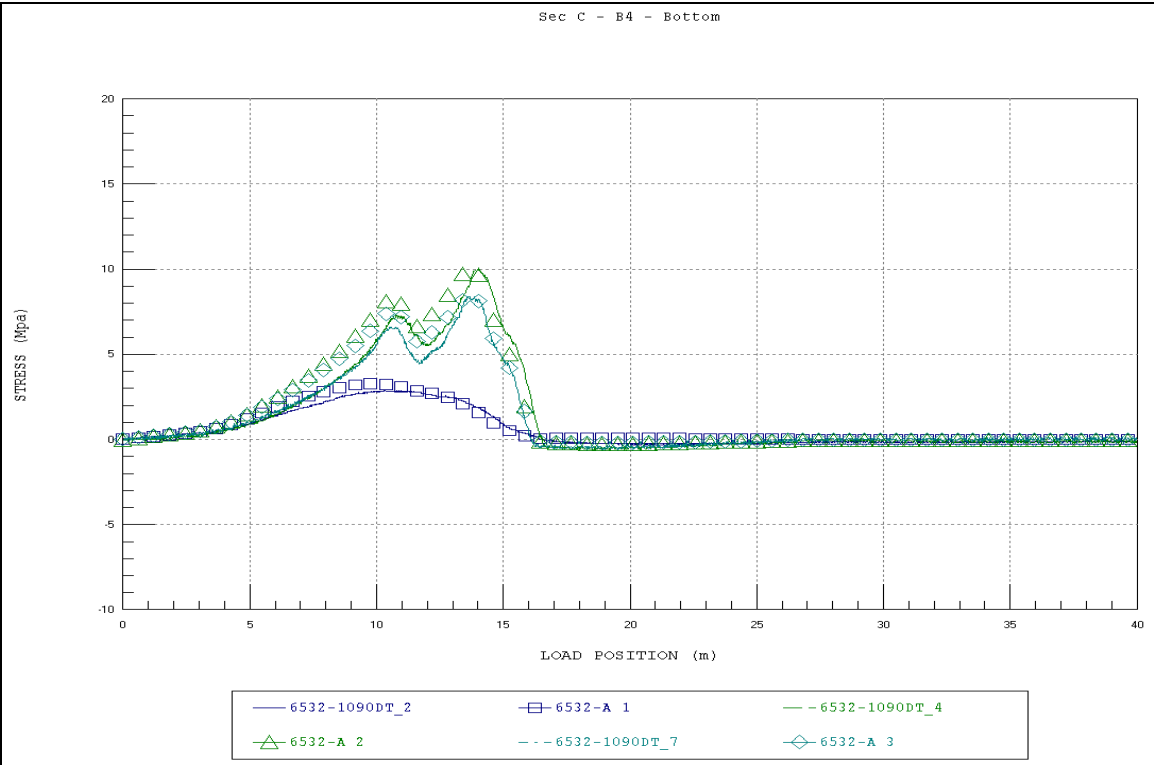
Figure A15. Section C – B4 – bottom.
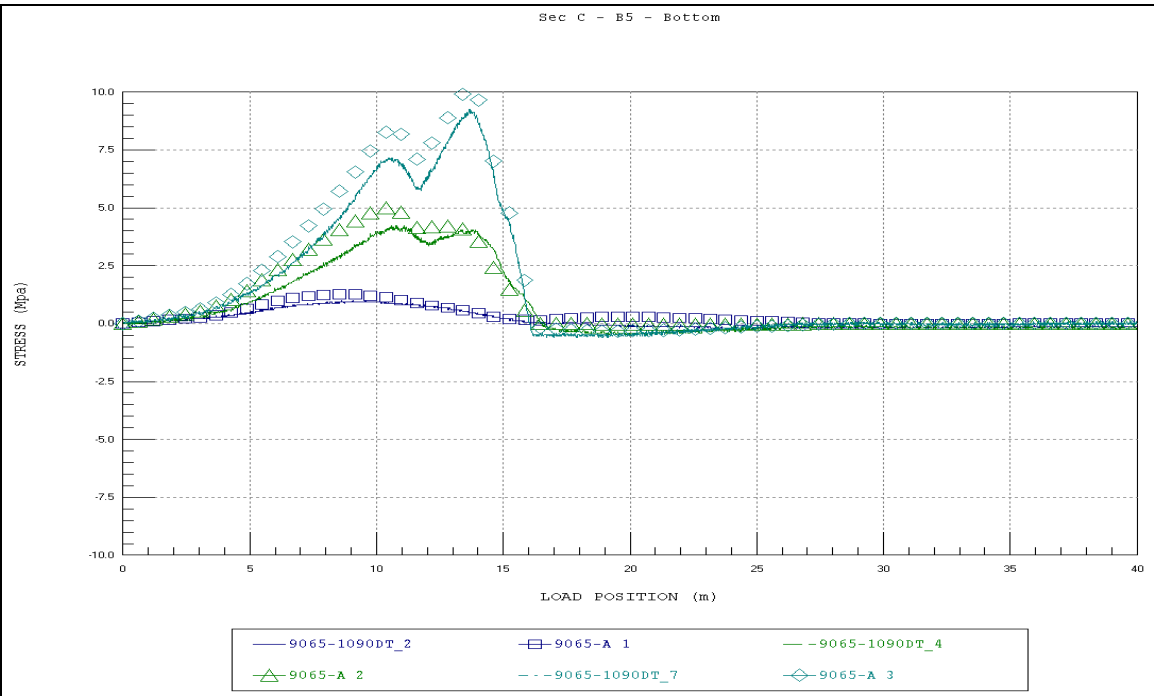
Figure A16. Section C – B5 – bottom.
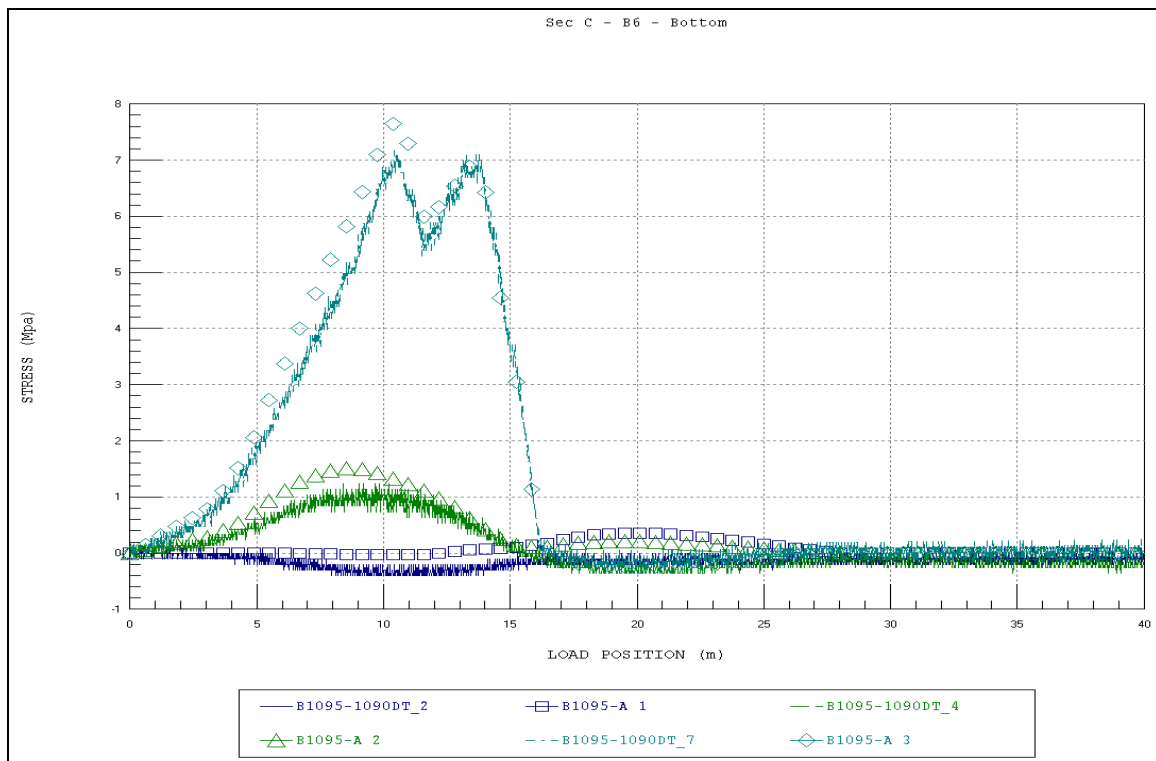
Figure A17. Section C – B6 – bottom.
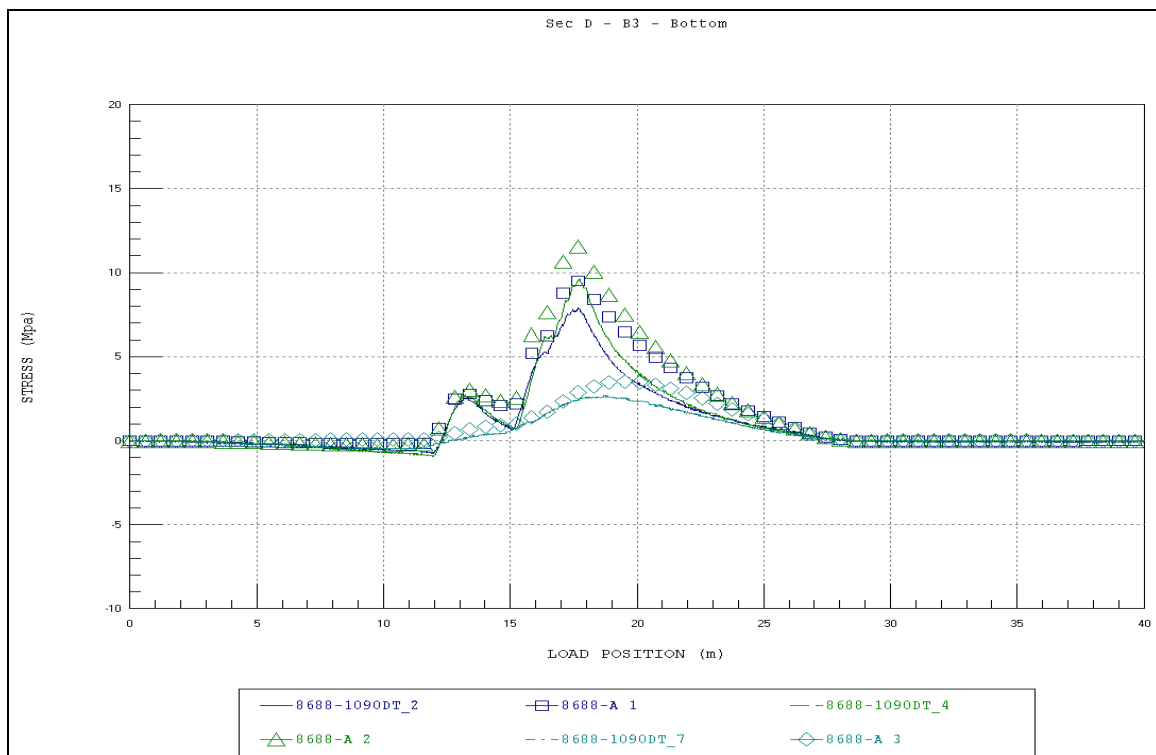
Figure A18. Section D – B3 – bottom.
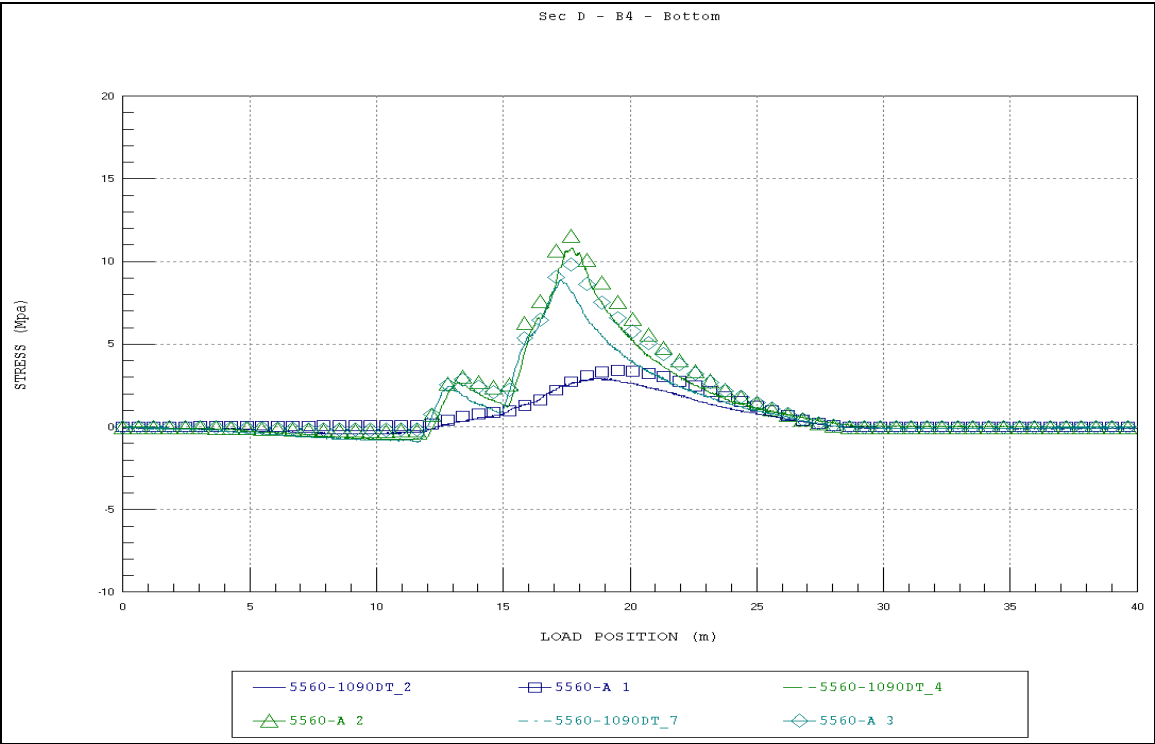
Figure A19. Section D – B4 – bottom.
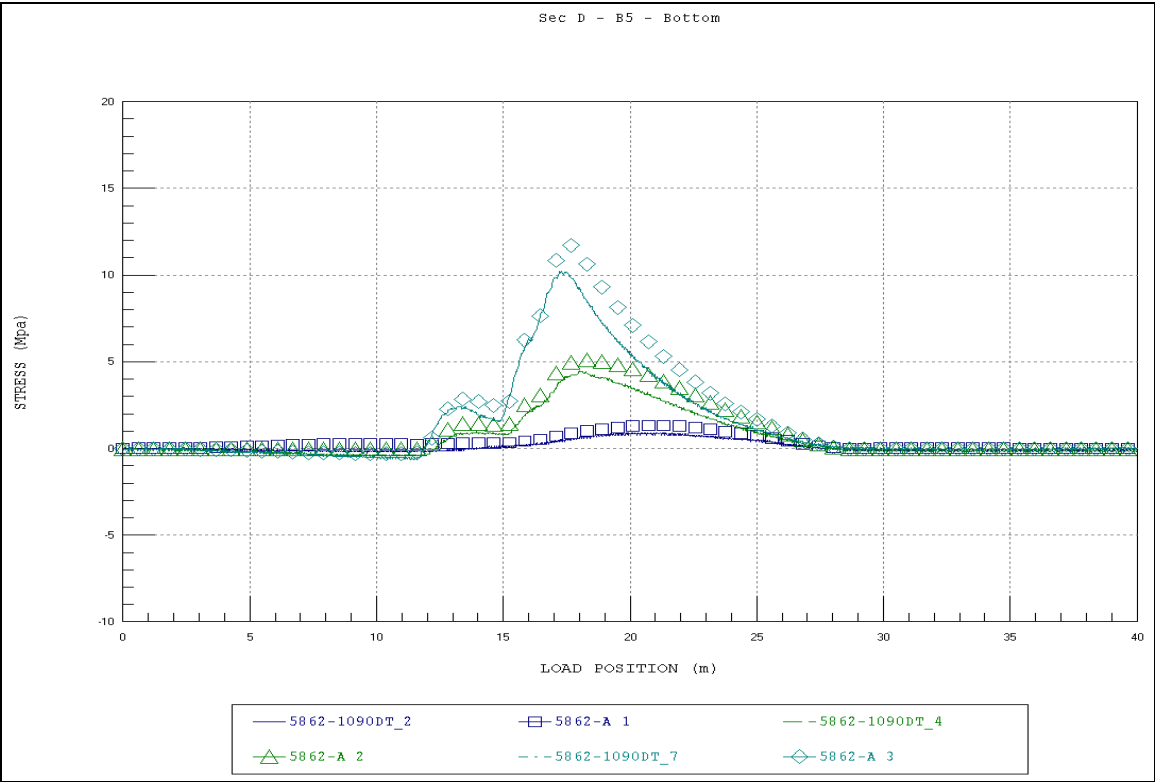
Figure A20. Section D – B5 – bottom.
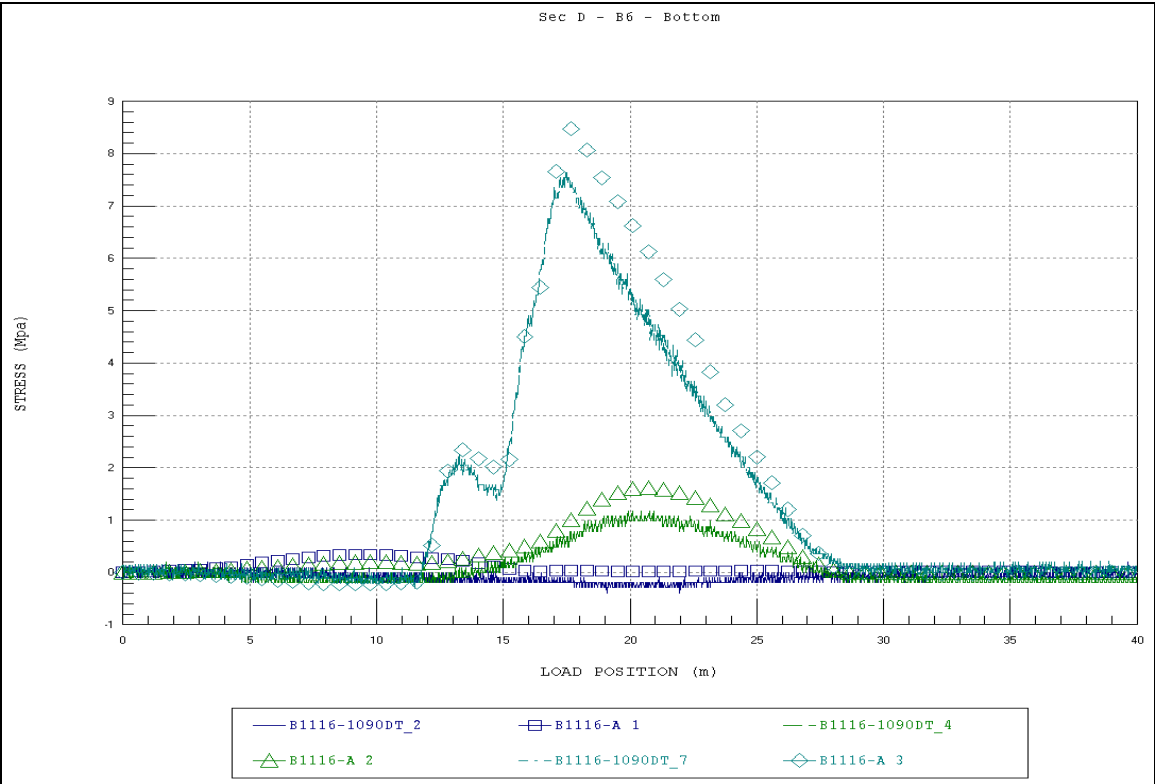
Figure A21. Section D – B6 – bottom.
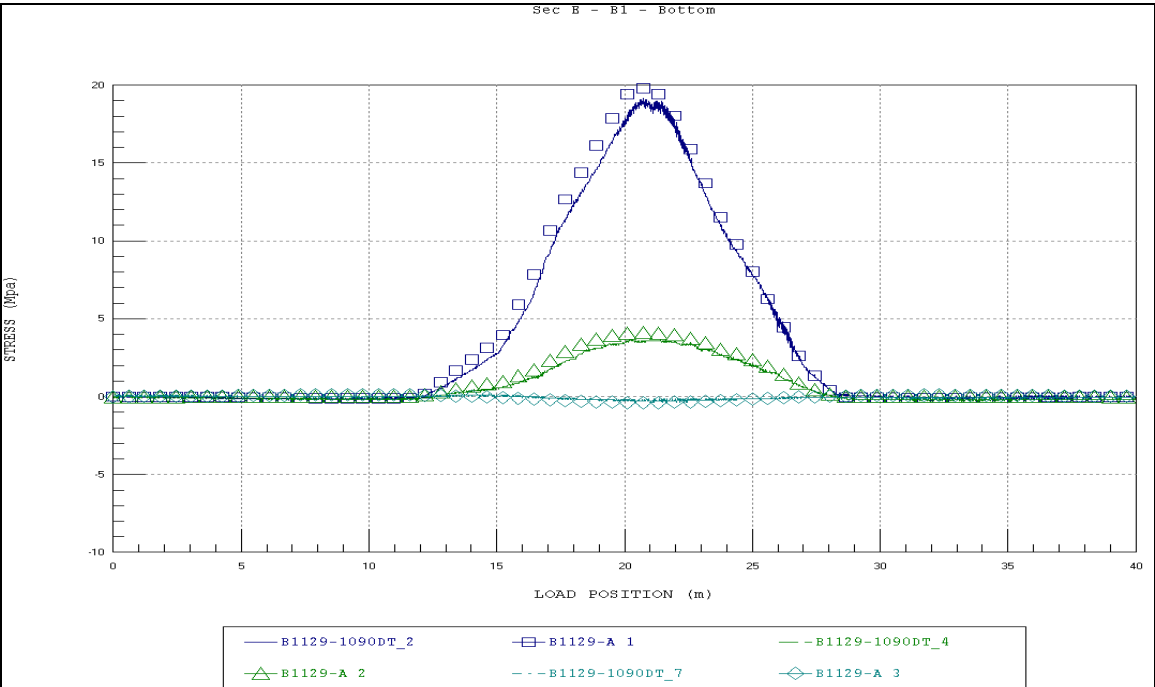
Figure A22. Section E – B1 – bottom.
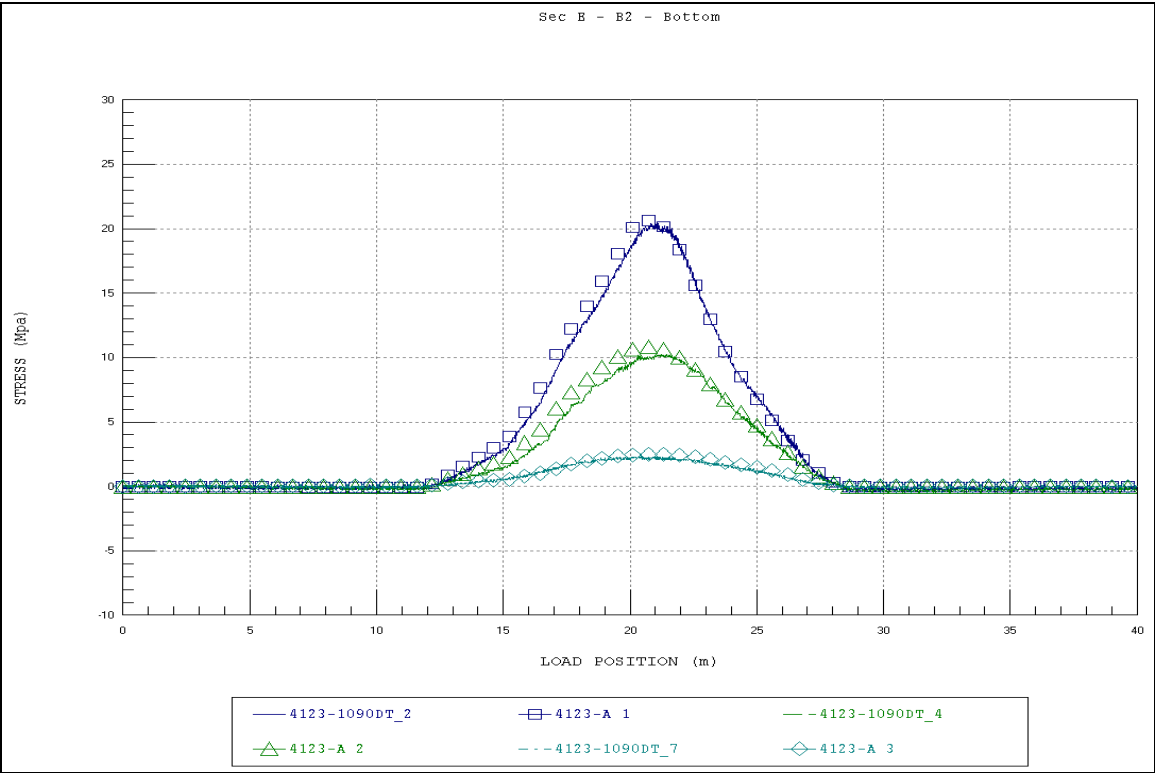
Figure A23. Section E – B2 – bottom.
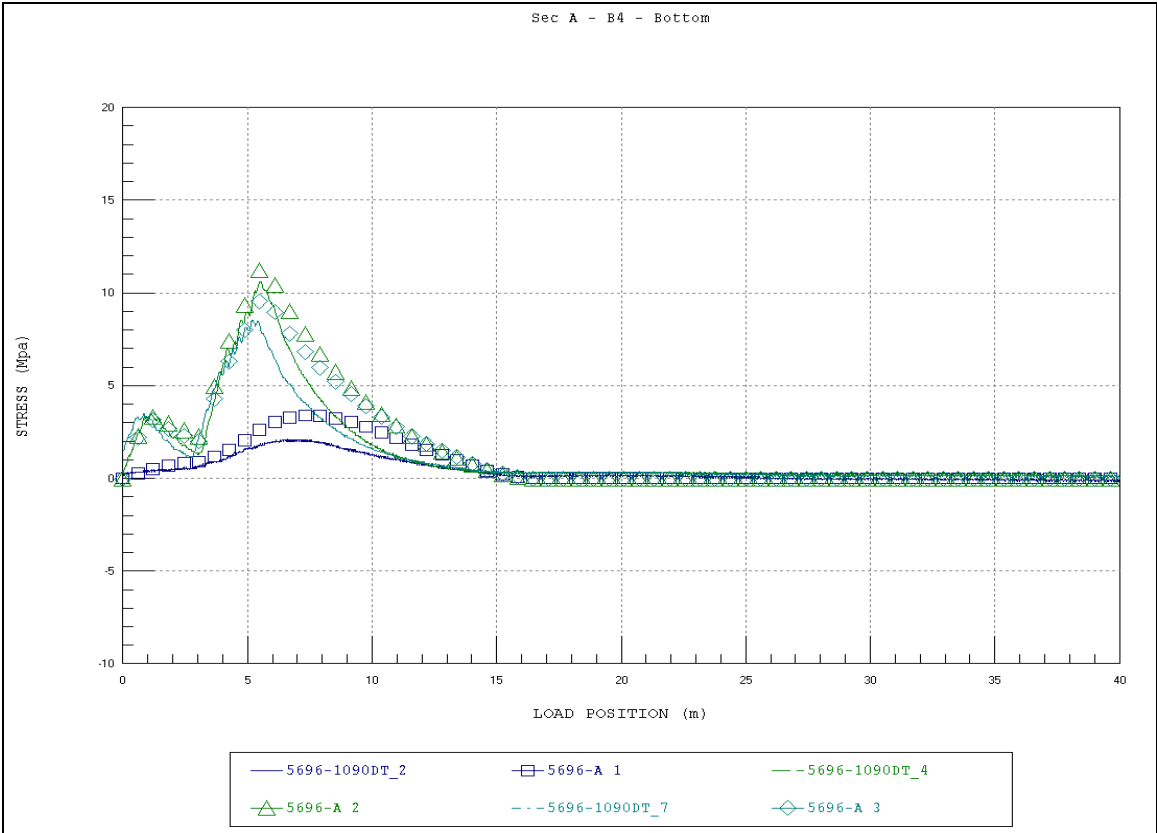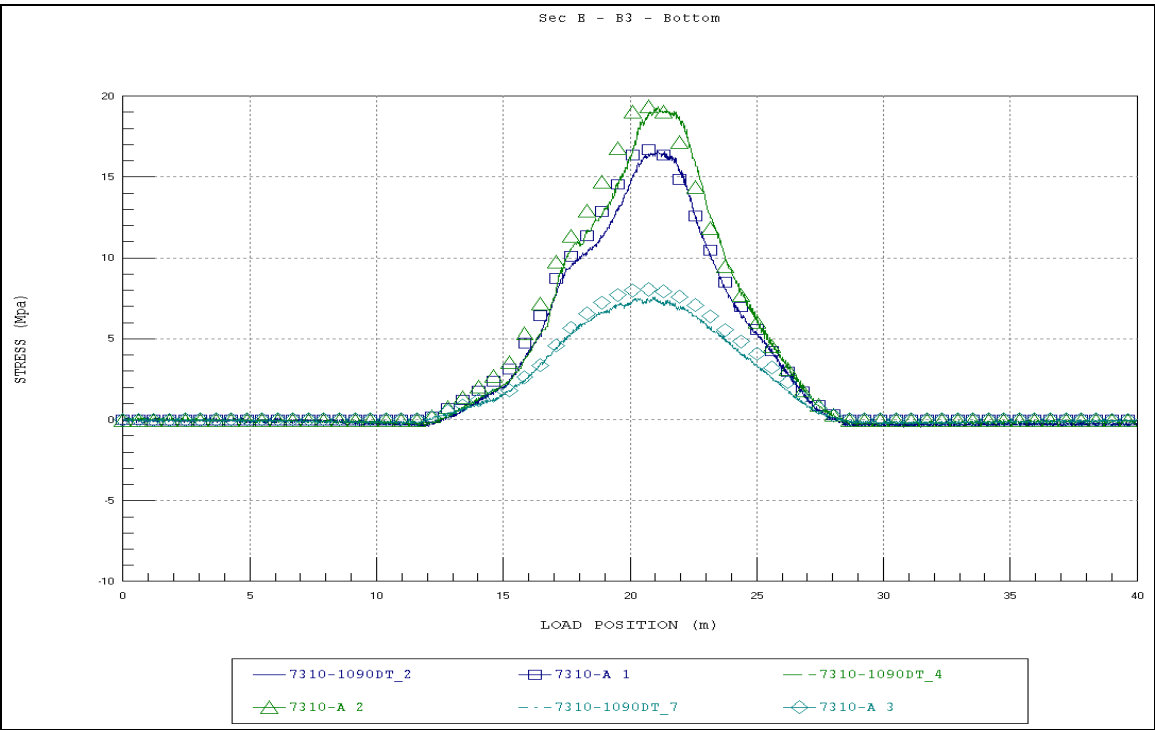

Figure A24. Section E – B3 – bottom.
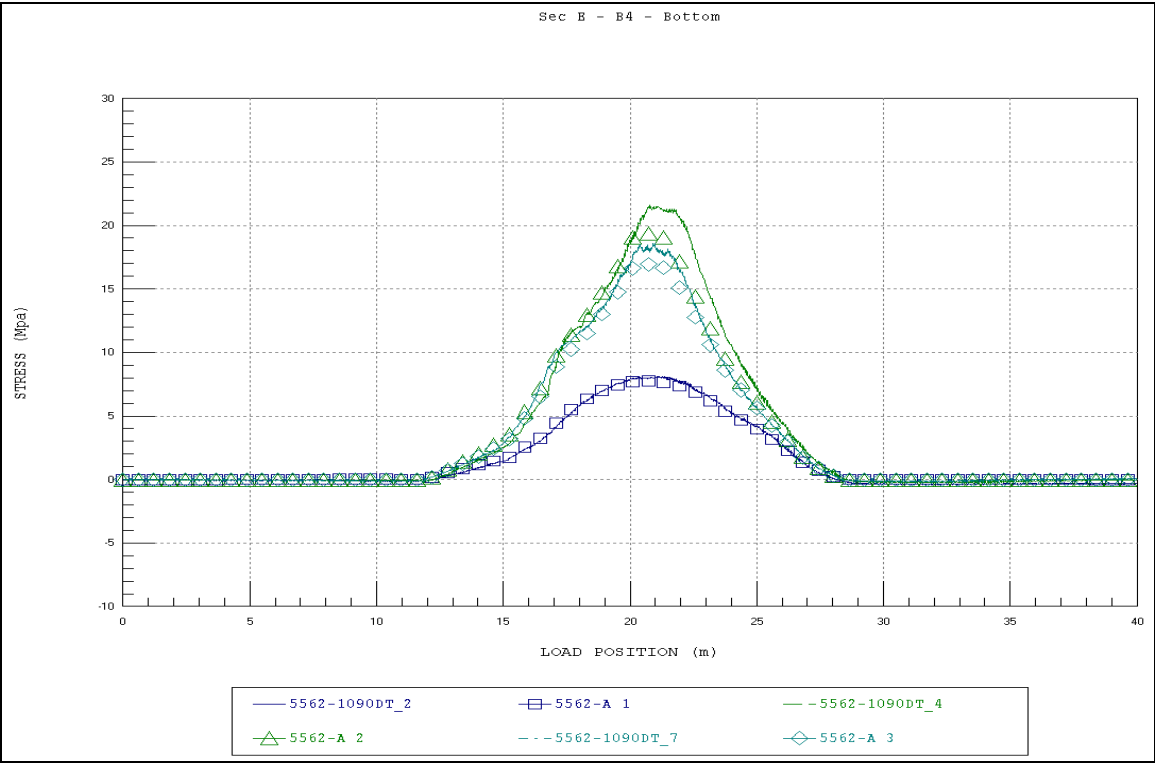
Figure A25. Section E – B4 – bottom.
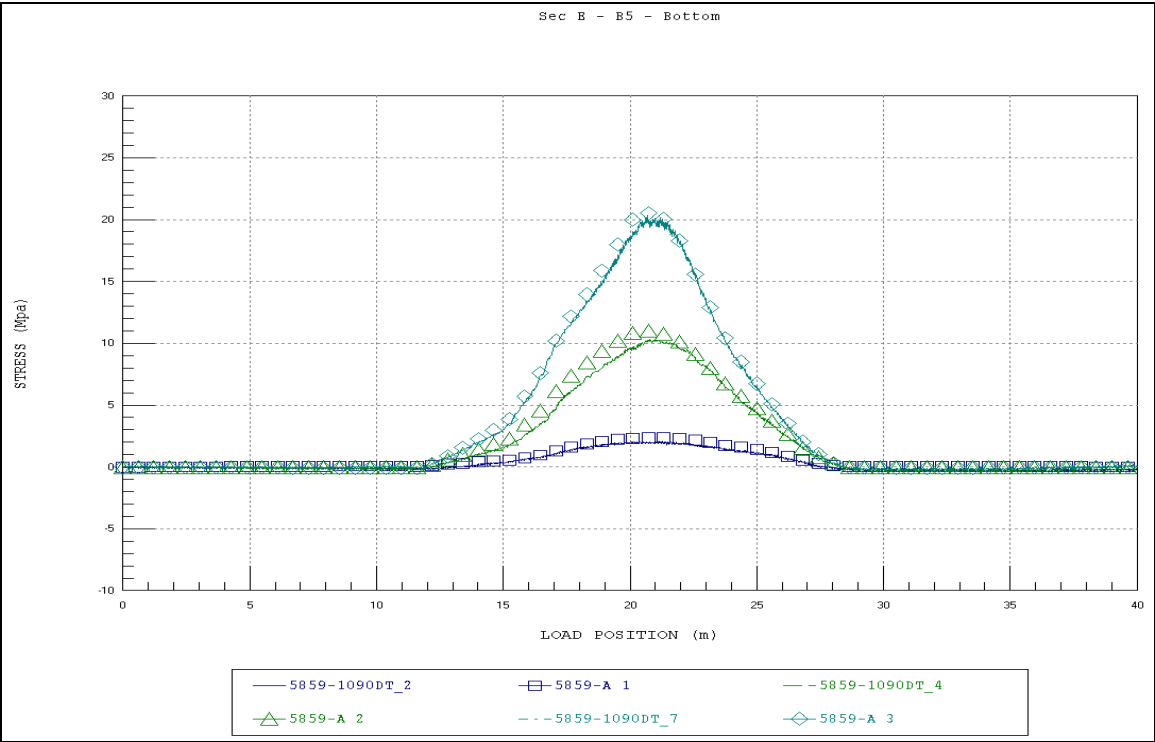
Figure A26. Section E – B5 – bottom.
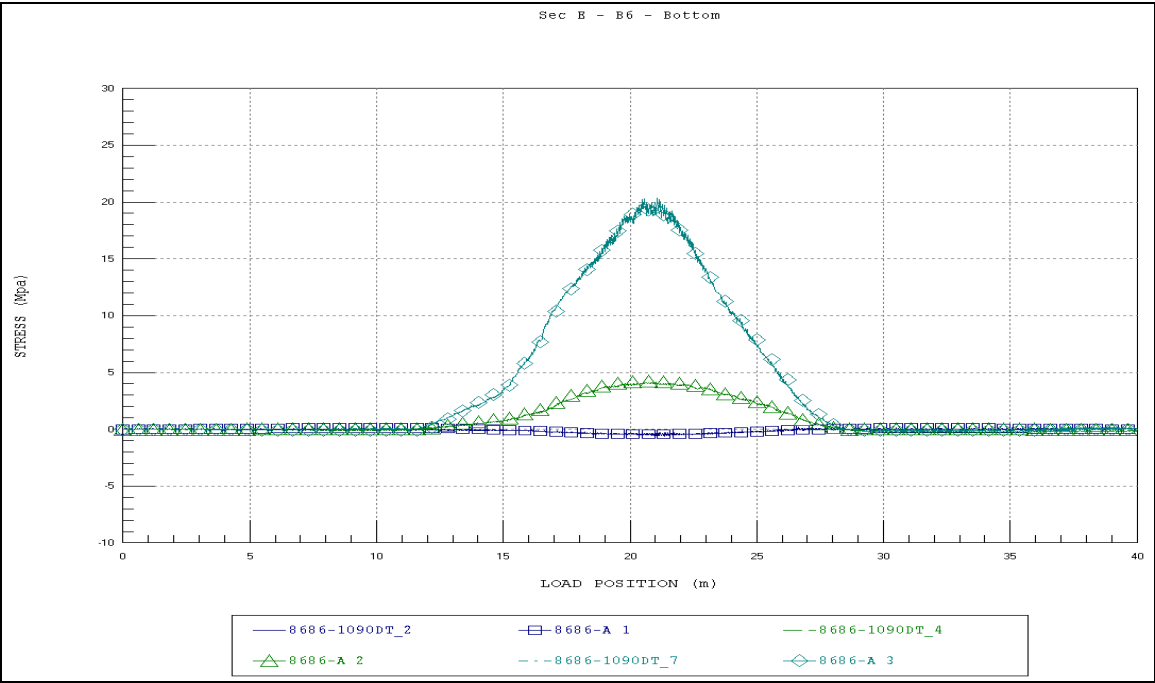
Figure A27. Section E – B6 – bottom.
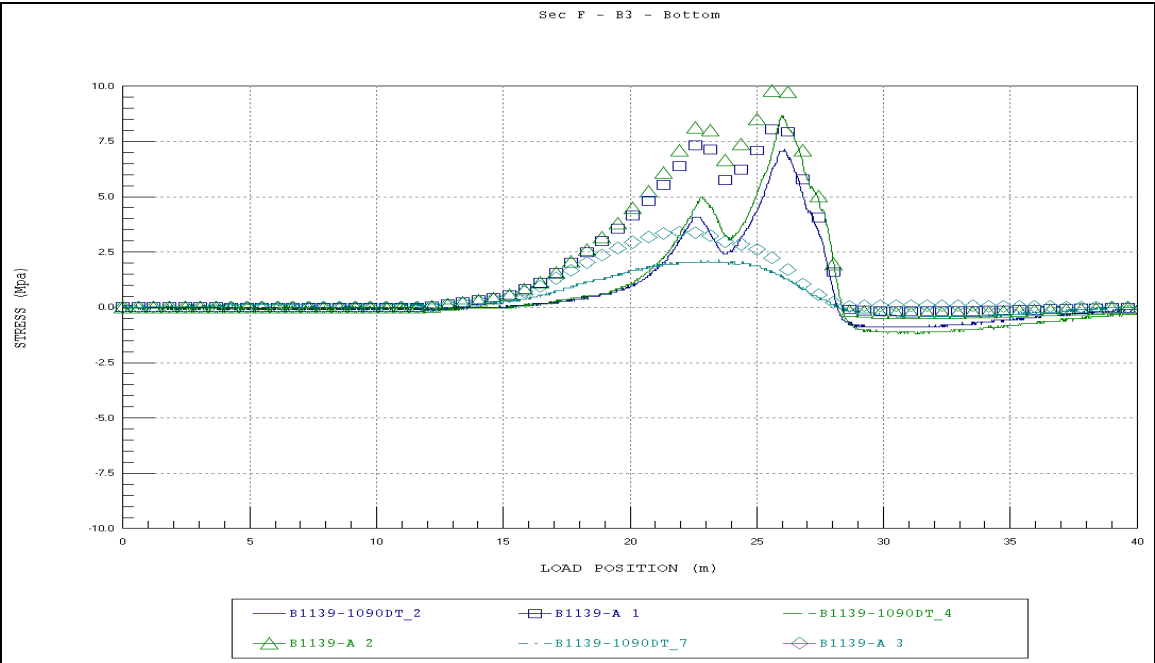
Figure A28. Section F – B3 – bottom.
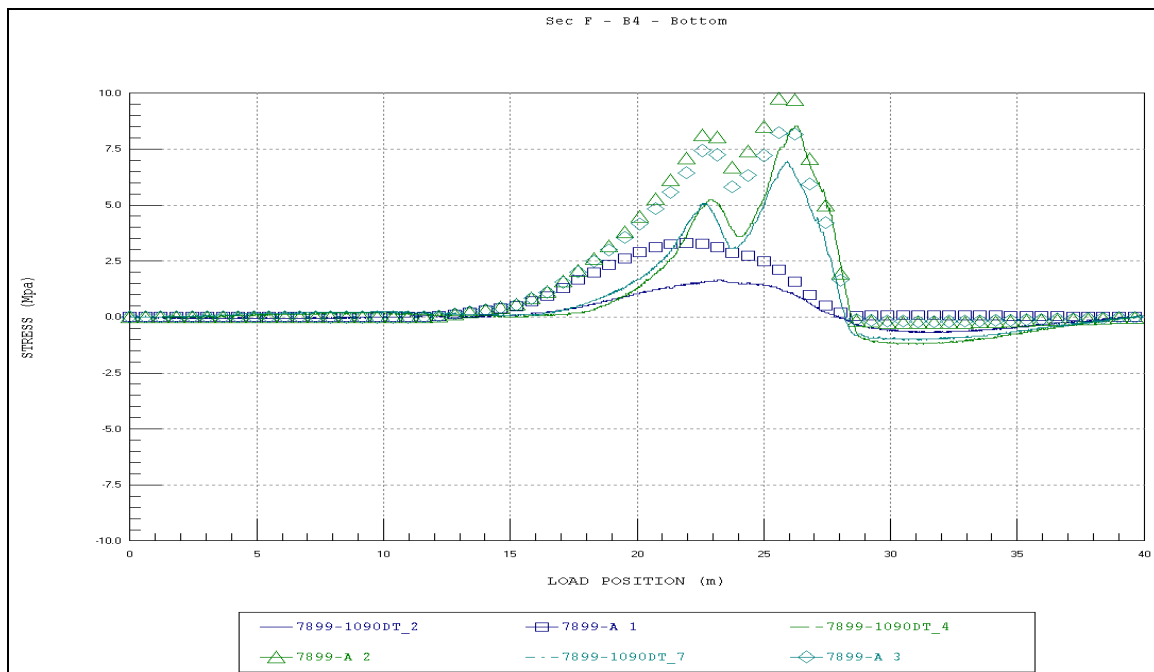
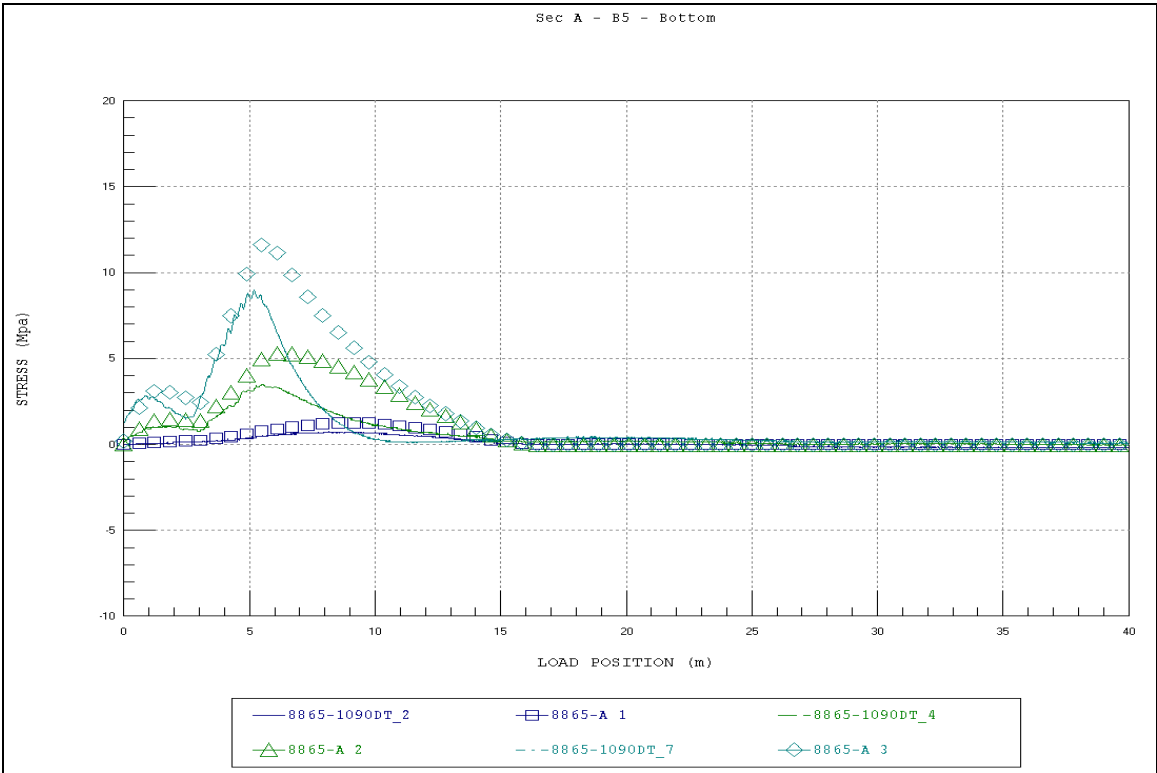Figure A29. Section F – B4 – bottom.
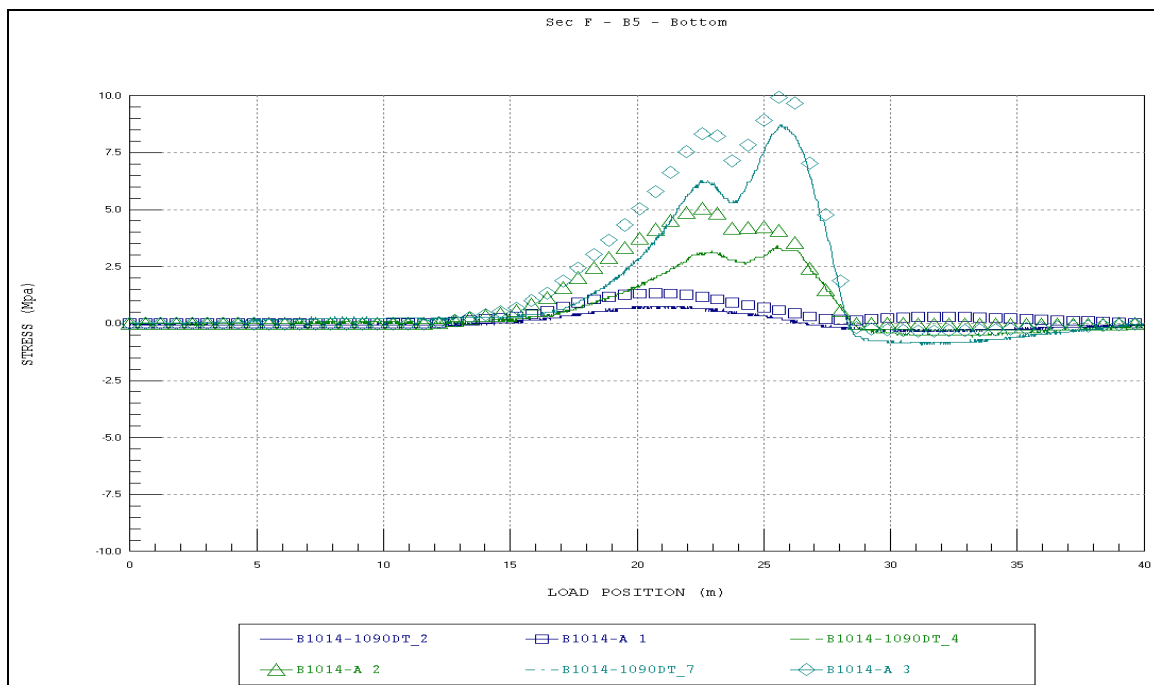
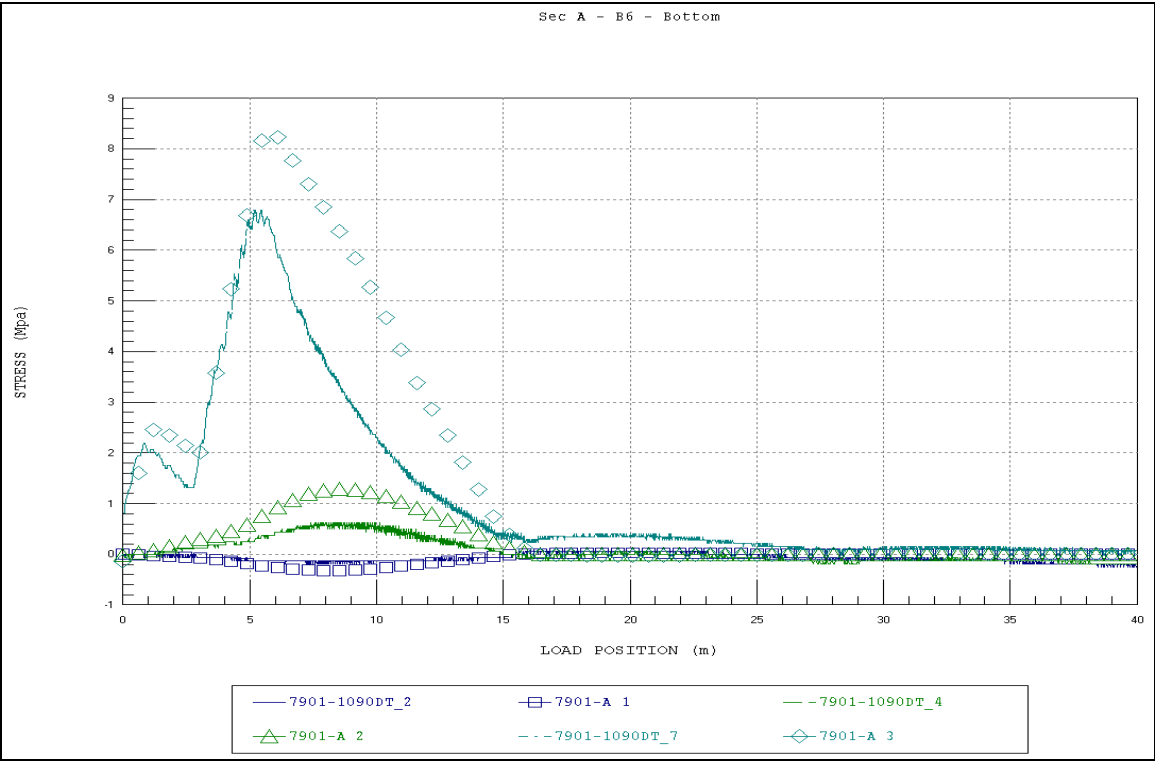Figure A30. Section F – B5 – bottom.
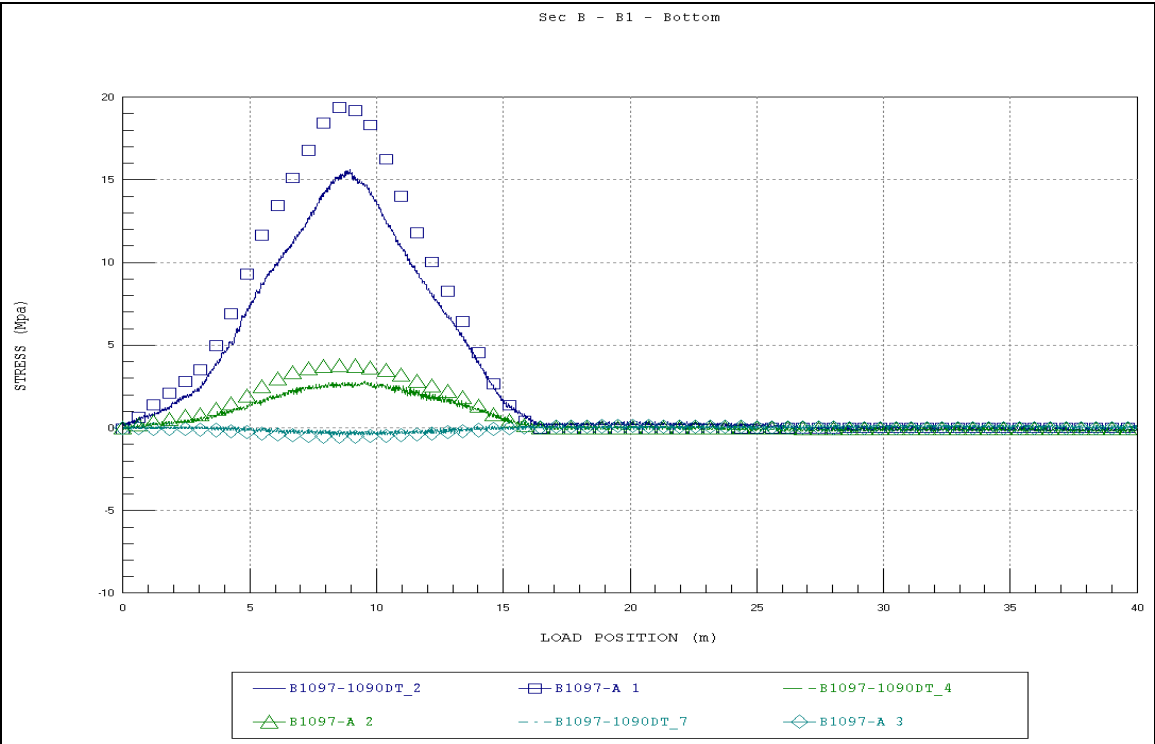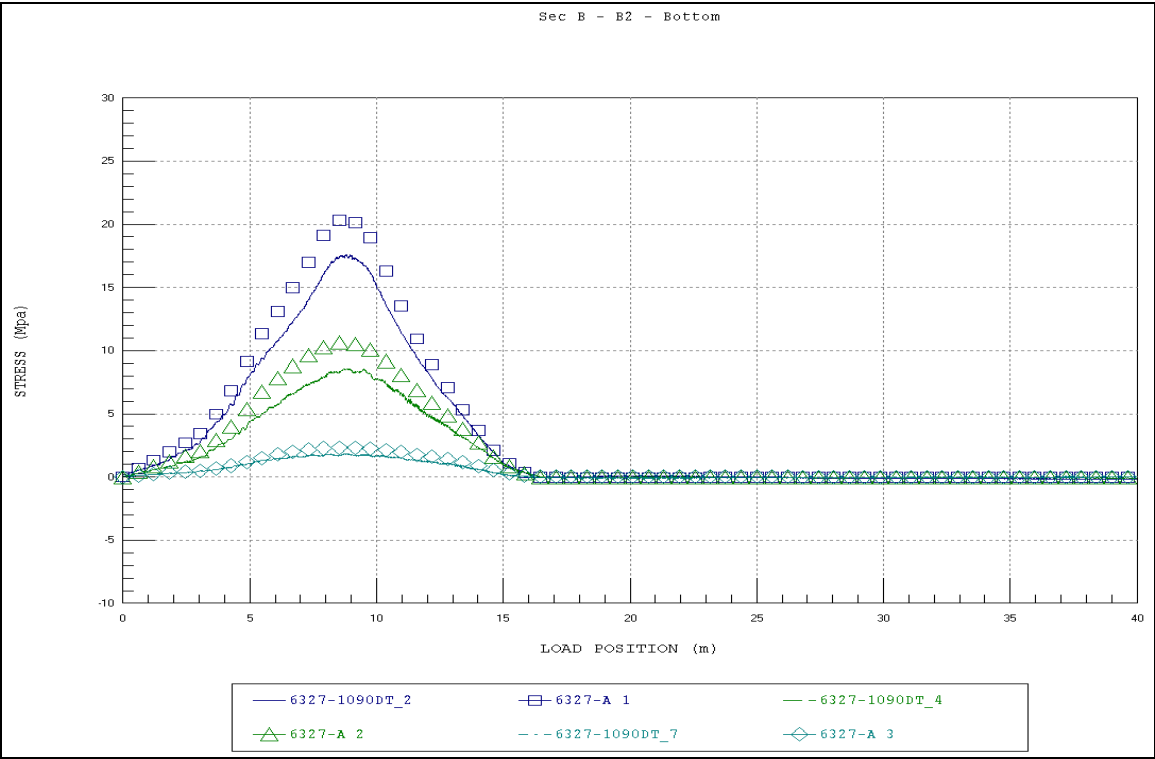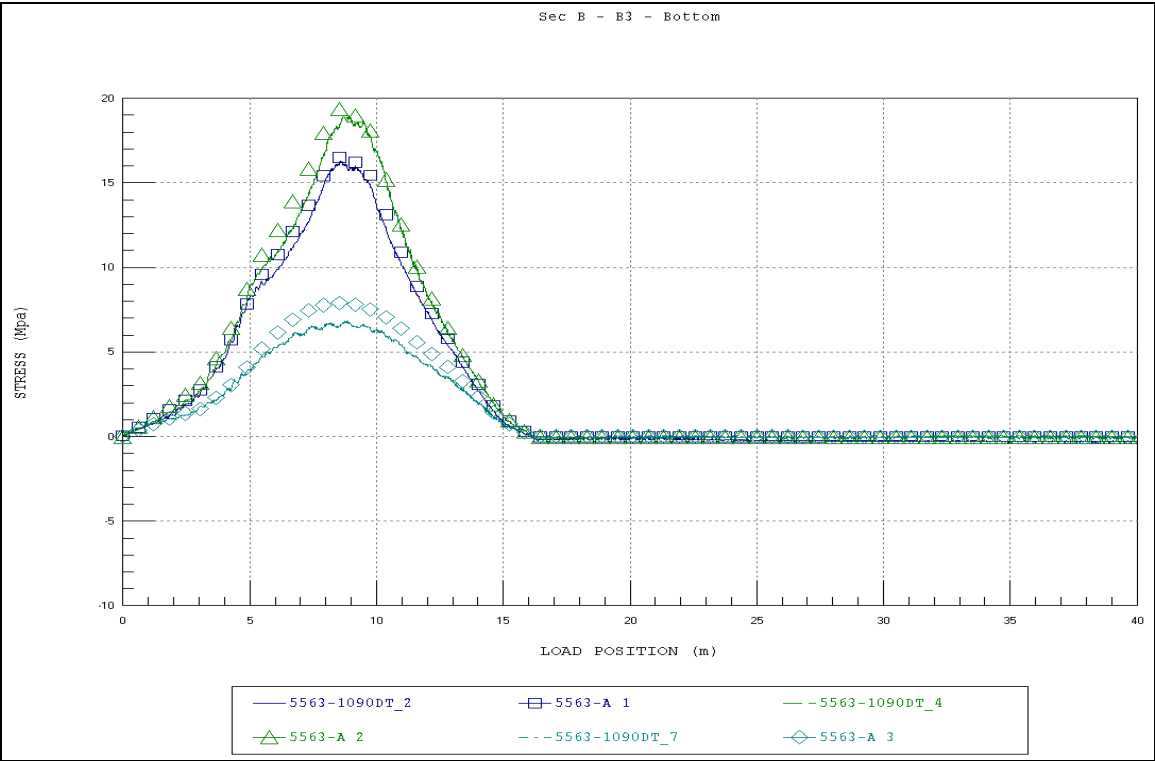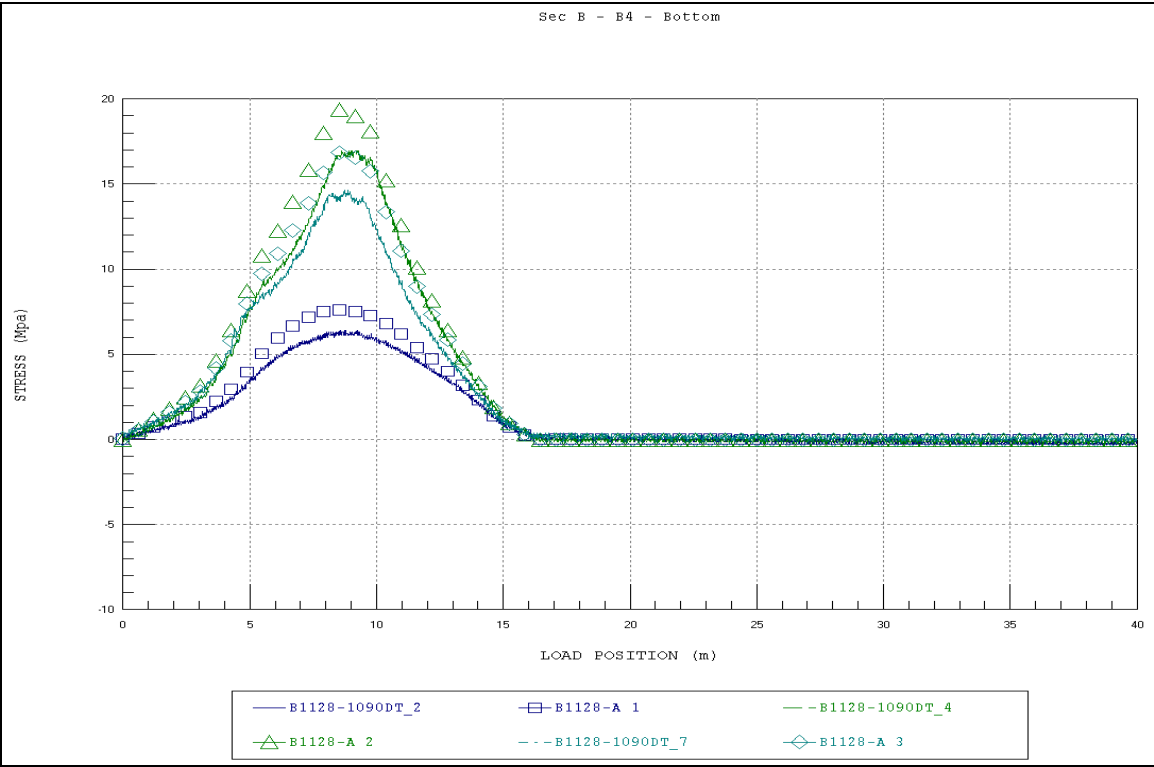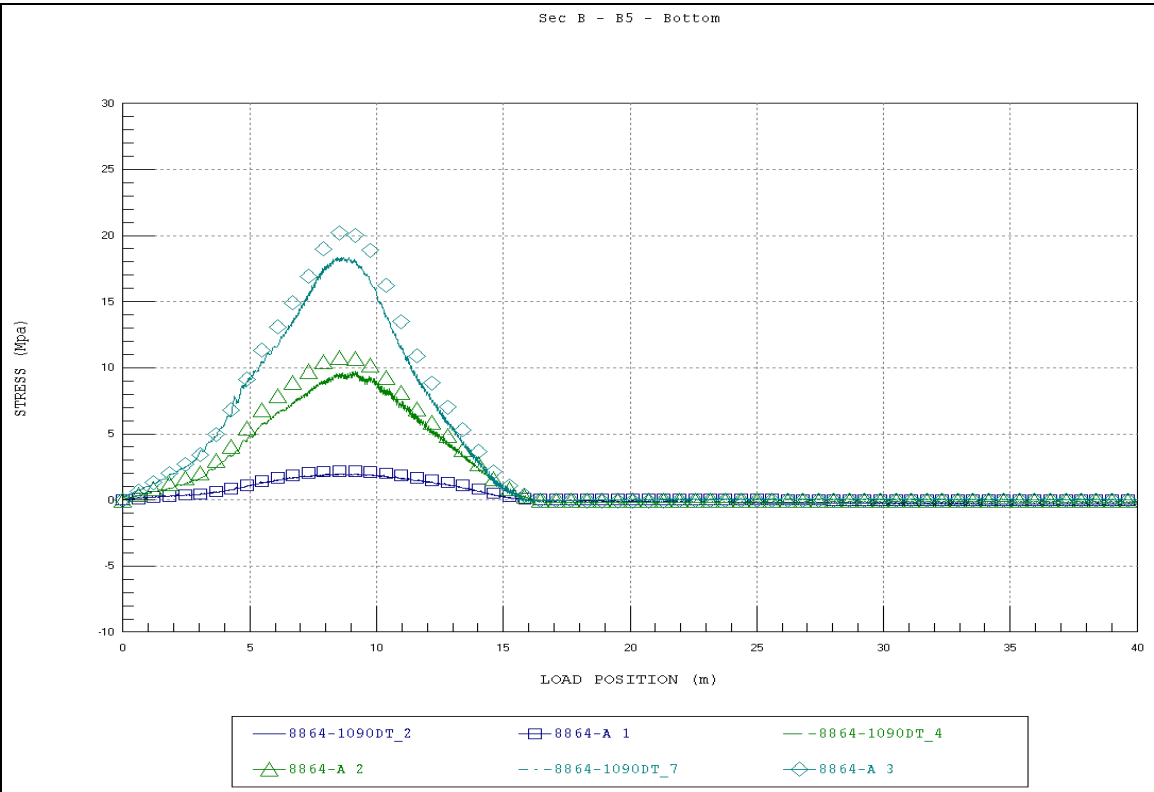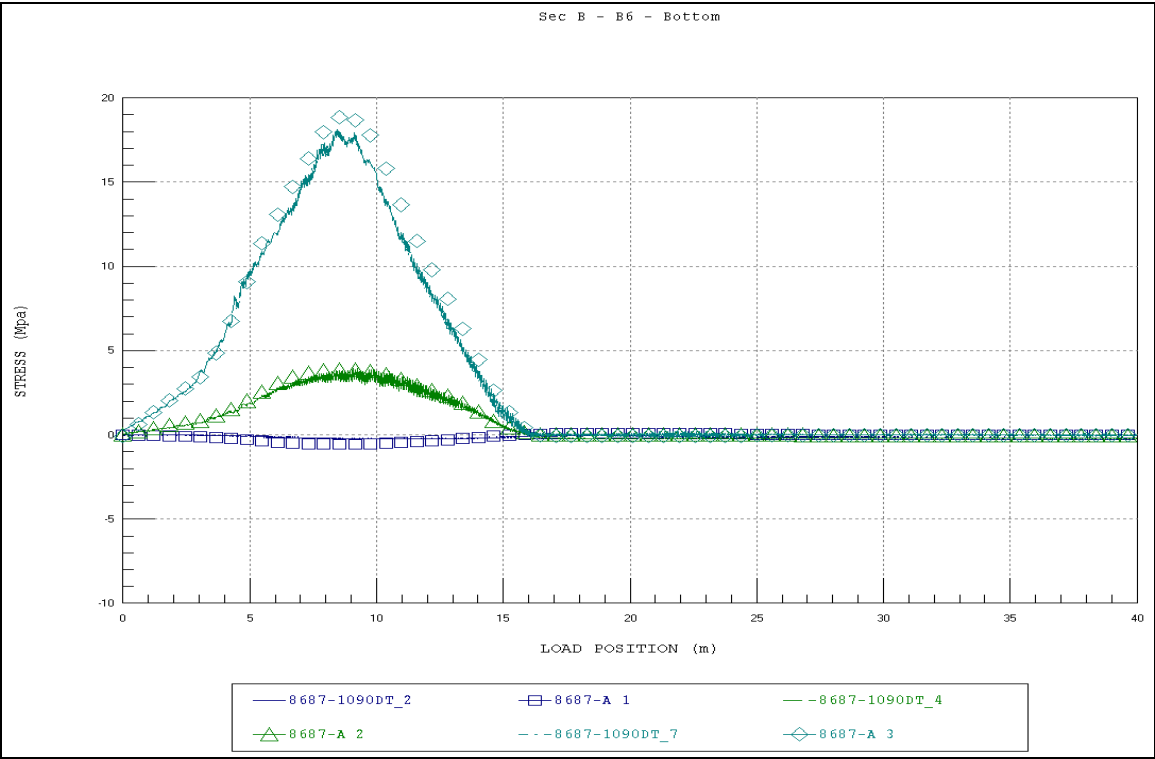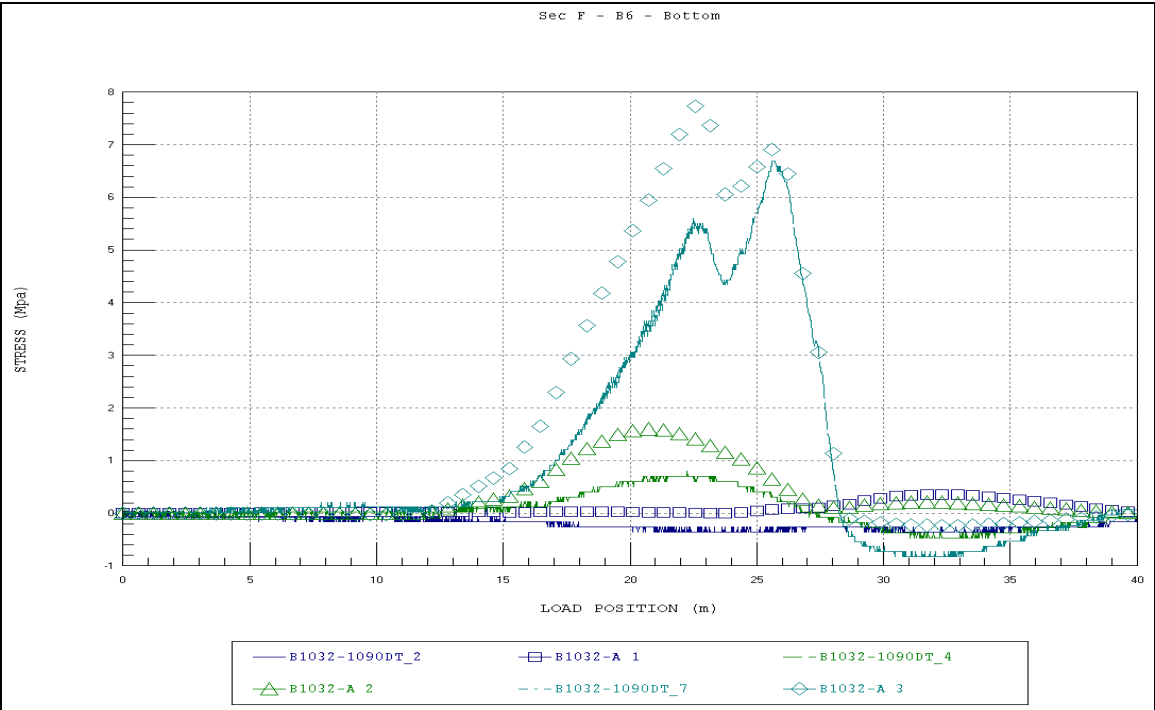
Figure A31. Section F – B6 – bottom.

Appendix B: Field Notes (Scanned)

FIELD NOTES & TESTING CHECKLIST
(TYPICAL BEAM-SLAB BRIDGES)

PROJECT NAME OR #: 1090   Camp Casey

FIELD NOTE TAKER: SA   DATE: 6/16/07

STRUCTURE NAME OR ID: 1090

3 CAD DRAWINGS: 1-Gage ID,   1-Gage Dimensions,   1-General Dimensions.

MEASUREMENTS AND GAGE INSTALLATION PROCEDURES (BELOW)

SPAN LENGTH(S): 40'

SKEW: YES   NO   ANGLE: N/A

BEAM SIZE: See Drawings   BEAM SPACING: 4'10"

DIAPHRAGM SPACING: 10'   SIZE: $L_f = 3"$ $D = 12"$ $t_f = 1/8"$ $t_w =$

BENT INFO: SIZE: ——   # OF PILES: ——   PILE SPACING: ——

GAGE INSTALLATION: 1. Measure gage location & write it on the beam.
2. Install gage and take picture(s) w/ a reference point.
3. Write gage ID and dimensions on CAD notes.
4. Repeat for every gage location!!!
5. Take multiple pics from different angles.

SUPPORT CONDITIONS: Simple w/ Bolt @ C.L.

ABUTMENT DETAILS: (Draw elevation detail) See Drawings

DECK THICKNESS: 6.5" (est.)   COMPOSITE: YES   NO

GENERAL OBSERVATIONS: Gap Between Beams Varies from top to bottom

1

MEASUREMENTS AND TESTING PROCEDURES (ABOVE)

BEGINNING OF WORLD (BOW)   VERIFY NORTH ON PLANS: YES   NO
(X=0, Y=0, location)   Edge of sidewalk
                        North East corner

BOW PHOTOS: ☑   ROAD MARKINGS PHOTOS: ☑

ROADWAY WIDTH (CURB-TO-CURB): 24'   SYMMETRIC: YES   NO

STRUCTURE WIDTH (Out-to-Out): 31' 3"

WEARING SURFACE: None   THICKNESS: —

STARTING TEST POSITION: —10' + ½ REV.   DIRECTION:

VEHICLE ROLL OUT (5 REVS!):   See Vehicles   A/C LOCATION: See Vehicle
*****MAKE SURE YOU PUT THE A/C ON THE SAME WHEEL AS WAS USED TO MEASURE THE ROLL OUT*****   info
                              info

VEHICLE MEASUREMENTS:

See Vehicle Info

AXLE WEIGHTS:
    FRONT: See Vehicle REAR: Info   GROSS:

VEHICLE PROVIDED BY: Army / PVD

TRAFFIC CONTROL PROVIDED BY: Terry / MP

ACCESS PROVIDED BY: PVD

2

<u>LATERAL TESTING POSITIONS:</u> (REFERENCED FROM BOW)

Y1: ~2' Pass   Y2: 15.5' Drive

Y3: 22' Drive   Y4: 15.5' Drive (Tank)

Y5:   Y6:

<u>LATERAL POSITIONS CHECKED BY:</u> SA

TESTING OPERATIONS (WINSTS)

VERIFY GAGE ID & # OF CHANNELS WITH WINSTS: ☑

RUN WINSTS TO VERIFY RESPONSES: GOOD   *6150 is noisy*

WEATHER CONDITIONS &
AMBIENT TEMPERATURE: Sunny ;   25°C ~ 30°C

<u>RUNNING THE FIELD TESTS</u>
STS OPERATOR: JLG   TRUCK OPERATOR: SA

<u>CONTROLLED SEMI-STATIC TESTS</u>
   SAMPLE RATE: 40 Hz
   GAIN: 1000

FILE NAME	LATERAL POSITION	COMMENTS
1090DT–1.dat	Y1	– variable speed – maybe missed ~ click @ ~72 sec.
–2.dat	Y1	GOOD
–3.dat	Y2	GOOD
–4.dat	Y2	Good
–5.dat	Y3	GOOD
–6.dat	Y3	missed clicks @ ~30, 51, 55, 68 ??
–7.dat	Y3	GOOD
–8.dat ←	Y2	Highspeed @ 32 kph sample rate = 66Hz
stop test on span #4		clicks: 2ⁿᵈ @ ~10' starting line
–9.dat	Y2	3ʳᵈ @ rear axle off bridge. GOOD
–10.dat	Y2	another brake test. (100Hz)

3

HIGH-SPEED TEST(S) OR ADDITIONAL TESTS   MIL vehicles.
        SAMPLE RATE: 40 Hz

FILE NAME	LATERAL POSITION	SPEED	COMMENTS
1090MI_1.dat	Y4	—	GOOD
1090MI_2.dat	Y4		GOOD
_3.dat	Y4	10 kph	Highspeed (10 kph) 66 Hz GOOD
_4.dat	Y4	Brake.	Stop on span 4 100Hz GOOD
1090HET_1.dat	Y2	EMPTY HET	off testing line by ~25'
_2.dat	Y2	"	GOOD (Tracking left ???) not sure - scott note.
_3.dat	Y2	"	GOOD
_4.dat	Y2	"	Highspeed (32 kph) maybe 2' off to the right @ Sheet.
_5.dat	Y2	-	Stop test on span 4 (100Hz)

BACKUP DATA FILES: 2 FLASH: ☑   2 PC'S: ☐   EMAIL: ☐

TAKE PICTURES OF NOTES: ☐   BACKUP PICS: ☐

ALL NOTES CHECKED BY: JLG

ANY ADDITIONAL TESTING COMMENTS:

✳ Gage 6150 is BAD → Destroy it!! ✳
     Name   Path   comments.

1090HETMI_1.dat	Y2	Truck is straight - Trailer is left by 5" ~GOOD
_2.dat	Y2	GOOD → same left 5"
_3.dat.	Y2	Highspeed (32kph) good.
_4.dat	Y2	Brake test 100 Hz GOOD

DONE !

SECTION A-A

3' from center of support

5564   6150   7906   5876   8865   7901

BAD

1.5" (Typ)   B1124   B1120

B1   B2   B3   B4   B5   B6

SECTION B-B

2"   2"

6" B1100   B1119   4050   6629   B1126   5565   1388   B1122

B1097   6359   5563   B1118   8854   8087   6"   1.5" (Typ)

16'9" to center of south support

B1   B2   B3   B4   B5   B6

SECTION C-C

3' to center of support

B1045   4118   9860   6530   9065   B1095

4079   5508   1.5" (Typ)

B1   B2   B3   B4   B5   B6

SECTION D-D

3' to center of support

8688   5580   5862   B1116

B1   B2   B3   B4   B5   B6

SECTION E-E

21"   21"

1"   6"

B1131 8863 B1044 B1123 9020 5569 5859 B1133

B1129 4123 7310 5562 5859 8686

B1   B2   B3   B4   B5   B6

SECTION F-F

3' to center of support

B1139 7879 B1014 B1031

B1   B2   B3   B4   B5   B6

2.25"
10"
42"
7.5"
13"
B.O.W.
41"

South support

Varies
0.5-1"
cent. of support
8" 13"

Piers

Varies 0.5" → 1.25"

10" 10"

Span 4 (Beam 2)

$0 - 90"$

$90" \sim 90" + 4'$

$90" + 4' \rightarrow C.L.$

Appendix C: Field Testing Procedures

Background

The motivation for developing a relatively easy-to-implement field-testing system was to allow short- and medium-span bridges to be tested on a routine basis. Original development of the hardware was begun in 1988 at the University of Colorado under a contract with the Pennsylvania Department of Transportation. Subsequent to that project, the Integrated Technique was refined on another study funded by the Federal Highway Administration in which 35 bridges located on the Interstate system throughout the country were tested and evaluated. Further refinement has been implemented over the years through testing and evaluating hundreds of bridges, lock gates, and other structures.

Structural testing hardware

The key to quickly completing the field testing is the use of strain trans-ducers (rather than standard foil strain gages) that can be attached to the structural members in just a few minutes. These sensors were originally developed for monitoring dynamic strains on foundation piles during the driving process. They have been adapted for use in structural testing through special modifications, have very high accuracy, and are periodic-ally recalibrated to standards of the National Institute of Standards and Technology. (Refer to Appendix D for specifications on the BDI strain transducers.)

In addition to the strain sensors, the data acquisition hardware has been designed specifically for structural live-load testing, which means it is extremely easy to use in the field. (See Appendix E for specifications on the BDI STS, or Structural Testing System.) Briefly, some of the features include military-style connections for quick assembly and self-identifying sensors that dramatically reduce bookkeeping efforts. The WinSTS testing software has been written to allow easy hardware configuration and data-recording operation. Other enhancements include the BDI AutoClicker, which is an automatic load position indicator that is mounted directly on the vehicle. As the test truck crosses the structure along the preset path, a communication radio sends a signal to the STS, which receives it and puts a mark in the data. This allows the field strains to be compared to

analytical strains as a function of vehicle position, not only as a function of time. (Appendix F presents the AutoClicker specifications.) The end result of using all of the above-described components is a system that can be used by people other than computer experts or electrical engineers. Typical testing time with the STS ranges from 20 to 60 channel tests being completed in 1 day, depending on access and other field conditions.

The following general directions outline how to run a typical diagnostic load test on a short- to medium-span highway bridge up to about 200 ft (60 m) in length. With only minor modifications, these directions can be applied to railroad bridges (use a locomotive rather than a truck for the load vehicle), lock gates (monitor the water level in the lock chamber), amusement park rides (track the position of the ride vehicle), and other structures in which the live-load can be applied easily. The basic scenario is to first instrument the structure with the required number of sensors, run a series of tests, and then remove all the sensors. These procedures can often be completed within 1 working day, depending on field conditions such as access and traffic.

Instrumentation of structure

This outline is intended to describe the general procedures used for completing a successful field test on a highway bridge using the BDI STS. For a detailed explanation of the instrumentation and testing procedures, contact BDI and request a copy of the Structural Testing System Operation Manual.

Attaching strain transducers

Once a tentative instrumentation plan has been developed for the structure in question, the strain transducers must be attached and the STS prepared for running the test. There are several methods for attaching the strain transducers to the structural members, depending on whether they are steel, concrete, timber, fiber-reinforced polymer (FRP), or other. For steel structures, quite often the transducers can be clamped directly to the steel flanges of rolled sections or plate girders. If significant lateral bending is assumed to be present, then one transducer may be clamped to each edge of the flange. In general, the transducers can be clamped directly to painted surfaces. The alternative to clamping is the tab attachment method that involves cleaning the mounting area and then using a fast-setting cyanoacrylate adhesive to temporarily install the transducers.

Small steel "tabs" are used with this technique and, after testing has been completed, these are removed and touch-up paint can be applied to the exposed steel surfaces.

Installation of transducers on pre-stressed concrete (PS/C) and FRP members is usually accomplished with the tab technique outlined above, while readily available wood screws and a battery-operated hand drill are used for timber members. Installing transducers on reinforced concrete (R/C) is more complex in that gage extensions are used and must be mounted with concrete studs.

If the above steps are followed, it should be possible to mount each transducer in approximately 5 to 10 min. The mounting of transducers on steel (Figure C1) and R/C (Figure C2) members is shown below.
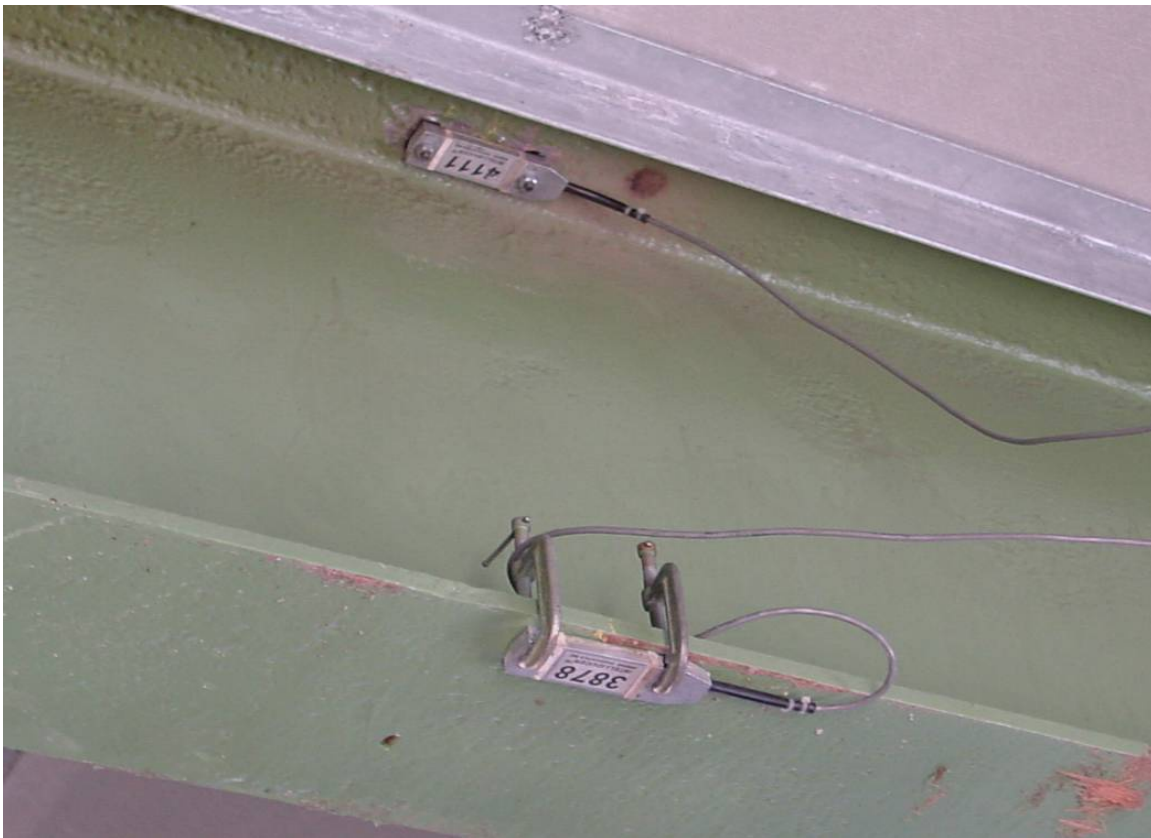
Figure C1. Strain transducers mounted on a steel girder.

Figure C2. Transducer with gage extensions mounted on R/C slab.

Assembly of system

Once the transducers have been mounted, they are connected to the four-channel STS units that are also located on the bridge. The STS units can be easily clamped to the bridge girders, or if the structure is concrete and no flanges are available on which to set the STS units, transducer tabs glued to the structure and plastic zip-ties or small wire can be used to mount them. Since the transducers will identify themselves to the system, there is no special order in which they must be plugged into the system. The only information that must be recorded is the transducer serial number and its location on the structure. Signal cables are then used to connect STS units together either in series or in a "tree" structure through the use of cable splitters. If several gages are close to each other, the STS units can be plugged directly to each other without the use of a cable.

Once all of the STS units have been connected, only one cable must be run and connected to the STS power supply located near the PC. Once power and communication cables are connected, the system is ready to acquire data. One last step entails installing the AutoClicker on the test vehicle, as shown in Figure C3.

Figure C3. AutoClicker mounted on test vehicle.

Establishing load vehicle positions

Once the structure is instrumented and the loading vehicle prepared, some reference points must be established on the deck in order to determine where the vehicle will cross. This process is important so that future analysis comparisons can be made with the loading vehicle in the same locations as it was in the field. Therefore, a "zero" or initial reference point is selected and usually corresponds to the point on the deck directly above the abutment bearing and the center line of one of the fascia beams. All other measurements on the deck will then be related to this zero reference point. For concrete T-beams, box beams, and slabs, this can correspond to where the edge of the slab or the beam web meets the face of the abutment. If the bridge is skewed, the first point encountered from the direction of travel is used. In any case, it should be a point that is easily located on the drawings of the structure.

Once the zero reference location is known, the lateral load paths for the
vehicle are determined. Often, the painted roadway lines are used for the
driver to follow if they are in convenient locations. For example, for a two-
lane bridge, a northbound shoulder line will correspond to Y1 (passenger-
side wheel); the center dashed line, to Y2 (center of truck); and the south-
bound shoulder line, to Y3 (driver's-side wheel). Often, the structure will
be symmetrical with respect to its longitudinal center line. If so, it is good
practice is to take advantage of this symmetry by selecting three Y loca-
tions that are also symmetric. This will allow for a data quality check since
the response should be very similar, say, on the middle beam if the truck is
on the left side of the bridge or the right side of the bridge. In general, it is
best to have the truck travel in each lane (at least on the lane line) and also
as close to each shoulder or sidewalk as possible. When the deck layout is
completed, the loading vehicle's axle weights and dimensions are
recorded.

Running the load tests

After the structure has been instrumented and the reference system laid
out on the bridge deck, the actual testing procedures are completed. The
WinSTS software is initialized and configured. When all personnel are
ready to commence the test, traffic control is initiated and the Run Test
option is selected, which places the system in an activated state. When the
truck passes over the first deck mark, the AutoClicker is tripped and data
are being collected at the specified sample rate. An effort is made to get the
truck across with no other traffic on the bridge. When the rear axle of the
vehicle completely crosses over the structure, the data collection is stopped
and several strain histories are evaluated for data quality. Usually, at least
two passes are made at each "Y" position to ensure data reproducibility
and, then, if conditions permit, high-speed or dynamic tests are
completed.

The use of a moving load as opposed to placing the truck at discrete loca-
tions has two major benefits. First, the testing can be completed much
quicker, meaning there is less impact on traffic. Second, and more impor-
tant, much more information can be obtained (both quantitative and
qualitative). Discontinuities or unusual responses in the strain histories,
which are often signs of distress, can be easily detected. Since the load
position is monitored as well, it is easy to determine what loading condi-
tions cause the observed effects. If readings are recorded only at discrete
truck locations, the risk of losing information between the points is great.

The advantages of continuous readings have been proven over and over again.

When the testing procedures are complete, the instrumentation is removed, and any touch-up work is completed.

Appendix D: Specifications – BDI Strain Transducers

Figure D1. BDI strain transducer.

Table D1. Strain transducer specifications.

Effective Gage Length:	3.0 in (76.2 mm); extensions available for use on R/C structures
Overall Size:	4.4 in. x 1.2 in. x 0.5 in. (110 mm x 33 mm x 12 mm)
Cable Length:	10 ft (3 m) standard, any length available
Material:	Aluminum
Circuit:	Full Wheatstone bridge with four active 350Ω foil gages, 4-wire hookup
Accuracy:	±2%, individually calibrated to NIST standards
Strain Range:	Approximately ±4000 $\mu\varepsilon$
Force Required for 1000 $\mu\varepsilon$:	Approximately 9 lb (40 N)
Sensitivity:	Approximately 500 $\mu\varepsilon$/mV/V
Weight:	Approximately 3 oz. (88 g)
Environmental:	Built-in protective cover, also water-resistant
Temperature Range:	-60 °F to 250 °F (-50 °C to 120 °C) operation range
Cable:	BDI RC-187: 22 gage, two individually shielded pairs with drain
Options:	Fully waterproofed, heavy-duty cable, special quick-lock connector
Attachment Methods:	C-clamps or threaded mounting tabs and quick-setting adhesive

Appendix E: Specifications – BDI Structural Testing System

Figure E1. BDI structural testing system.

Table E1. Structural testing system specifications.

Channels	4 to 128, expandable in multiples of four
Hardware Accuracy	±0.2% (2% for strain transducers)
Sample Rates	0.01 to 1,000 Hz sample rate; Internal over-sampling rate is 15 KHz
Max Test Lengths	20 min at 100 Hz; 128K samples per channel maximum test length
Gain Levels	1, 250, 500, 1000
Digital Filter	Fixed by selected sample rate
Analog Filter	200 Hz, -3db, 3rd-order Bessel
Max. Input Voltage	±10V
Power	85 - 264 VAC, 47-440 Hz; -25 to 55 °C
12VDC Power	External inverter included
Excitation Voltages: Standard: LVDT:	5V DC @ 200 mA; ±15V DC @ 200 mA
A/D Resolution	2.44 uV/bit (14-bit ADC)
PC Requirements	Windows 2000, XP

PC Interface	USB 1.1 Port (compatible with USB 2.0)
Self-Balancing Range	±20 mV @ input with 350Ω Wheatstone bridge
Enclosures	Aluminum, splash-resistant
Cable Connections	All aluminum military grade, circular bayonet "snap" lock
Vehicle Tracking:	See "AutoClicker" specifications
Sensors	See "BDI Strain Transducer" specifications; Also supports LVDTs, foil strain gages, accelerometers, various DC output sensors; Single RS232 serially interfaced sensor
Weights: Power Unit: STS Unit	 6.2 lb (2.8 kg) 1.6 lb (0.7 kg)
Dimensions: Power Unit: STS Unit:	 13.5 x 9.5 x 2.4 in. (343 x 242 x 61 mm) 11.8 x 3.4 x 1.7 in. (300 x 87 x 44 mm)

Appendix F: Specifications – BDI AutoClicker

Figure F1. AutoClicker mounted on test truck.

Table F1. AutoClicker specifications.

Three Handheld Radios	Motorola P1225 two-channel (or equal) modified for both "Rx" and "Tx"
Power	9V battery
Mounting	Universal front fender mounting system
Target	Retroreflective tape mounted on universal wheel clamp
Bands/Power	VHF/1-watt or UHF/2-watt
Frequencies	User-specified
Data Acquisition System Requirements	TTL/CMOS input (pull-up resistor to 5V)
Output	Isolated contact closure (200V 0.5A max switch current)

Appendix G: Modeling and Analysis – The Integrated Approach

Introduction

In order for load testing to be a practical means of evaluating short- to medium-span bridges, it is apparent that testing procedures must be economic to implement in the field and the test results translatable into a load rating. A well-defined set of procedures must exist for the field applications as well as for the interpretation of results. An evaluation approach based on these requirements was first developed at the University of Colorado during a research project sponsored by the Pennsylvania Department of Transportation (Commander 1989; Goble et al. 1992). Over several years, the techniques originating from this project have been refined and expanded into a complete bridge rating system.

The ultimate goal of the "integrated approach" is to obtain realistic rating values for highway bridges in a cost-effective manner. This is accomplished by measuring the response behavior of the bridge due to a known load and determining the structural parameters that produce the measured responses. With the availability of field measurements, many structural parameters in the analytical model can be evaluated that are otherwise conservatively estimated or ignored entirely. Items that can be quantified through this procedure include the effects of structural geometry, effective beam stiffness, realistic support conditions, effects of parapets and other nonstructural components, lateral load transfer capabilities of the deck and transverse members, and the effects of damage or deterioration. Often, bridges are rated poorly because of inaccurate representations of the structural geometry or because the material and/or cross-sectional properties of main structural elements are not well defined. A realistic rating can be obtained, however, when all of the relevant structural parameters are defined and implemented in the analysis process.

One of the most important phases of this approach is a qualitative evaluation of the raw field data. Much is learned during this step to aid in the rapid development of a representative model.

Initial data evaluation

The first step in structural evaluation consists of a visual inspection of the data in the form of graphic response histories. Graphic software was developed to display the raw strain data in various forms. Strain histories can be viewed in terms of time or truck position. Since strain transducers are typically placed in pairs, neutral axis (NA) measurements, curvature responses, and strain averages can also be viewed. Linearity between the responses and load magnitude can be observed by the continuity in the strain histories. Consistency in the NA measurements from beam to beam and as a function of load position provides great insight into the nature of the bridge condition. The direction and relative magnitudes of flexural responses along a beam line are useful in determining if end-restraints play a significant role in the response behavior. In general, the initial data inspection provides the engineer with information concerning modeling requirements and can help locate damaged areas.

Having obtained strain measurements at two depths on each beam cross section, the flexural curvature and the location of the NA can be computed directly from the field data. Figure G1 illustrates how curvature and NA values are computed from the strain measurements.

$$\bar{y} = \frac{\varepsilon_B \, d}{\varepsilon_T - \varepsilon_B}$$

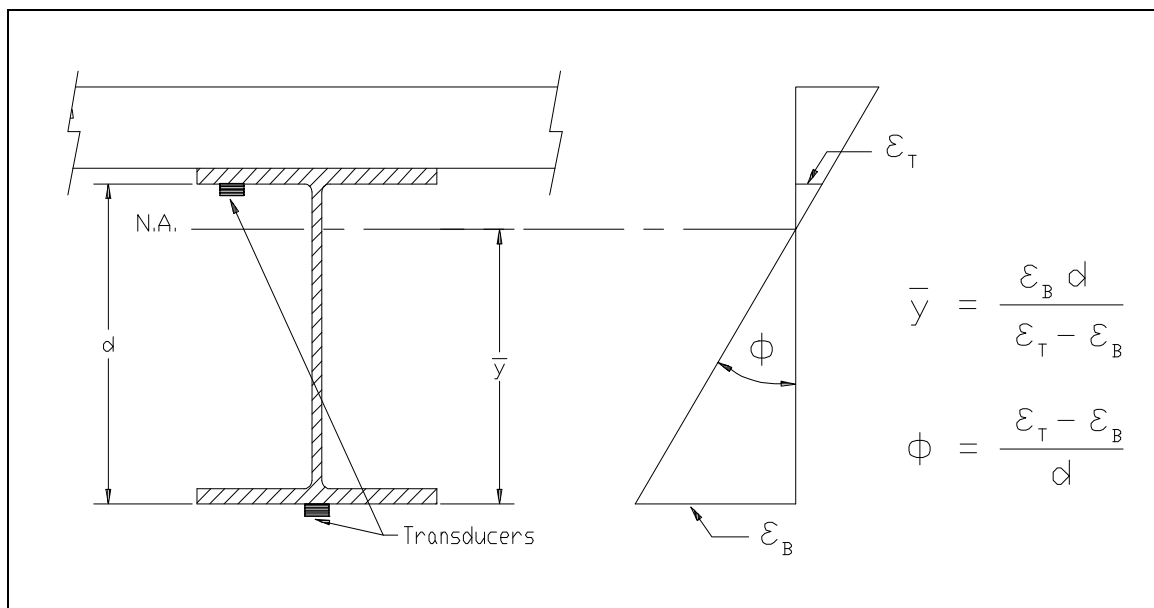$$\phi = \frac{\varepsilon_T - \varepsilon_B}{d}$$

Figure G1. Illustration of neutral axis and curvature calculations.

The consistency in the NA values between beams indicates the degree of consistency in beam stiffness. Also, the consistency of the NA measurement on a single beam as a function of truck position provides a good quality check for that beam. If for some reason a beam's stiffness changes with respect to the applied moment (i.e. loss of composite action or loss of effective flange width due to a deteriorated deck), it will be observed by a shift in the NA history.

Since strain values are translated from a function of time into a function of vehicle position on the structure and the data acquisition channel and the truck position tracked, a considerable amount of bookkeeping is required to perform the strain comparisons. In the past, this required manipulation of result files and spreadsheets, which was tedious and a major source of error. This process in now performed automatically by the software, and all of the information can be verified visually.

Finite element modeling and analysis

The primary function of the load test data is to aid in the development of an accurate finite element model of the bridge. Finite element analysis is used because it provides the most general tool for evaluating various types of structures. Since a comparison of measured and computed responses is performed, it is necessary that the analysis be able to represent the actual response behavior. This requires that actual geometry and boundary conditions be realistically represented. In maintaining reasonable modeling efforts and computer run times, a certain amount of simplicity is also required, so a planar grid model is generated for most structures and linear-elastic responses are assumed. A grid of frame elements is assembled in the same geometry as the actual structure. Frame elements represent the longitudinal and transverse members of the bridge. The load transfer characteristics of the deck are provided by attaching plate elements to the grid. When end-restraints are determined to be present, elastic spring elements having both translational and rotational stiffness terms are inserted at the support locations.

Loads are applied in a manner similar to the actual load test. A model of the test truck, defined by a two-dimensional group of point loads, is placed on the structure model at discrete locations along the same path that the test truck followed during the load test. Gage locations identical to those in the field are also defined on the structure model so that strains can be computed at the same locations under the same loading conditions.

Evaluation of rotational end-restraint

A common requirement in structural identification is the need to determine effective spring stiffness values that best represent in situ support conditions. Whereas it is generally simple to evaluate a spring constant in terms of moment per rotation, the value generally has little meaning to the engineer. A more conceptual approach is to evaluate the spring stiffness as a percentage of a fully restrained condition (Gerstle and Ackroyd 1990), with 0 percent being a pinned condition and 100 percent being fixed, for example. This is best accomplished by examining the ratio of the beam or slab stiffness to the rotational stiffness of the support.

As an illustration, a point load is applied to a simple beam with elastic supports (see Figure G2). By examining the moment diagram, it is apparent that the ratio of the end moment to the midspan moment (M_e/M_m) equals 0.0 if the rotational stiffness (K_r) of the springs is equal to 0.0. Conversely, if the value of K_r is set to infinity (rigid), the moment ratio will equal 1.0. If a fixity term is defined as the ratio (M_e/M_m), which ranges from 0 to 100 percent, a more conceptual measure of end-restraint can be obtained.
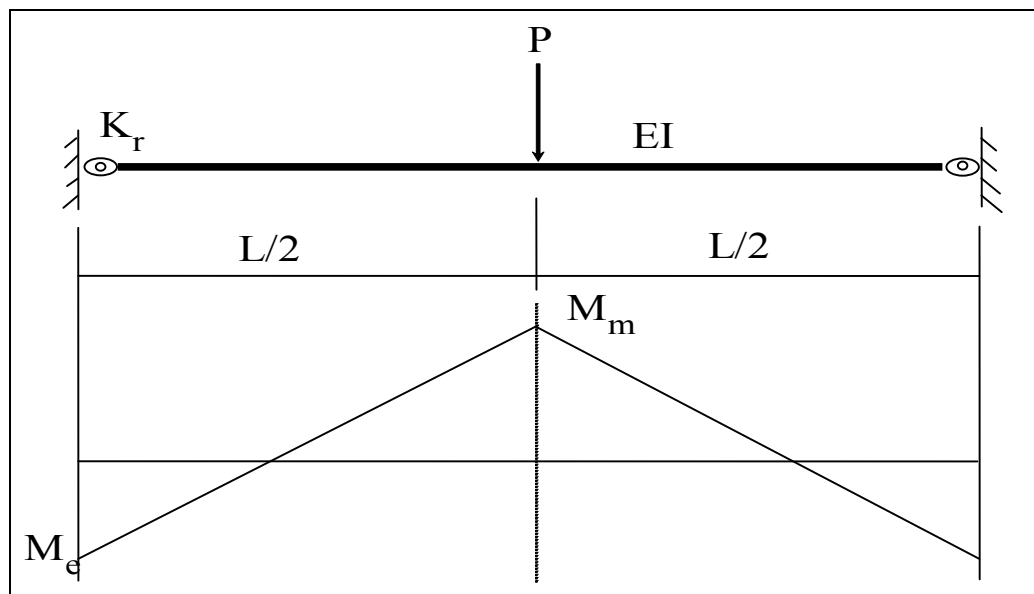
Figure G2. Moment diagram of beam with rotational end-restraint.

The next step is to relate the fixity term to the actual spring stiffness (K_r). The degree to which the K_r affects the fixity term depends on the beam or slab stiffness to which the spring is attached. Therefore, the fixity term must be related to the ratio of the beam/spring stiffness. Figure G2 contains a graphical representation of the end-restraint effect on a simple

beam. Using the graph presented as Figure G3, a conceptual measure of end-restraint can be defined after the beam and spring constants are evaluated through structural identification techniques.
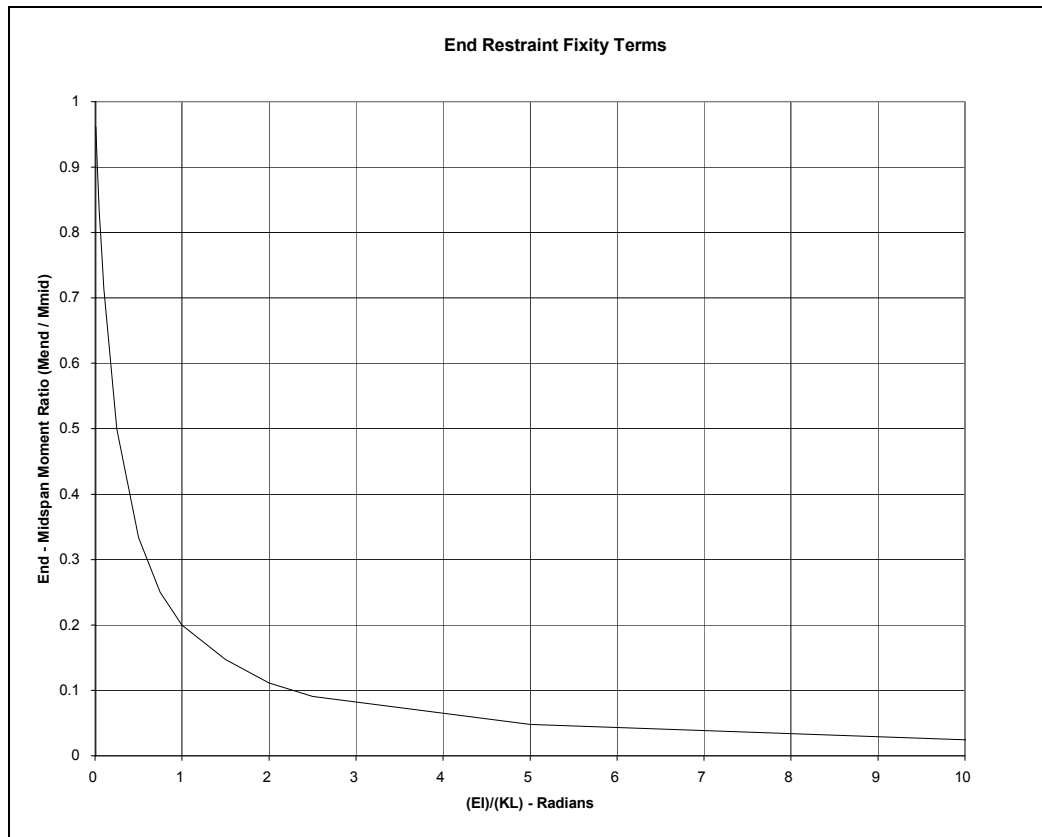
Figure G3. Relationship between spring stiffness and fixity ratio.

Model correlation and parameter modification

The accuracy of the model is determined numerically by the analysis using several statistical relationships and through visual comparison of the strain histories. The numeric accuracy values are useful in evaluating the effect of any changes to the model, whereas the graphical representations provide the engineer with the best perception for why the model is responding differently from what the measurements indicate. Member properties that cannot be accurately defined by conventional methods or directly from the field data are evaluated by comparing the computed strains with the measured strains. These properties are defined as variable and are evaluated such that the best correlation between the two sets of data is obtained. It is the engineer's responsibility to determine which parameters need to be refined and to assign realistic upper and lower limits to each parameter. The evaluation of the member property is

accomplished with the aid of a parameter identification process (opti-mizer) built into the analysis. In short, the process consists of an iterative procedure of analysis, data comparison, and parameter modification. It is important to note that the optimization process is merely a tool to help evaluate various modeling parameters. The process works best when the number of parameters is minimized and reasonable initial values are used.

During the optimization process, the analysis program computes various error values, which provide a quantitative measure of the model accuracy and improvement. The error is quantified in four ways, each providing a different perspective of the model's ability to represent the actual struc-ture: an absolute error, a percent error, a scale error, and a correlation coefficient.

The **absolute error** is computed from the absolute sum of the strain differences. Algebraic differences between the measured and theoretical strains are computed at each gage location for each truck position used in the analysis; therefore, several hundred strain comparisons are generally used in this calculation. This quantity is typically used to determine the relative accuracy from one model to the next and to evaluate the effect of various structural parameters. It is used by the optimization algorithm as the objective function to minimize. Because the absolute error is in terms of micro-strain (mε), the value can vary significantly depending on the magnitude of the strains, the number of gages, and number of different loading scenarios. For this reason, it has little conceptual value except for determining the relative improvement of a particular model.

A **percent error** is calculated to provide a better qualitative measure of accuracy. It is computed as the sum of the strain differences squared divided by the sum of the measured strains squared. The terms are squared so that error values of different sign will not cancel each other out, and to put more emphasis on the areas with higher strain magnitudes. A model with acceptable accuracy will usually have a percent error of less than 10 percent.

The **scale error** is similar to the percent error except that it is based on the maximum error from each gage divided by the maximum strain value from each gage. This number is useful because it is based only on strain measurements recorded when the loading vehicle is in the vicinity of each gage. Depending on the geometry of the structure, the number of truck

positions, and various other factors, many of the strain readings are essentially negligible. This error function uses only the most relevant measurement from each gage.

Another useful quantity is the **correlation coefficient,** which is a measure of the linearity between the measured and computed data. This value determines how well the shapes of the computed response histories match the measured responses. The correlation coefficient can have a value between 1.0 (indicating a perfect linear relationship) and -1.0 (exact opposite linear relationship). A good model will generally have a correlation coefficient greater than 0.90. A poor correlation coefficient is usually an indication that a major error in the modeling process has occurred. This is generally caused by poor representations of the boundary conditions or the loads being applied incorrectly (i.e., truck traveling in wrong direction).

Table G1 contains the equations used to compute each of the statistical error values.

Table G1. Error functions.

Error Function	Equation
Absolute error	$\sum \lvert \varepsilon_m - \varepsilon_c \rvert$
Percent error	$\sum (\varepsilon_m - \varepsilon_c)^2 / \sum (\varepsilon_m)^2$
Scale error	$\dfrac{\sum \max \lvert \varepsilon_m - \varepsilon_c \rvert_{gage}}{\sum \max \lvert \varepsilon_m \rvert_{gage}}$
Correlation coefficient	$\dfrac{\sum (\varepsilon_m - \overline{\varepsilon_m})(\varepsilon_c - \overline{\varepsilon_c})}{\sum \sqrt{(\varepsilon_m - \overline{\varepsilon_m})^2 (\varepsilon_c - \overline{\varepsilon_c})^2}}$

In addition to the numerical comparisons made by the program, periodic visual comparisons of the response histories are made to obtain a conceptual measure of accuracy. Again, engineering judgment is essential for determining which parameters should be adjusted so as to obtain the most accurate model. The selection of adjustable parameters is performed by determining what properties have a significant effect on the strain comparison and determining which values cannot be accurately estimated through conventional engineering procedures. Experience in examining

the data comparisons is helpful; however, two general rules apply concerning model refinement. When the shapes of the computed response histories are similar to the measured strain records but the magnitudes are incorrect, this implies that member stiffness must be adjusted. When the shapes of the computed and measured response histories are not very similar, the boundary conditions or the structural geometry are not well represented and must be refined.

In some cases, an accurate model cannot be obtained, particularly when the responses are observed to be nonlinear with load position. Even then, a great deal can be learned about the structure, and intelligent evaluation decisions can be made.

Appendix H: Load Rating Procedures

A load rating factor is a numeric value indicating a structure's ability to carry a specific load. Load rating factors were computed by applying standard design loads along with the structure's self-weight and asphalt overlay. Rating factors are computed for various structural components and are equal to the ratio of the component's live-load capacity and the live-load applied to that component; including all appropriate load factors. A load rating factor greater than 1.0 indicates that a member's capacity exceeds the applied loads with the desired factors of safety. A rating factor less than 1.0 indicates a member is deficient such that a specific vehicle cannot cross the bridge with the desired factor of safety. A number near 0.0 indicates the structure cannot carry its own dead weight and maintain the desired safety factor. The lowest-component rating factor generally controls the load rating of the entire structure. Additional factors are applied to account for variability in material, load application, and dynamic effects. Two levels of load rating are performed for the bridge. An Inventory Level rating corresponds to the design stress levels and/or factors of safety and represents the loads that can be applied on a daily basis. The Operating Rating levels correspond to the maximum load limits above which the structure may experience damage or failure.

For borderline bridges (those for which calculations indicate a posting is required), the primary drawback to conventional bridge rating is an over-simplified procedure for estimating the load applied to a given beam (i.e., wheel load distribution factors) and a poor representation of the beam itself. Due to lack of information and the need for conservatism, material and cross-section properties are generally underestimated, and beam end supports are assumed to be simple when, in fact, even relatively simple beam bearings have a substantial effect on the midspan moments. Inaccuracies associated with conservative assumptions are compounded with complex framing geometries. From an analysis standpoint, the goal is to generate a model of the structure that is capable of reproducing the measured strains. Decisions concerning load rating are then based on the performance of the model once it is proven to be accurate.

The main purpose for obtaining an accurate model is to evaluate how the bridge will respond when standard design loads, rating vehicles, or permit

loads are applied to the structure. Since load testing is generally not performed with all of the vehicles of interest, an analysis must be performed to determine load rating factors for each truck type. Load rating is accomplished by applying the desired rating loads to the model and computing the stresses on the primary members. Rating factors are computed using the equation specified in the AASHTO (2003) (see Equation H1).

It is important to understand that diagnostic load testing and the integrated approach are most applicable to obtaining Inventory (service load) rating values. This is because it is assumed that all of the measured and computed responses are linear with respect to load. The integrated approach is an excellent method for estimating service load stress values, but it generally provides little additional information regarding the ultimate strength of particular structural members. Therefore, Operating rating values must be computed using conventional assumptions regarding member capacity. This limitation of the integrated approach is not viewed as a serious concern, however, because load responses should never be permitted to reach the inelastic range.

Operating and/or Load Factor rating values must also be computed to ensure a factor of safety between the ultimate strength and the maximum allowed service loads. The safety to the public is of vital importance, but as long as load limits are imposed such that the structure is not damaged. safety is no longer an issue.

Following is an outline describing how field data are used to help in developing a load rating for the superstructure. These procedures will only complement the rating process, and must be used with due consideration to the substructure and inspection reports.

1. **Conduct preliminary investigation**: Verify linear and elastic behavior through continuity of strain histories, locate neutral axis of flexural members, detect moment resistance at beam supports, and qualitatively evaluate behavior.
2. **Develop representative model**: Use graphic pre-processors to represent the actual geometry of the structure, including span lengths, girder spacing, skew, transverse members, and deck. Identify gage locations on model identical to those applied in the field.
3. **Simulate load test on computer model**: Generate two-dimensional model of test vehicle and apply to structure model at discrete positions

along same paths defined during field tests. Perform analysis and compute strains at gage location for each truck position.

4. **Compare measured and initial computed strain values**: Compute various global and local error values at each gage location and make visual comparisons with post-processor.

5. **Evaluate modeling parameters**: Improve model based on data comparisons. Engineering judgment and experience is required to determine which variables are to be modified. A combination of direct evaluation techniques and parameter optimization is used to obtain a realistic model. General rules have been defined to simplify this operation.

6. **Model evaluation**: In some cases it is not desirable to rely on secondary stiffening effects if it is likely they will not be effective at higher load levels. It is beneficial, though, to quantify their effects on the structural response so that a representative computer model can be obtained. The stiffening effects that are deemed unreliable can be eliminated from the model prior to the computation of rating factors. For instance, if a noncomposite bridge is exhibiting composite behavior, it can conservatively be ignored for rating purposes. However, if it has been in service for 50 years and it is still behaving compositely, chances are that very heavy loads have crossed over it and any bond-breaking would have already occurred. Therefore, probably some level of composite behavior can be relied upon. When unintended composite action is allowed in the rating, additional load limits should be computed based on an allowable shear stress between the steel and concrete and an ultimate load of the noncomposite structure.

7. **Perform load rating:** Apply HS-20 and/or other standard design, rating, and permit loads to the calibrated model. Rating and posting load configurations recommended by AASHTO are shown in Figure H1.

8. The same rating equation specified by the **AASHTO - Manual for the Condition Evaluation of Bridges** is applied:

$$RF = \frac{C - \gamma_{DC}(DC) - \gamma_{DW}(DW) \pm \gamma_P(P)}{\gamma_{LL}(LL + IM)} \qquad \text{(H1)}$$
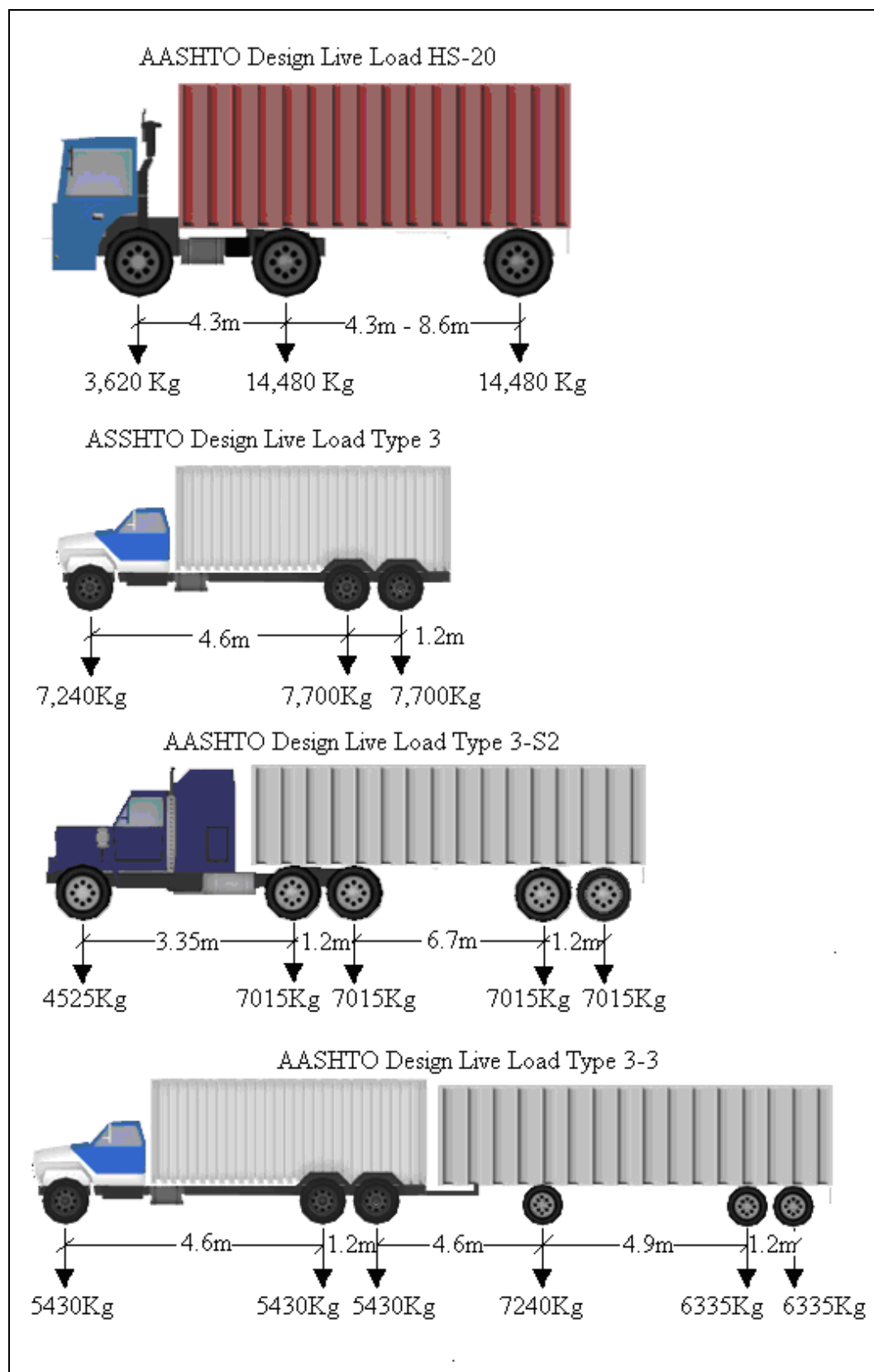
Figure H1. AASHTO rating and posting load configurations (SI).

where:

RF = rating factor for individual member

C = member capacity

γ_{DC} = LRFD load factor for structural components and attachments

DC = dead-load effect due to structural components

γ_{DW} = LRFD load factor for wearing surfaces and utilities

DW = dead-load effect due to wearing surface and utilities

γ_P = LRFD load factor for permanent loads other than dead-loads = 1.0

P = permanent loads other than dead-loads

γ_{LL} = LRFD load factor for live-load

LL = live-load effect

IM = impact effect, either AASHTO or measured

The only difference between this rating technique and standard beam rating programs is that a more realistic model is used to determine the dead-load and live-load effects. Two-dimensional loading techniques are applied because wheel load distribution factors are not applicable to a planar model. Stress envelopes are generated for several truck paths; envelopes for paths separated by normal lane widths are combined to determine multiple-lane loading effects.

9. **Consider other factors**: Other factors such as the condition of the deck and/or substructure, traffic volume, and other information in the inspection report should be taken into consideration and the rating factors adjusted accordingly (Tables H1 and H2).

The configuration and layout of all the vehicles used in the load rating and axle spacings for each vehicle are shown in Figures H2–H4 and Tables H3–H7.

Table H1. LRFR load and resistance factors.

Dead-Load	DC (dead-load effects due to structural components and attachments)	1.25
	DW (dead-load effects due to wearing surface and utilities)	1.50
Live-Load	Inventory	1.75
	Operating	1.35
Condition Factor, φ_c	Good or satisfactory	1.00
	Fair	0.95
	Poor	0.85
System Factor, φ_s	Welded members in two-girder/truss/arch bridges	0.85
	Riveted members in two-girder/truss/arch bridges	0.90
	Multiple eyebar members in truss bridges	0.90
	Three-girder bridges with girder spacing ≤6 ft	0.85
	Four-girder bridges with girder spacing ≤4 ft	0.95
	All other girder bridges and slab bridges	1.00
	Floorbeams with spacing >12 ft and noncontinuous stringers	0.85
	Redundant stringer subsystems between floorbeams	1.00

Table H2. LRFD resistance factors.

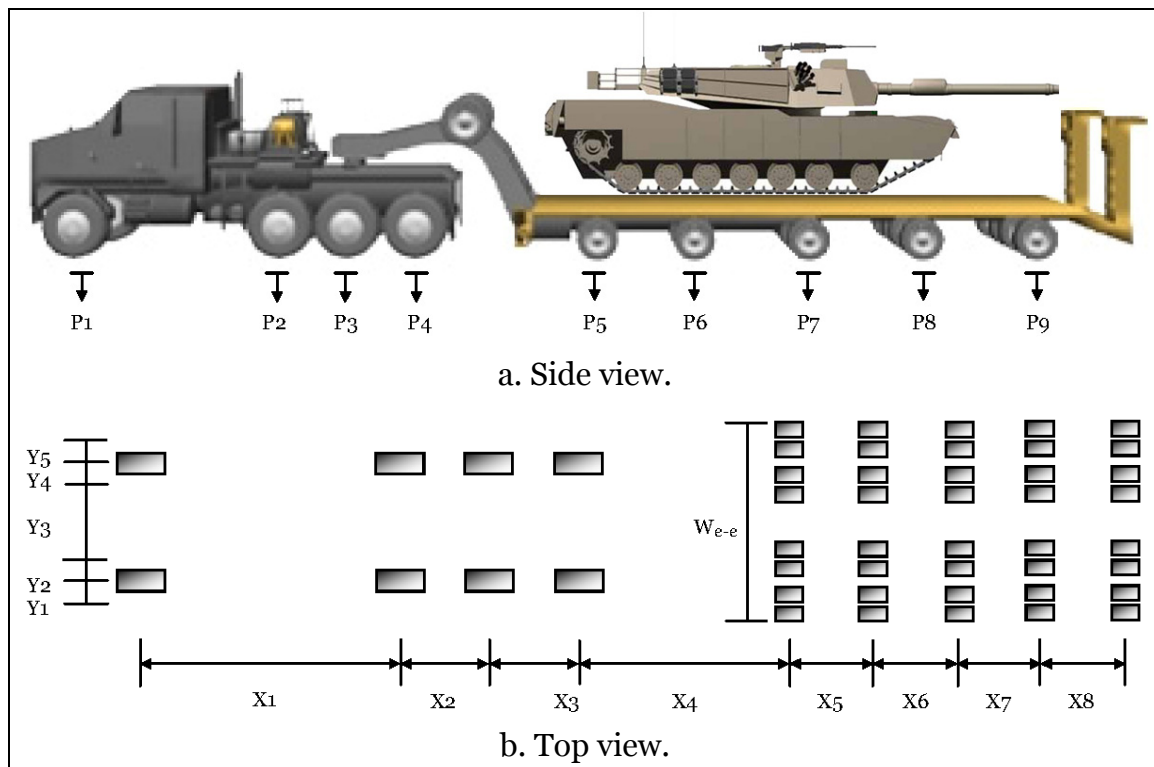| Capacity	Steel Resistance Factor	R/C Resistance Factor	PS/C Resistance Factor
Flexure, Φ_b	1.00	0.90	1.00
Shear, Φ_v	1.00	0.90	0.90

a. Side view.

b. Top view.

Figure H2. Configuration of HETS vehicle load distribution.

Table H3. Loading data and dimensions of HETS with M1A1.

Loading Data								
Axle Loads (kg)	P1	P2	P3	P4	P5	P6	P7	P8	P9
	9820	10090	9820	9005	12217	13440	12670	12670	14210
Dimensions								
Transverse Spacing (m)	We-e	Y1	Y2	Y3	Y4	Y5			
	3.66	0.51	0.34	1.48	0.34	0.51			
Longitudinal Spacing (m)	X1	X2	X3	X4	X5	X6	X7	X8	
	3.94	1.52	1.52	4.86	1.81	1.81	1.81	1.81	

Table H4. Loading data and dimensions of empty HET.

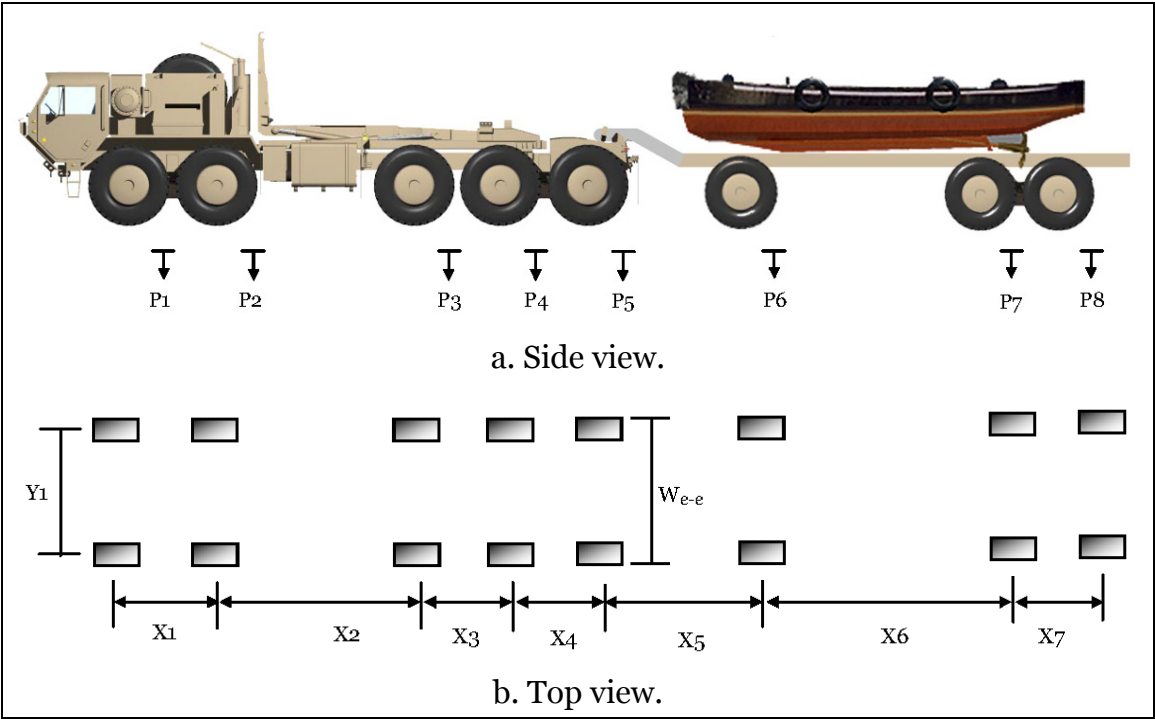| Loading Data								
Axle Loads (kg)	P1	P2	P3	P4	P5	P6	P7	P8	P9
	8890	5020	5050	4890	3780	3620	3760	5520	5590
Dimensions								
Transverse Spacing (m)	We-e	Y1	Y2	Y3	Y4	Y5			
	3.66	0.509	0.341	1.48	0.341	0.509			
Longitudinal Spacing (m)	X1	X2	X3	X4	X5	X6	X7	X8	
	3.94	1.52	1.52	4.86	1.81	1.81	1.81	1.81	

a. Side view.

b. Top view.

Figure H3. Configuration of PLS vehicle load distribution.

Table H5. Loading data and dimensions of PLS.

Loading Data								
Axle Loads (kg)	P1	P2	P3	P4	P5	P6	P7	P8
	5158	5158	9593	9593	9593	4434	9321	9321
Dimensions								
Transverse Spacing (m)	W$_{e-e}$	Y1						
	2.44	2.03						
Longitudinal Spacing (m)	X1	X2	X3	X4	X5	X6	X7	
	1.52	3.41	1.52	1.52	2.59	3.05	1.40	

Table H6. MLC Loading data and dimensions

MLC	Tracked	Wheeled*
60	54300Kg 4.27m 0.7m 3.35m	63350Kg 3.7m 1.5m 4.6m 1.2m 7240Kg 16290Kg 16290Kg 11765Kg 11765Kg
70	63350Kg 4.6m 0.8m 3.5m	72850Kg 3.7m 1.5m 4.6m 1.2m 9500Kg 19000Kg 19000Kg 12670Kg 12670Kg

a. Side view.

b. Top view.

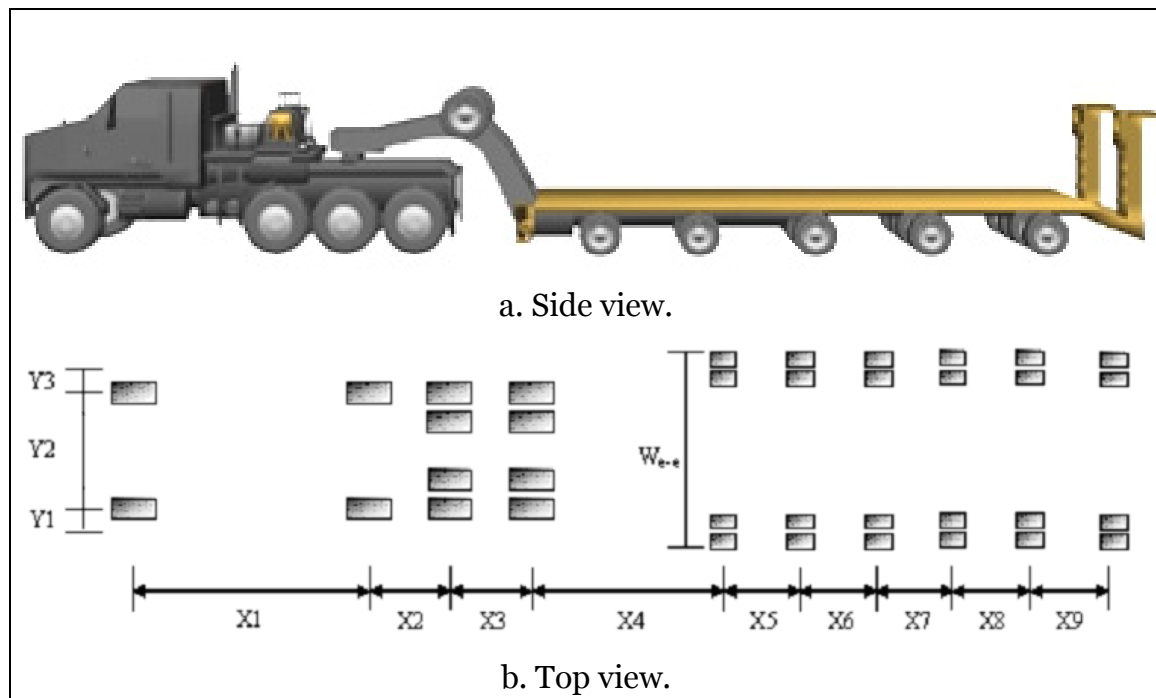Figure H4. Configuration of Korean MHET vehicle load distribution.

Table H7. Loading Data and Dimensions of Korean MHET.

Loading Data									
Axle Loads (kg)	P1	P2	P3	P4	P5	P6	P7	P8	P9	P10
	7560	9980	12000	11300	9320	9590	9460	9860	9710	9520
Dimensions									
Transverse Spacing (m)	We-e	Y1	Y2	Y3					
	3.25	0.357	2.03	0.357					
Longitudinal Spacing (m)	X1	X2	X3	X4	X5	X6	X7	X8	X9
	1.70	3.20	1.35	5.92	1.30	1.30	1.30	1.30	1.30

1. REPORT DATE (DD-MM-YYYY)	2. REPORT TYPE	3. DATES COVERED (From - To)
May 2008	Final report	

4. TITLE AND SUBTITLE

Field Testing and Load Rating Report, Bridge S-1090

5a. CONTRACT NUMBER

5b. GRANT NUMBER

5c. PROGRAM ELEMENT NUMBER

6. AUTHOR(S)

Brett Commander, Jesse Grimson, Wilmel Varela-Ortiz, Terry R. Stanton, Carmen Y. Lugo, and Gerald M. Hansler

5d. PROJECT NUMBER

5e. TASK NUMBER

5f. WORK UNIT NUMBER

7. PERFORMING ORGANIZATION NAME(S) AND ADDRESS(ES)

Bridge Diagnostics, Inc., 1965 57th Court North, Suite 106, Boulder, CO 80301-2826;
U.S. Army Engineer Research and Development Center
Geotechnical and Structures Laboratory
3909 Halls Ferry Road, Vicksburg, MS 39180-6199;
Eighth U.S. Army, Seoul, South Korea

8. PERFORMING ORGANIZATION REPORT NUMBER

ERDC/GSL TR-08-8

9. SPONSORING / MONITORING AGENCY NAME(S) AND ADDRESS(ES)

Headquarters, Installation Management Command (IMCOM)
Arlington, VA 22202

10. SPONSOR/MONITOR'S ACRONYM(S)

11. SPONSOR/MONITOR'S REPORT NUMBER(S)

12. DISTRIBUTION / AVAILABILITY STATEMENT
Approved for public release; distribution is unlimited.

13. SUPPLEMENTARY NOTES

14. ABSTRACT
In June 2007, Bridge Diagnostics, Inc. (BDI), was contracted by the U.S. Army Corps of Engineers to perform live-load testing and load rating on Bridge S-1090 at Camp Casey, South Korea, in conjunction with two other structures, S-4360 and S-1801. The general goal of the live-load testing was to obtain and then utilize field measurements to verify an analytical model from which accurate load ratings could be obtained. A more specific purpose of the load test was to determine if the use of the Heavy Equipment Transporter System (HETS) to transport an M1A1 tank across the bridge was more or less severe than the M1A1 tank crossing on its own.

Controlled load tests were performed with a three-axle dump truck, an empty HETS, an M1A1 tank, and a HETS carrying an M1A1 tank. The load test data were examined to obtain a direct comparison of load responses from the different load configurations. The conclusion obtained directly from the load test data was that the HETS/M1A1 load combination produced lower stresses than the M1A1 tank by itself. Subsequent modeling and analysis of the bridge further verified that the HETS was the best option for transporting the M1A1 across the bridge. Load ratings were performed for the standard American Association of State Highway and Transportation Officials (AASHTO) vehicles and several military load configurations in accordance with AASHTO Load and Resistance Factor Design–Bridge Design Specifications 2004 and Manual for Condition Evaluation and Load and Resistance Factor Rating of Highway Bridges 2003. It was found that the structure can safely carry all of the AASHTO vehicles and military load configurations considered in this report.

15. SUBJECT TERMS

Distribution factor	Load rating	Military vehicles
Finite element analyses	Load test	Steel beam bridge

16. SECURITY CLASSIFICATION OF:			17. LIMITATION OF ABSTRACT	18. NUMBER OF PAGES	19a. NAME OF RESPONSIBLE PERSON
a. REPORT	**b. ABSTRACT**	**c. THIS PAGE**			
UNCLASSIFIED	UNCLASSIFIED	UNCLASSIFIED		102	**19b. TELEPHONE NUMBER** (include area code)